Femtosecond Pump probe Spectroscopy of Light harvesting Complexes and Phthalocyanines

by

Saturnin OMBINDA LEMBOUMBA

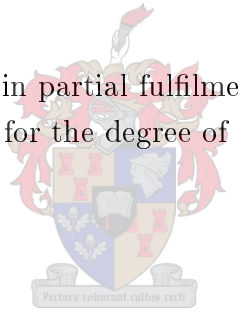

Dissertation presented in partial fulfilment of the requirements for the degree of

Doctorate of Physics

at Stellenbosch University

Study Leaders:
Dr Anton du Plessis, Dr Christine M. Steenkamp, Prof. Erich G. Rohwer

December 2011

Declaration

By submitting this thesis/dissertation electronically, I declare that the entirety of the work contained therein is my own, original work, that I am the sole author thereof (save to the extent explicitly otherwise stated), that reproduction and publication thereof by Stellenbosch University will not infringe any third party rights and that I have not previously in its entirety or in part submitted it for obtaining any qualification.

December 2011

Abstract

The generation of ultrafast light pulses and the development of time–resolved spectroscopic techniques, such as the femtosecond pump–probe spectroscopy technique, have facilitated the study of ultrafast energy transfer in the photosynthetic systems of green plants and photodynamic therapy drugs. It has allowed the investigation of biological and chemical processes that take place on the ultrafast timescale and has allowed us to obtain spectral and kinetic information on energy transfer. In addition, it has allowed time–resolved experiments in which the transient absorption of species under investigation was observed and has elucidated molecular dynamics. In the present work this was done with a temporal resolution of approximately 200 fs and covering a pump-to-probe delay range of 300 fs to 2 ns.

The main aims of this study were to characterise the femtosecond pump–probe spectroscopy system, to investigate the energy transfer in the natural light harvesting complex II (LHC II) in view of future expansion to the study of synthesized artificial functional light harvesting complexes and finally to study ultrafast processes in zinc phthalocyanine (ZnPc) systems.

In photosynthetic organisms, LHC II is the most abundant light–harvesting complex and it plays an important role in light harvesting and photoprotection. The light energy is absorbed by light–harvesting complexes and transferred to a reaction centre (RC) in an ultrafast timescale.

Phthalocyanines are a new class of photosensitiser used for photodynamic therapy. These drugs are used to treat small and superficial tumours. The energy transfer from the singlet–excited state to the triplet–excited state occurs on an ultrafast timescale. However, recent work done on zinc phthalocyanine has proved that the determination of the ultrafast component remains a challenge. Several ultrafast studies carried out on ZnPc in solvents have been not only unsuccessful to give a clear picture of the ultrafast dynamics but have also produced divergent results.

In this study, a characterisation of the femtosecond pump–probe spectroscopy setup was done. The samples under investigation were probed by a white–light continuum. The generation of the white–light continuum introduced chirp, which influenced the temporal evolution of the transient absorption results. The technique used to correct the chirp introduced by white–light generation is discussed in detail. Our femtosecond pump–probe spectroscopy setup was benchmarked by using a well–known dye, namely malachite green. In addition, the investigation of the transient absorption change of LHC II, an active component in photosynthesis, as extracted from spinach leaves and the ultrafast dynamics of a promising photosensitiser ZnPc in dimethyl sulfoxide (DMSO) as

well as in dimethyl formamide (DMF) was done. The spectral and dynamic results obtained using these three samples are described and exponential fits to the absorbance decay curves used to estimate the timescales of the energy–transfer processes are presented. In this experiment, the dynamics and measured time constants related to the energy transfer between the different types of chlorophyll in LHC II was monitored, whereas with ZnPc, the dynamics and the measured time constants associated with solvation dynamics and vibrational relaxation was examined.

Opsomming

Die vorming van ultravinnige lig pulse en die ontwikkeling van tyd–opgelosde spektroskopiese tegnieke, soos die femtosekonde pomp–proef spektroskopie tegniek, het die studie van ultravinnige energie oordrag in fotosintetiese stelsels van groen plante en chemiese prosesse gefasiliteer, wat kan plaasvind op die ultravinnige tyd skaal en laat dit toe om spektrale en kinetiese informasie oor die energie oordrag te kan bepaal. Dit het ook dit moontlik gemaak om tyd–opgelosde eksperimente te kan doen waarin ons veranderlike absorbsie van die monster kon ondersoek en die molekulere dinamika kon ontrafel. In hierdie werk is dit gedoen met n tyd resolusie van omtrent 200 fs termyl 'n pomp-tot-proef tydvertraging van 300 fs tot 2 ns gebruik is.

Die hoof doelwitte van hierdie werk was om 'n femtosekonde pomp–proef spektroskopie stelsel te karakteriseer, die energie oordrag in die natuurlike lig-oes kompleks II te ondersoek met die toekomstige uitbreiding van die studie na sintetiese lig-oes komplekse as oogmerk en laastens om ultravinnige prosesse in Sink Ftalosianiene stelsels te ondersoek.

In fotosintetiese organismes, is lig–oes kompleks II die mees volop lig–oes kompleks en speel 'n belangrike rol in lig–oes en foto–skerming. Die lig energie word geabsorbeer deur lig–oes komplekse en dan oorgedra na reaksie middelpunte in 'n ultravinnige tydskaal.

Ftalosianiene is 'n nuwe klas fotosensiteerder wat gebruik word in fotodinamiese terapie. Hierdie dwelms word gebruik om klein en oppervlakkige gewasse te behandel. Die energie oordrag van die opgewekte singlet tot die triplet toestand vind plaas op die ultravinnige tydskaal. Onlangse navorsingswerke het getoon dat die bepaling van die ultravinnige komponent 'n uitdaging bly. Verskeie vorige ondersoeke is gedoen op Sink Ftalosianiene in verskeie oplosmiddels, en nie net het hierdie studies nie 'n helder prentjie verskaf van die ultravinnige dinamika nie, maar het ook divergerende resultate opgelewer.

In hierdie werk word 'n karakterisering van die femtosekonde pomp–proef spektroskopie stelsel gedoen. Die monsters is ondersoek met 'n wit–lig kontinuum proef. Die vorming van die wit–lig kontinuum het tjirp veroorsaak, wat die tyd–evolusie van die veranderlike absorbsie resultate beinvloed het. Die tegniek wat gebruik was om die tjirp te korregeer word bespreek. Ons femtosekonde pomp–proef spektroskopie stelsel is gestandardiseer deur die wel–bekende kleurstof malachiet groen. Ons het ook die veranderlike absorbsie van lig–oes kompleks II ondersoek, 'n aktiewe komponent in fotosintese, soos dit onttrek is uit spinasie blare, asook die ultravinnige dinamika van die belowende photosensitizer Sink Ftalosianiene in DMSO asook DMF. Die spektrale en dinamiese resultate verkry vanaf hierdie drie monsters word beskryf en eksponensiele passings aan die ab-

sorbsie verval kurwes is gebruik om die tydskale van die energie oordrag prosesse te skat. In hierdie eksperiment is dinamika en gemete tydkonstantes waargeneem wat toegeskryf kan word aan die energie oordrag tussen verskillende soorte chlorofil in lig–oes kompleks II. In die Sink Ftalosianien eksperimente is dinamika en gemete tydkonstantes waargeneem wat toegeskryf kan word aan solverings–dinamika asook vibrasionele ontspanning.

Acknowledgments

I would like to thank the following people and institutions:

- Dr Anton du Plessis, for his excellent supervision, guidance and expertise, as well as the time spent on academic discussions and technical advice given to me in the laboratory
- Dr Christine M. Steenkamp, for her time, comments, invaluable input and efficiency in the completion of the work as well as her inspiring approach and dedication to research
- Prof Erich G. Rohwer, for his supervision and contribution of his knowledge to the project
- All the members of the femtosecond research group at the CSIR–NLC, who provided support especially Ludwig De Clercq and Palesa Molukanele
- The African Laser Centre, the National Laser Centre (CSIR) and the Gabonese government for funding the project and my studies
- My family, who have always supported me with my studies. I will always be grateful and I would never been where i am without their help
- To my wife, Thembisa Ombinda (Dodo), who provide me with support, encouragement, motivation and love
- To my little boy, Athenkosi D. Ombinda, for bringing me joy when I was frustrated
- To the Gabonese community, who supported me in Stellenbosch as well as in Pretoria

Contents

List of Figures

List of Tables

Chapter 1

General introduction

1.1 General overview

The use of the pump–probe technique in most ultrafast spectroscopy measurements has brought a better understanding of dynamic processes in many branches of physics, chemistry and biology. It has been used to detect and monitor fast transient chemical processes in living cells [1] or in solution [2], and to study fast chemical reactions [3, 4, 5]. The femtosecond research group at CSIR–NLC have developed a pump–probe femtosecond transient absorption system. This system can be used to investigate ultrafast energy–transfer events that occur on time scales from 300 fs to 2 ns, in particular light–gathering and transfer mechanisms, in photosynthetic light–harvesting complexes (LHCs) and energy transfer in photodynamic therapy (PDT) drugs that lead to the destruction of cancer.

The state of the art in femtosecond pump–probe spectroscopy is that various groups around the world are focusing their efforts on biological applications. LHCs is currently the "hot topic" in femtosecond spectroscopy and will remain so for a number of years, until the energy–transfer processes are fully understood and systems can be synthesised such that the energy transfer can be controlled and manipulated. Commercial relevance is found in potentially highly efficient biological solar cells, among others. On the other hand, the processes of light absorption and energy transfer are also at the heart of PDT. Phthalocyanines are a new class of photosensitiser used for PDT. These drugs are used to treat small and superficial tumours. In recent years, particular attention has been given to zinc phthalocyanine (ZnPc) in order to find suitable photosensitisers that can be clinically used as photodynamic cancer drugs. There are ultrafast processes that are used for the destruction of the cancer.

Research into the fundamental processes that are involved in chemical re-

action mechanisms is of critical importance for understanding chemical and biological phenomena. Many of these processes occur on the picosecond and femtosecond timescale. Time–resolved femtosecond pump–probe spectroscopic techniques are often the only available methods capable of detecting and monitoring these events. Internationally, there are several laboratories that have such facilities and that are active in this research field, but none in Africa until recently. This area of research is at the forefront of many areas of study and is a significant growth area in current research in the fields of physics and biology. The strategic importance of the work lies in the fact that femtosecond science is one of the newest and most rapidly developing application fields of lasers in the world. On the basic science side, it has already had a major impact on the understanding of basic chemical and biological systems.

1.2 Objectives

The first objective of this work was to characterise and benchmark a pump–probe femtosecond transient absorption system. This system can be used to investigate ultrafast energy–transfer events, such as light–gathering and energy transfer mechanisms, in photosynthetic LHCs and ultrafast processes in ZnPc.

The second objective was to acquire an experimental basis for understanding the fast processes that occur in LHCs and ZnPc. The third objective was to measure the ultrafast energy–transfer events that take place in biological samples containing LHCs and ZnPc. Furthermore, once this had been done, the fundamental research question involved the interpretation of these results to improve our understanding of these fundamental processes. The main goal was to investigate the dynamics of energy transfer in LHCs and ultrafast processes in PDT drugs (ZnPc) over a timescale that ranges from roughly 300 fs to 2 ns and to understand the dynamics of these processes.

The investigation on the LHCs was done with the hope of obtaining artificial LHCs that could be compared to the natural ones but the acquisition of artificial LHCs did not materialise. However the results obtained with natural LHC II serves to confirm previous work. In addition previous work done on ultrafast processes in ZnPc presented a lack of data in the picosecond time scale [6]. The pump-probe setup used in this work was suitable to fill the gap observed in previous work [6]. In addition discrepancies were noted in literature whereby Rao and Rao attributed the time constant of 35 ps to the depopulation of the excited state S_1 of ZnPc [7], whereas the depopulation of S_1 is given as 3 ns elsewhere [8]. In order to resolve these discrepancies and fill that gap, a study of ultrafast processes in ZnPc was done not only by exciting ZnPc at different pump wavelengths than reported elsewhere, but also by investigating the ZnPc

ultrafast processes in different solvents.

1.3 Dissertation layout

The general overview of the dissertation is briefly outlined in Chapter 1.

In Chapter 2, the general background of pump–probe spectroscopy is given, which entails the basic principles and the theory of the pump–probe spectroscopy technique, and the expected pump–probe measured signal. In addition, the samples under investigation are presented.

In Chapter 3, the experimental setups for transient absorption measurement are described. In addition, methods used not only for sample preparation but also for measurement and analysis of transient absorption data are shown.

In Chapter 4, results of the investigation of energy transfer in LHCs and ZnPc in solvent are presented and discussed.

In Chapter 5, conclusions of the investigation are presented and recommendations for further study are given.

Chapter 2

Literature review

2.1 Introduction

Many biological and chemical processes occur on relatively long timescales (from milliseconds to seconds). These long processes are the result of combinations of several very fast elementary processes, ranging from femtoseconds to picoseconds [9]. In photosynthesis systems, the transfer of energy inside LHCs and to the reaction centre (RC) occurs on a timescale of 100 fs to several picoseconds [9, 10, 11, 12] whereas the energy transfer within an aggregated chain of complexes takes places on a timescale of microseconds to milliseconds. The energy transfer occurring on a femtosecond to picosecond timescale is generally referred to as the ultrafast regime. In order to observe ultrafast processes, such as the translation or rotation of parts of a molecule, energy transfer, charge transport or the formation or breaking of a chemical bond, a measurement technique with a temporal resolution in the range of femtoseconds to picoseconds is required. However, most detectors are not fast enough to resolve such timescales [13].

The ultrafast pump–probe spectroscopy technique allows one to resolve changes on these timescales, typically from tens or hundreds of femtoseconds up to hundreds of picoseconds or even a few nanoseconds. In this technique, ultrafast laser pulses are used to pump (excite) sample molecules to an excited state, and probe pulses are used to monitor changes by delaying the probe pulse relative to the pump pulse. The detector therefore does not require fast response, as the temporal information is provided by having short laser pulses, shorter than the process to be monitored. This has become a powerful, unique tool and a relevant technique for the investigation of various ultrafast processes. The advantages of this technique are the investigation of ultrafast dynamics of biological or chemical systems in real time and the observation of the movement of individual particles such as electrons or atoms and energy–transfer processes

taking place in biological and chemical molecular systems.

The use of the pump–probe technique has provided physicists, chemists and biologists with the resources to probe and understand the ultrafast dynamics of molecular interactions [13, 14]. The "transient absorption" spectroscopy (pump–probe) technique has been used in studies on ultrafast transient chemical processes in liquids, gases, clusters, semiconductors and large biochemical systems [5, 14, 15]. For example, numerous transient absorption spectroscopy studies have been done on LHCs and bacterial photosynthesis dynamics [16, 17, 18, 19]. These studies of dynamic events have also been extended to nanoparticles as new targets for drug–delivery mechanisms [14], understanding the chemical modification of DNA when it absorbs UV light [14], artificial LHCs in order to produce efficient solar cells [12] and dye cluster and PDT drugs to understand the mechanism of drug action [20]. The pump–probe technique is used to probe and characterise excited states, and particularly the lifetimes of these states, of the molecules under investigation.

2.2 Review of pump–probe spectroscopy

2.2.1 The basic principles of the pump–probe technique

The pump–probe technique uses two different laser pulses: the pump and probe pulses. The pump pulse excites the sample at a given wavelength and the probe pulse, delayed in time, explores the absorption of the sample and its change, usually at different wavelengths and various delay times. In the pump–probe method, there are two important requirements that should be satisfied.

The first one is that the pump and the probe should be independently tunable in order to excite the sample at resonance and to probe different optical transitions of the sample that are taking place [9, 21, 22, 23]. The tunability of the pump and probe pulses allows more detailed investigations compared to the restricted use of fixed frequencies. However to simplify the pump–probe experiment, probe pulses that cover an ultrabroad spectral range at once are used. This wider probe spectrum allows the simultaneous monitoring of the transient species involved in a photoprocess induced by the pump pulse.

The second requirement that should be satisfied is that the pulse duration of the pump and the probe pulses must be shorter than the timescale of the dynamic that one wants to observe [9, 22]. The shorter the pump and probe pulses are, the better one can monitor the fast processes. In addition, the temporal resolution of the pump–probe technique is determined not only by the duration of the pump and probe pulses, but also by the degree of experimental control over the time delay between the pump and probe pulses.

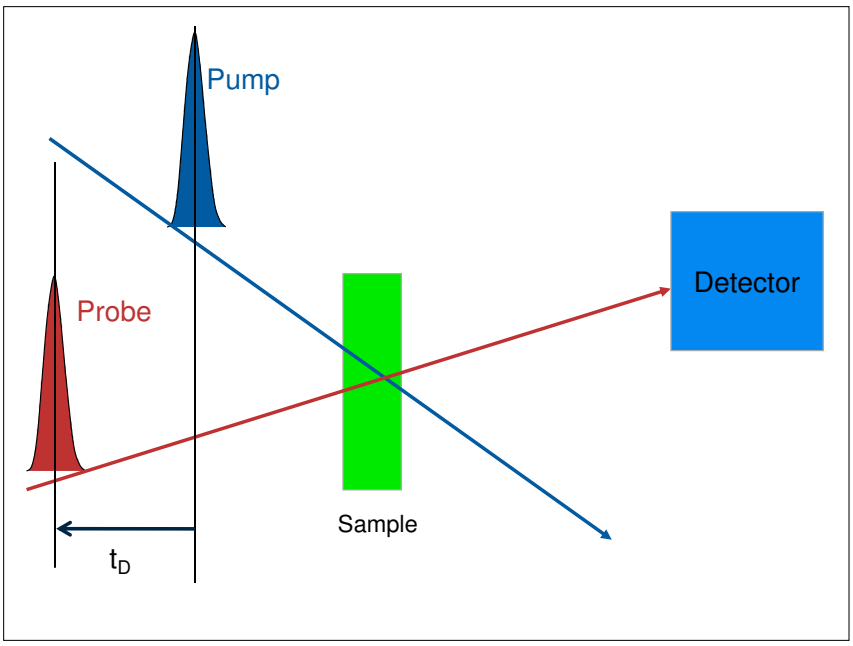

Figure 2.1: The basic principle of the pump–probe spectroscopy technique illustrated with probe pulse arriving at the sample a delay time t_D after the pump pulse

The pump and probe pulses are sent through different optical paths and are then focused into the sample with a time delay t_D between them, as shown in Figure 2.1. The pump is used to trigger a photo–induced process, such as an electronic excitation in the sample, atoms or molecules, and the probe beam is used to probe the atoms or molecules after excitation, as shown in Figure 2.2. The evolution of this process can then be followed by varying the time delay t_D and monitoring the delayed probe pulse. For instance, Figure 2.3 shows the evolution of the "transient concentration" of the excited state of such a hypothetical system, which corresponds to a measurement of the population of the excited state of Figure 2.2 at different times after excitation. In the pump–probe spectroscopy technique, the more intense pump pulse is used to induce the transient changes in the sample, whereas the weak probe pulse is used to measure the photo–induced changes of the sample. In addition, the probe pulse energy should be at least two orders of magnitude less than the pump pulse energy, which is a crucial requirement in order not to disturb the sample [24].

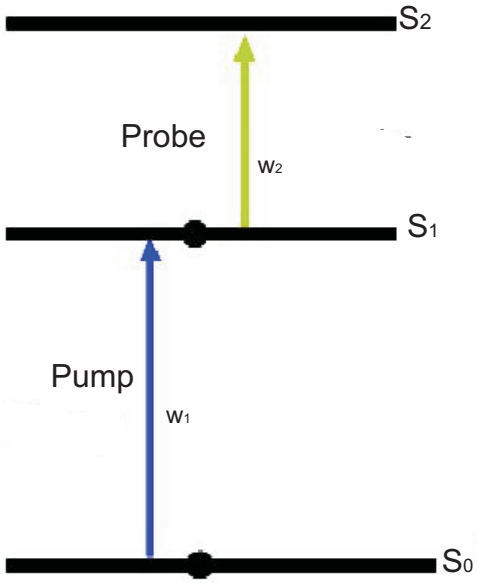

Figure 2.2: Basic energy–level diagram of a hypothetical system, indicating a pump–probe experiment where w_1 populates and w_2 absorption provide temporal information of the population in state S_1. The principle applies to a large number of atoms or molecules.

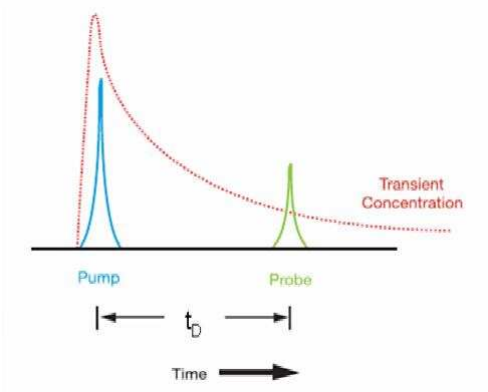

Figure 2.3: Monitoring the transient concentration of an excited state in a pump–probe setup [15]. In this example, excited–state absorption (ESA) provides the spectroscopic and temporal information.

2.2.2 Theory of pump–probe spectroscopy

By comparison of the pumped and non–pumped probe spectra ($\triangle A$), it is possible to find information about the excited molecules or atoms in the system at a specific given delay. Time resolution and information about the kinetics of these molecules or atoms can be obtained by measuring $\triangle A$ at various delays. The pump–probe signal is expressed as the difference in absorption (or transmission), as mentioned above. Using the Beer–Lambert law, the pump–probe signal is derived as follows:

$$I_{transmitted} = I_{incident} e^{-\varepsilon dc} = I_{incident} e^{A}$$

$$A = -\varepsilon dc$$

$$A = -log\left(\frac{I_{transmitted}}{I_{incident}}\right)$$

$$A = log\left(\frac{I_{incident}}{I_{transmitted}}\right) \tag{2.1}$$

where ε is the absorption coefficient, d is the absorption path length and c is the concentration.

Therefore

$$\triangle A = A_{pumpON} - A_{pumpOFF} = log\left(\frac{I_{ref}}{I_{signal}}\right)_{ON} - log\left(\frac{I_{ref}}{I_{signal}}\right)_{OFF} \tag{2.2}$$

The question arising from this equation is whether this equation holds for all situations, e.g. when the reference beam passes through the sample or not. First examine the case when the reference beam is passing through the sample, as indicated in Figure 2.4.

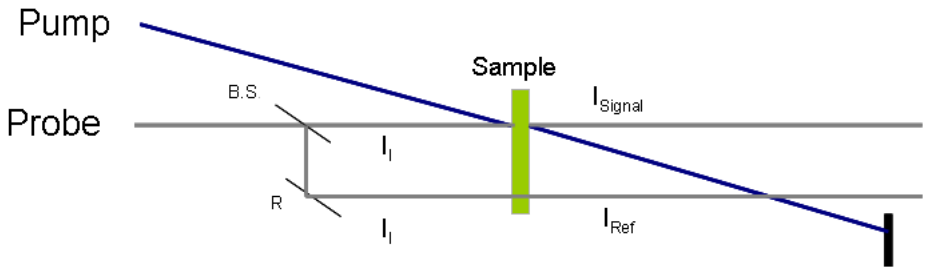

Figure 2.4: The overlap of pump and probe beams: The two probe beams are shown – the signal and the reference are passing through the sample

When the pump is off, the equation 2.1 becomes

$$A_{pumpOFF} = log\left(\frac{I_I}{I_{signal}}\right)_{OFF} \tag{2.3}$$

when the pump is on, the equation 2.1 becomes

$$A_{pumpON} = log\left(\frac{I_I}{I_{signal}}\right)_{ON} \tag{2.4}$$

then

$$\triangle A = A_{pumpON} - A_{pumpOFF} = log\left(\frac{I_I}{I_{signal}}\right)_{ON} - log\left(\frac{I_I}{I_{signal}}\right)_{OFF} \tag{2.5}$$

In addition, it was assumed that the pump signal does not influence the reference beam. Therefore, whether the pump is on or off, the following relationship is obtained

$$A = log\left(\frac{I_I}{I_{ref}}\right) \Longrightarrow I_I = I_{ref}e^A$$

Putting this expression into the previous two equations (2.3) and (2.4), the Beer-Lambert law becomes

$$A_{pumpOFF} = log\left(\frac{I_{ref}e^A}{I_{signal}}\right)_{OFF}$$

$$A_{pumpON} = log\left(\frac{I_{ref}e^A}{I_{signal}}\right)_{ON}$$

therefore, by inserting these expressions into equation, (2.2) the absorbance change equation becomes

$$\triangle A = A_{pumpON} - A_{pumpOFF} = log\left(\frac{I_{ref}}{I_{signal}}\right)_{ON} - log\left(\frac{I_{ref}}{I_{signal}}\right)_{OFF} \tag{2.6}$$

In the case where the reference beam is passing out of the sample as indicated in Figure 2.5

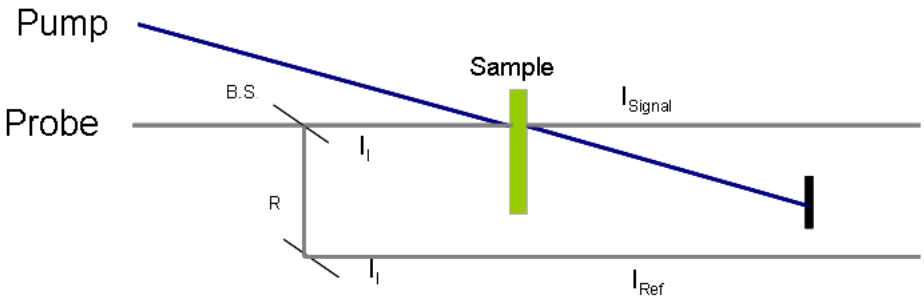

Figure 2.5: The overlap of pump and probe beams: The two probe beams are shown – the signal is passing through the sample and the reference out of the sample

again

$$\triangle A = A_{pumpON} - A_{pumpOFF} = log\left(\frac{I_I}{I_{signal}}\right)_{ON} - log\left(\frac{I_I}{I_{signal}}\right)_{OFF}$$

In this case

$$I_I = I_{ref} \tag{2.7}$$

therefore, replacing I_I with I_{ref} in the equation, the absorbance change becomes

$$\triangle A = A_{pumpON} - A_{pumpOFF} = log\left(\frac{I_{ref}}{I_{signal}}\right)_{ON} - log\left(\frac{I_{ref}}{I_{signal}}\right)_{OFF} \tag{2.8}$$

This indicates that the transient absorption obtained does not depend on the reference beam going through the sample.

2.2.3 Generation of ultrafast pulses and white–light

Ultrafast pulses Ultrafast pulses are generated in an oscillator laser resonator that contains a nonlinear optical element with a broad–gain medium such as Ti:Sapphire crystal. To obtain short pulses, many longitudinal modes propagating inside the laser resonator cavity must be mode–locked. In a multi–mode laser resonator, the longitudinal modes oscillate independently and have arbitrary phases relative to one another. However, the laser output is the outcome of the superposition of these modes. As a result, the interference between the modes produces a noise–like, fluctuating laser output. To overcome these noise–like outputs, the phases of the modes are manipulated in such a

way that there is a fixed phase between the modes. These modes of the laser, held in phase, will all periodically interfere constructively with one another to generate a short laser pulse. Various methods have been used to achieve mode–locking in such lasers. Nowadays in solid–state mode–locked lasers, ultrafast pulses are generated by using self–mode–locking. In a Ti:Sapphire laser, the self–mode–locking is achieved through the action of an instantaneous nonlinear Kerr lens effect inside the active medium. When a high–intensity electric field is applied to the crystal, a third–order nonlinear effect occurs, which leads to a change of the index of refraction of the crystal (Kerr lens effect). This Kerr lens effect leads to the refractive index to be intensity–dependent as indicated in equation 2.9

$$n = n_0 + n_2 I \tag{2.9}$$

where n_0 is the linear refractive index and n_2 is the nonlinear refractive index coefficient.

The formation of a Kerr lens causes the beam to undergo stronger self–focusing when it travels through the sapphire crystal on each pass. This means that the crystal behaves like a converging lens. Therefore, the strong, intense modes in the laser resonator will be enhanced and will be more strongly focused than the weaker modes. By introducing an appropriate slit or aperture in the laser resonator, an intensity–dependent loss mechanism can be achieved. The greater part of weak–intensity peaks are stopped while most of the higher–intensity peaks are let through. The mode–locking can then occur.

In order to obtain ultrafast pulses, longitudinal modes in the resonator must remain in phase. However, when a laser pulse is propagating through a nonlinear medium, positive chirp is introduced to the pulse. This chirp is based on group velocity dispersion (GVD) theory. The GVD increases the duration of the short laser pulses. The pulse duration increase occurs because low frequency components propagate faster than the higher frequency components. As a result, there will be a temporal broadening of the pulse. However, over a large bandwidth, the modes in the resonator cannot be held in phase. To achieve short pulses, GVD should be compensated by inserting in the resonator a dispersion compensation element such as a prism pair.

For many applications in femtosecond spectroscopy, the pulse energy needs to be higher than that produced by a laser oscillator. In order to generate higher energy pulses, the chirped pulse amplification (CPA) technique is used. A femtosecond pulse is propagated through a dispersive medium, which will result in the temporal stretching of the pulse. This chirped pulse can be amplified and subsequently recompressed to the original pulse duration.

White–light continuum With the development and commercialisation of femtosecond lasers in recent years, the white–light continuum has been used in many fields of research. In particular, white–light continuum has been used for time–resolved pump–probe spectroscopy experiments as a probe beam. The white–light continuum is generated by focusing an ultrafast laser pulse of high peak power onto a small area of nonlinear optical media. The propagation of this ultrafast pulse produces a broadening of its spectrum. The white–light continuum generation has been observed in various media, namely in crystal, glass, fibres, photonic crystal fibres, liquid and gas [25]. Many physical processes have been proposed to explain the white–light continuum generation. The major physical processes involved in white–light continuum generation are self–phase modulation, four–wave mixing, self–focusing and stimulated Raman scattering. However, several studies have shown that the process of white–light continuum generation is most probably generated by self–phase modulation [13, 25, 26]. The propagation of femtosecond laser pulse through a medium to generate a white–light continuum produces a group velocity dispersion effect. The increase of the pulse duration of the chirped white–light continuum can be measured or calculated [25].

2.2.4 Detection systems

There are several detection systems that can be used in pump–probe experiments. Popular detection systems used in transient absorption spectroscopy are multichannel detectors, such as the linear photodiode arrays (PDAs) [27, 28] or charge couple device (CCD), and the single–channel detectors such as double photodiodes [15, 21] or photodiode [9]. The configuration of the multichannel detector includes a spectrograph combined with a PDA or CCD detection system [27, 28, 29], whereas the single–channel detector is a combination of a spectrograph with photodiode(s). In addition, for high– and low–repetition rate measurement lock–in amplification or boxcar integrator is used respectively [29] in the case of single–channel detectors. These different detector systems are usually used according to certain needs and requirements of the experiment. In our experiment, a multichannel detector using a dual PDA detection system was the detector used.

The multichannel detector system configuration is composed of a spectrometer combined with a dual PDA detection system. The dual photodiode array detection system is placed behind the spectrometer in order to measure the signal and reference pulses (white–light continuum). Two separate sets of data are recorded at a fixed pump–probe delay when the pump irradiates the sample and when the pump is blocked from irradiating the sample, as indicated in equa-

tions (2.3) and (2.4). As a result, the absorbance changes $\triangle A$ are calculated, as indicated in equation (2.2) for the entire probe wavelength spectrum. The advantages of using PDAs in the multichannel detection are first of all that the data of many wavelengths can be acquired simultaneously due to the fact that the PDAs contain hundreds or thousands of photodiodes [27]. Secondly the PDAs have beneficial characteristics, such as low dark current and high saturation charge [27], which allow longer time integration. A longer time integration permits a better or a higher signal to noise ratio. In fact, the signal will be larger and the noise will be averaged toward zero as the integration time becomes longer. Thirdly, the PDAs have a high UV sensitivity with good stability and excellent output linearity [27].

2.2.5 Expected transient absorption signals from pump–probe measurement

For the analysis of the pump–probe measurement, three different techniques can be used: the transient absorption, the differential transmission and the transient reflection. The transient absorption is the technique by which the variation of the absorption of the probe beam is recorded when the sample is pumped and not pumped ($\triangle A = A_{pumped} - A_{notpumped}$), whereas the pump–probe differential transmission and pump–probe transient reflection are recorded using the variation of the intensity of the probe signal transmitted or reflected respectively [9, 30] when the sample is pumped and not pumped. In this study the focus was on transient absorption. It is possible to find information about the excited molecules or atoms at a specific time after excitation. Time resolution and information about the kinetics of these molecules or atoms can be obtained by measuring at various times after excitation or delays between pump and probe pulses. When the sample absorbs a photon from the pump beam and is promoted to the excited state, three phenomena can occur. Thus three expected signals are observed in the pump–probe spectroscopy in liquid phase.

The first of the possible signals that can be observed in the pump–probe experiment is ground–state bleaching (GSB) or photobleaching (PB), which is due to the fact that the pump excites many molecules into the higher excited state, which results in a reduction of the number of molecules in the ground state. Therefore, when the probe beam arrives, there will be fewer molecules in the ground state [12] (as indicated in Figure 2.6 with the red arrow). There will be an absorption decrease at the wavelengths where the molecule absorbs in the ground state. A negative signal of absorbance change ($\triangle A < 0$), as shown in Figure 2.6 a) [9] will be obtained.

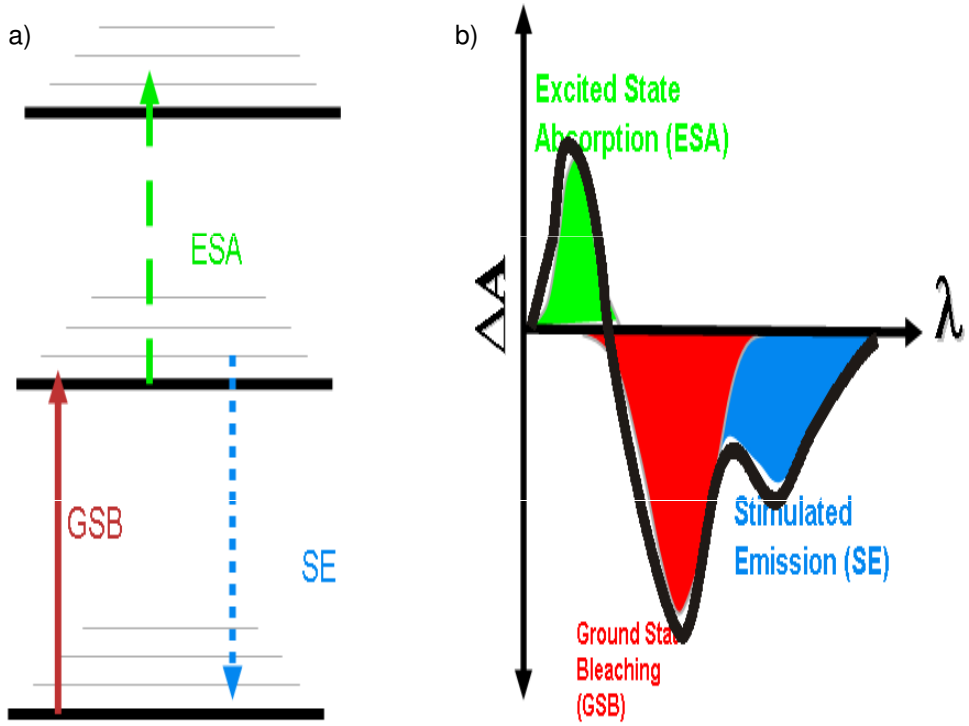

Figure 2.6: a) Energy level scheme of a molecular system showing different physical processes that generate transient absorption signals in a pump–probe experiment. b) Decomposing a transient absorption spectrum from a transient absorption experiment at a particular delay time t_D into ground state bleaching (GSB) (photobleaching), stimulated emission (SE) and excited state absorption (ESA) (photoabsorption)[12].

The second signal is stimulated emission (SE). The pump populates the excited state in such a way that the probe can stimulate those molecules at the excited state to return back to the ground state (see Figure 2.6 a), blue arrow) and a photon identical to the excited photon will be released. The quantity of photon release will increase and the detector will perceive this increase of photons as a decrease in absorption. Therefore, a negative signal will be recorded ($\triangle A$<0) [29]. This phenomenon occurs at the same time as GSB and at wavelengths equal to or longer than the ground–state absorption [9]. When a molecule absorbs light, it can be excited to a higher vibrational state of the electronic excited state. The molecule will dissipate part of its absorbed energy as vibrational energy. It will then end up at the lowest vibrational state of the electronic excited state. For SE, a lower energy photon, compared to the excitation photon, will be emitted. Therefore, the SE spectrum is always red–shifted

relative to the excitation wavelength.

The third signal is excited state absorption (ESA) or photoinduced absorption (PA). This signal is caused by the excited–state population, which can be excited further to a higher energy level by the probe pulse (see Figure 2.6 a), green arrow). There will an increase of the absorption by the probe beam, therefore the absorbance change will be positive ($\triangle A > 0$) [31]. The ESA signal occurs at frequencies of the probe pulse according to the energy level structure of the molecule under investigation [9].

These three processes can occur at the same time and with relatively similar signal strengths. Figure 2.6 b shows the decomposition of a typical pump–probe signal at one delay time and interprets the transitions responsible for these different signals. The black curve indicates the resulting signal.

2.3 Transient absorption of biological systems

2.3.1 Light–harvesting complex II

Photosynthesis is the process by which light energy is converted into chemical energy and then through a complex series of biochemical and biophysical processes to any one of a number of bio–machines [32]. There is a large diversity of photosynthetic organisms, higher plants, cyanobacteria and photosynthetic bacteria [10]. However, some fundamental processes remain consistent. These are light absorption, excitation energy transfer, charge separation and vectoral charge transfer [32]. In photosynthesis, chlorophylls are light absorbing pigments that are bound to proteins and are also known as pigment–proteins. These pigment–proteins have two main functions. They form light–harvesting antenna complexes that are organised into an antenna system to absorb light and they transfer the excitation energy to the second functional entity, called a reaction center. It is at the reaction center that charge separation and transfer occurs [32, 33].

In the natural state, there is a high degree of disorder within the system. This is due to natural light from the sun irradiating the photosynthetic pigments with a range of different wavelengths of light, which the pigments can absorb. This means that the energy of the photons, the intensity of the light and the time between photon excitations occur in a random manner. The environmental conditions in which these systems grow also vary [34]. In order to investigate the processes of light absorption and energy transfer, these variables need to be reduced for which a number of strategies are used. Over recent years, a number of photosynthetic components have been isolated and detailed structural information has been obtained using crystallographic data [35, 36, 37] and atomic

force microscopy (AFM) [38, 39, 40]. A significant amount of the work on elucidating the structures of energy–transfer processes within LHCs and (RCs) has been conducted on purple photosynthetic bacteria [10].

In photosynthetic organisms such as the bacteria *Rhodobacter sphaeroides (R.sphaeroides)* there are two types of light harvesting antenna complexes – types 1 and 2. These are termed LH1 (B875) and LH2 (B800/850). In the more general case of non–bacterial organisms, these light–harvesting complexes are termed LHC I and LHC II. LHC II acts as light absorbing and transferring complexes. LHC I is closely associated with a RC [41, 42]. In all species of purple bacteria, the LH1 surrounds the RC [10]. LHC I and LHC II are constructed on the same modular basis [43, 44]. This organisation of RCs surrounded by aggregates of chlorophylls and associated "carotenoid" seems to be universal to photosynthetic bacteria and higher plants and is called the photosynthetic unit (PSU) [45].

When photons are absorbed by one of the chromophores in the LHC II antenna, non–radiative photo–physical processes occur in a series that channels the excitation energy with high efficiency from the site of absorption. There are two types of ultrafast photo–physical processes that are occurring. One is energy migration (exciton process), which is the reversible series of energy–transfer processes that occurs between identical coupled chromophores, in this case between LHC II antenna of the photosynthetic membrane. The other is energy transfer, which refers to the down–hill energy–transfer process that will then terminate the exciton process [46] within the PSU. Energy transfer takes place in the order LHC II $\rightarrow$ LHC I $\rightarrow$ RC. In the RC, an irreversible electron–transfer reaction occurs at a special pair of chromophores, preventing any possible back–transfer of energy [46]. Both of these occur in the singlet (S1) state of an excited pigment [46]. The energy transfer is a sequential process, is multi–exponential and occurs in a total time of less than 100 ps at approximately 95% efficiency [45]. Within a bacteriochlorophyll ring, it is estimated that energy transfer around the ring takes place in a few hundreds of femtoseconds [18, 47]. The LH2 $\rightarrow$ LH1 transfer time is 3–5 ps [48]. Energy transfer from LH1 $\rightarrow$ RC is 30–50 ps [19]. This longer time is due to the greater LH1 – RC distance.

One line of study is to isolate these functional components and study the energy–transfer characteristics separately. The energy–transfer processes of these photosynthetic systems can be investigated using ultrafast pump–probe transient absorption spectroscopic techniques [31, 49, 50]. The use of ultrafast pulsed lasers enables the pigments to be excited in unison. This pump pulse excites the pigments at a pre–set temporal origin, after which the energy transfer can be probed by a second pulse with an adjustable delay [34].

In the experiments conducted in this study, the sample was isolated LHC II

from spinach leaves. The LHC II is the most abundant antenna in the "Photosystem II" (PS II). The function of the LHC II is to transfer excitation energy towards a reaction centre of PS II. Normally, there are four LHC II trimers per PS II reaction centre [51]. In addition to LHC II, the PS II contains other complexes, such as CP29, CP26, CP47, CP43, D1 and D2. The CP43, CP 47, D1 and D2 form the PS II core complex [52, 53, 54]. In its native form, the LHC II is a trimeric protein.

The structure of this complex was first described in 1994 [55]. Each monomer contains 7–8 chlorophyll a, 4–5 chlorophyll b and 3 carotenoids, namely lutein, neoxanthin and violaxanthin [27, 56]. These chlorophylls have been assigned specific site energies. Those of chlorophyll a are **a**602–**a**604 and **a**610–**a**614, those of chlorophyll b are **b**601 and **b**605–**b**609 [35]. These chlorophylls are arranged in two separate layers: one close to the stromal surface and the other by the luminal surface with a distance ranging from 13.9 to 18Å between them. Close to the stromal surface of the membrane are three clusters of chlorophylls. There is a chlorophyll a trimer (**a**610–**a**611–**a**612) and a Chlorophyll a dimer (**a**602–**a**603). These are closely associated with three Chlb (**b**601, **b**608 and **b**609) molecules. On the luminal side of the membrane there is a chlorophyll a cluster (**a**613 and **a**614), a group of chlorophyll b (**b**606, **b**607 and **b**605) and a single chlorophyll a (**a**604) [57]. When assembled, the LHC II trimer contains between 36 and 42 chlorophyll molecules as well as 10 to 12 xanthophyll (lutein, neoxanthin and violaxanthin) molecules. Figure 2.7 indicates the chemical structure of chlorophyll a and chlorophyll b. In vivo and vitro there is a further level of structural organisation that LHC II can adopt. This is a regular lamellar sheet mainly 2D in shape, or alternatively in 3D structures, or thirdly as a dis–ordered 3D structure [58]. Thus LHC II has a large degree of flexibility in its structural organisation with accompanying changes in optical properties.

The interpretation of pump–probe transient absorption data is highly complex and the results obtained are influenced by many factors, such as the degree of aggregation of the LHC II [52] or whether the complexes are in the monomeric or trimeric state [52, 59]. The absorption spectrum shows one main peak in the red region, around 675 nm, which is mainly due to chlorophyll a [60] and a shoulder at 650 nm, which is related mostly to chlorophyll b. In addition, the absorption spectrum exhibits a broad band from 400 nm to 520 nm with the main peak positioned at 440 nm and shoulders on both sides of this. The peak at 440 nm represents chlorophyll a, while the peak at 470 nm represents chlorophyll b [27].

Several transient absorption studies have been done on the energy transfer among the chlorophylls and these have shown that the transfer takes place mainly from chlorophyll b to chlorophyll a [33, 61]. In addition to the transfer

from chlorophyll b to chlorophyll a, there is also energy equilibration that can take place from chlorophyll a to chlorophyll a and from chlorophyll b to chlorophyll b. The LHC II monomer is composed of 7–8 chlorophyll a, 4–5 chlorophyll b and 3 carotenoids, which give a chlorophyll a:b ratio range of 1.6:1–2:1. The energy transfer from chlorophyll b to chlorophyll a within this monomer exhibits three components: a very fast component that occurs around 100–150 fs and two further components that have lifetimes of 600–800 fs and 5–7 ps [61]. The time constant of the major component of energy transfer from chlorophyll b to chlorophyll a was reported in the literature to be approximately 600 fs [17, 33, 61, 62, 63]. In addition to chlorophyll b to chlorophyll a energy–transfer time, there is also energy equilibration from chlorophyll a to chlorophyll a, which takes place in a time constant of around 300 fs and 6 ps [63].

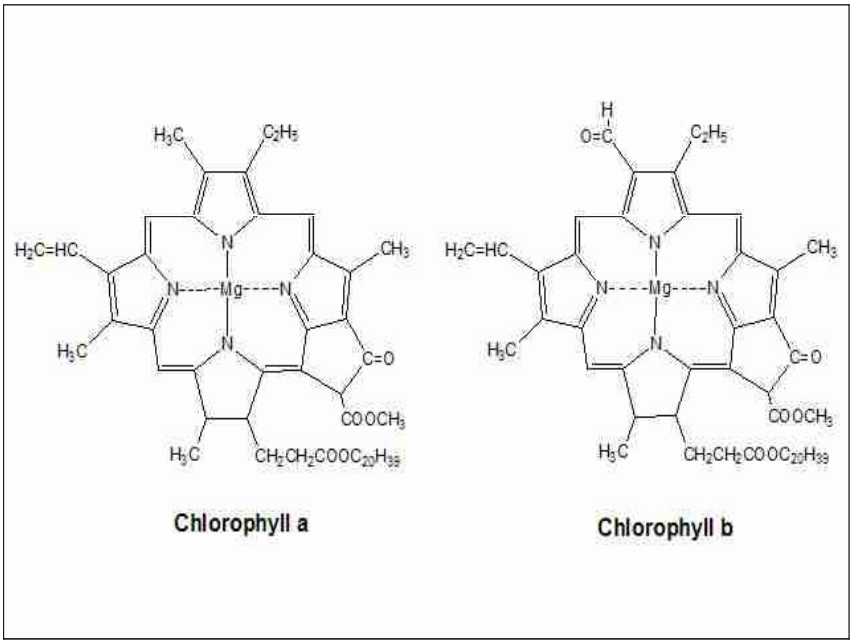

Figure 2.7: Chemical structures of Chlorophyll a and Chlorophyll b [64]

When molecules are in an excited state, a slower process, called annihilation may take place. The excited molecules may collide and transfer the energy that they carried to other molecules in the excited state, which will then be promoted to the higher excited state. This slower process appears to be energy–transfer limited [17]. When transient absorption is performed, two different processes of annihilation can be observed, namely singlet–singlet annihilation which takes place in timescales of 12–20 ps, and singlet–triplet annihilation which takes place in timescales around 40 ps.

2.3.2 Zinc phthalocyanine

Phthalocyanines are multipurpose components that have a variety of applications, which range from chemical sensors and nonlinear optical devices to various optical uses such as inks and dyes [65, 66]. In addition, phthalocyanines are a new class of photosensitiser used for PDT. These drugs are used to treat small and superficial tumours [30, 67] and may also be used for blood sterilisation and as sunlight–activated herbicides and insecticides [6].

In recent years, particular attention has been given to phthalocyanines in the search for photosensitisers that can be clinically used as a PDT cancer drug. In the designing of the photosensitiser there are some factors that one has to consider. The most important is a high absorption coefficient at a wavelength suitable for the application. This means that the absorption region of the designed photosensitiser should overlap with the absorption window of the skin in order to facilitate light penetration into the localised tumour. It is also important to take into account the light sources available, the photophysical properties, such as energy transfer, the singlet state and triplet state lifetime of the photosensitiser and triplet state quantum yield. The excited triplet state of the photosensitiser molecules should be close to the resonance of the oxygen molecules and must have a relatively long lifetime, such that the excited photosensitiser molecule can be quenched by molecular oxygen with high yield.

The processes of light absorption and energy transfer are at the heart of photodynamic therapy. PDT is based on the complete introduction of a tumor–localising photosensitiser and then optically exciting the photosensitiser with an appropriate wavelength of a light source. Following the absorption of light, the photosensitiser is excited from the ground state S_0, which has two electrons with opposite spins in the low–energy molecular orbital, to the singlet excited state S_1 (generally the first excited singlet state). In fact, one of the electrons is promoted into a high–energy orbital, but keeps its spin. At the first excited state, the photosensitiser has a relatively short lifetime (in the order of nanoseconds) and can relax back to the ground state S_0 by emitting a photon (fluorescence) or by a nonradiative process (internal conversion) into heat.

In addition, there is another radiationless deactivation pathway from the excited singlet S_1 to the triplet state, known as intersystem crossing (ISC). Transition from a singlet state to the triplet is quantum mechanically forbidden by the spin–selection rule. But under certain conditions, such as spin–orbital coupling, this transition can occur. The first excited singlet state will have a large probability of transferring its energy to the first excited triplet state T_1. In fact, the first excited singlet state undergoes ISC, whereby the spin of the excited electron inverts to form an excited triplet state that has parallel electron spins

consequently a long lifetime (from microsecond to millisecond). The triplet state may release its energy through the emission of light (phosphorescence) and the photosensitiser end up at its ground state. The fluorescence, internal conversion and phosphorescence can occur simultaneously and compete among each another.

In PDT, the triplet state of the photosensitiser plays a central role in cancer cell destruction. By quenching of the triplet state of the photosensitiser T_1, there will be an energy transfer that generates an electronically excited state of the oxygen S_1 [20]. Figure 2.8 presents the process of generating the singlet oxygen. The excited singlet oxygen is regarded as a highly cytotoxic agent in PDT. The presence of the singlet oxygen will lead to the destruction of the cancer cell or tumour.

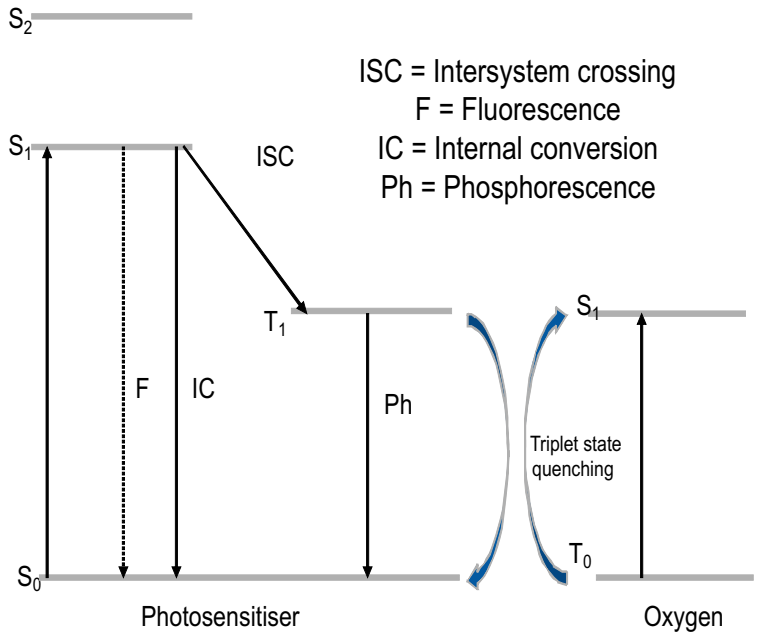

Figure 2.8: Energy–level diagram of the photodynamic therapy photosensitiser showing processes leading to the production of the singlet oxygen[20]

The triplet state of the photosensitiser can undergo two types of reaction that lead to the destruction of the cancer cell. Figure 2.9 illustrates the type of reactions that are involved in cancer cell damage. The triplet state of the photosensitiser gains an electron by reacting directly with a solvent or a substrate molecule to form a free radical anion. This radical anion can further react with environmental oxygen to produce a reactive oxygen species, namely superoxide

anion. This reaction again involves an electron transfer. The superoxide anion does not involve itself in oxydative damage of the tumour but reacts with hydrogen species to generate highly reactive hydroxyl radicals and hydrogen peroxide. This reaction procedure that involves electron/hydrogen transfer is called a type I reaction [20]. The second reaction is called a type II reaction. This reaction is based on energy transfer [68]. The photosensitiser triplet state transfers its energy directly to the oxygen to produce the singlet oxygen [20, 67, 69, 70]. The singlet oxygen is oxidising representative that reacts directly with cancer cells. Both type I and type II reactions can take place at the same time, but it has been shown that the oxygen singlet state is the most reactive product generated and that the type II reaction, the energy transfer, is the main pathway of oxygen singlet generation and the more efficient in PDT [67].

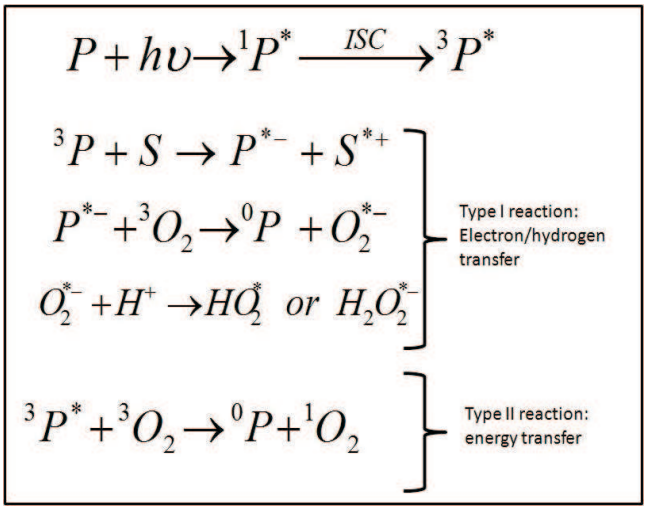

Figure 2.9: Graph of the mechanisms involved in photodynamic therapy, indicating the two types of reactions that lead to the generation of the oxygen singlet with P: photosensitiser, S: substrate, O:oxygen and H: hydrogen[20].

ZnPc is a promising PDT photosensitiser that exhibits a photodynamic activity. A strong absorption band in the near–infrared in close proximity to the optical window of human tissue [6, 30] and a triplet state near resonance with the transition of the oxygen from ground to excited singlet state make ZnPc a suitable candidate for PDT. ZnPc has been reported to have suitable photophysical properties. It has a relatively long lifetime excited singlet state (3–8 ns) and a long lifetime of triplet state with a high-quantum yield. These long lifetimes constitute an important advantage for ZnPc. Long lifetimes enhance the number of interactions between the ZnPc excited triplet state and the ground state of the environmental oxygen, thereby increasing the oxygen quantum yield.

Figure 2.10 shows the chemical structure of zinc phthalocyanine.

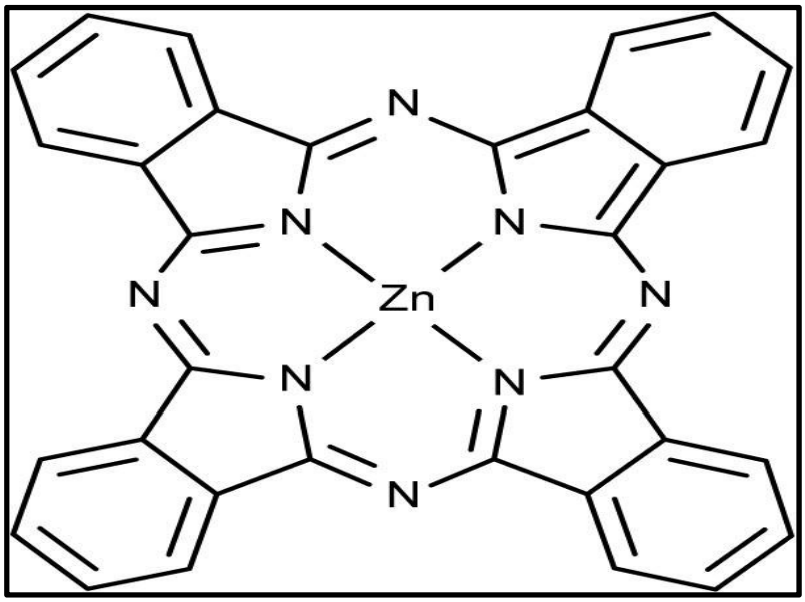

Figure 2.10: Chemical structure of Zinc Phthalocyanine [6]

However, the lifetimes of the singlet and triplet excited states vary with the solvent used. The singlet excited state of ZnPc dissolved in dimethy sulfoxide (DMSO) has a lifetime of around 3 to 8 ns [30] and the excited triplet state has a long lifetime of 350 μs [6, 71], whereas in tetrahydrofuran (THF), the triplet state lifetime is 230 μs. These lifetimes hold if there is no oxygen species in the medium. The presence of oxygen shortens the triplet state lifetime. The other important factor of ZnPc is its solubility. It has been reported in the literature that ZnPc is not soluble in water. To overcome this difficulty, ZnPc is for instance synthesised with hydrophilic groups such as SO_3 [71, 72], which allow ZnPc to dissolve in water.

Spectroscopic studies of ZnPc in DMSO have shown two absorption bands, as indicated in Figure 2.11. The first absorption band is the B–band in the ultraviolet region with a major peak at 345 nm, which corresponds to the $S_0 \rightarrow S_2$ transition [6]. The second absorption band is the Q–band in the red part of the spectrum with a strong absorption peak at 672 nm, which relates to the $S_0 \rightarrow S_1$ transition. In addition, the Q–band has a shoulder at around 645 nm assigned to vibronic transition and a small peak at 606 nm [6]. However, the incorporation of the hydrophilic group to ZnPc and the use of different solvents produce shifts of these absorption peaks [8, 68, 73, 74, 75, 76]. For instance, the absorption spectra of tetrasulfonated zinc phthalocyanine ($ZnPcS_4$) in DMSO

has absorption B–band peaks at 350 nm in the UV and 613 nm and 679 nm with a shoulder at 652 nm in Q–band [73], whereas in THF, ZnPc has for instance a major Q–band peak at around 666 nm [8, 68].

In addition to the spectral characteristics described above, it has been reported that the ground-state electronic absorption spectra of ZnPc indicate that ZnPc in DMSO is a monomeric form [6, 66]. This was observed by comparing the absorption spectra profiles of ZnPc in DMSO and water [66]. The absorption B- and Q-bands of ZnPc in DMSO are red-shifted and narrowed compared with the absorption bands of ZnPc in water. In addition, there is a relative increase of the Q–band intensity in the monomeric form. This shows that ZnPc in DMSO is mostly in a monomeric form.

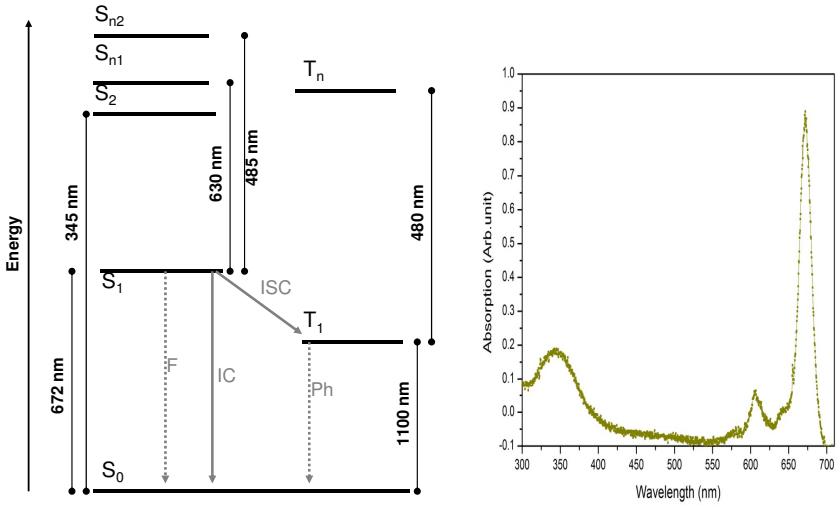

Figure 2.11: Energy-level diagram with the absorption wavelength of the electronical states and absorption spectrum of zinc phthalocyanine[6].

Several femtosecond studies have indicated that phthalocyanines in solution exhibit ultrafast excited-state dynamics [6, 77]. Understanding these dynamics is of the essence of PDT. Femtosecond transient absorption pump–probe spectroscopy has shown the existence of ultrafast energy transfers in phthalocyanines [6, 77]. These ultrafast energy transfers play an important role in the photophysics of ZnPc. Before looking at the energy transfer, the lifetime of the first excited state is an important factor that one needs to consider. The first excited state (S_1) lifetime or fluorescence lifetime measurement obtained in diverse environments has comparable values for different studies. The mea-

sured value of fluorescent lifetime is approximately 2.8 ns [6, 8]. However, work done on $ZnPcS_4$ in DMSO shows that the first excited-state decays with a time constant of 160 ps [66]. In addition, degenerate four-wave mixing measurements done on ZnPc in DMSO indicates a decay time constant of 35 ps [7]. Note that ISC ($S_1 \rightarrow T_1$) contributes to the decay time of S_1 as well as the recovery time of the ground state (S_0). Extensive work done on ZnPc in toluene has indicated that the decay time constant of fluorescence (k_F) is around 9.1 ns with a quantum yield of 0.34±0.03 [78]. In addition, the decay time constants of the non–radiative pathways are 38.5 ns with a quantum yield of 0.08±0.11 for the internal conversion ($S_1 \rightarrow S_0$) and 5.6 ns with quantum yield of 0.58±0.08 for the intersystem crossing ($S_1 \rightarrow T_1$) [78]. More recently it was shown that the energy transfer from the singlet state ZnPc occurs at timescale of less than 100 fs. This was observed when the ZnPc was linked to the carotenoid molecule while an investigation was carried out on artificial LHCs [79].

Ultrafast studies of ZnPc seem to indicate that there are different lifetime values associated to the depopulation of the S_1 state of ZnPc in solution. The values for the lifetime of the S_1 state (35 ps by Rao and Rao [7], 160 ps by Howe and Zhang [66], 2.8 ns by Savolainen et al [6] and 9.1 ns by Bishop et al [78]) differ significantly. The time constants of 35 ps found by Rao and Rao and 160 ps reported by Howe and Zhang attributed to depopulation of S_1 do not agree with the 3 ns value of fluorescence lifetime of S_1 [6, 8]. In addition the work presented by Savolainen et al lacks data in the picosecond time scale. In the work of Savolainen et al, only investigation of the time scales 200-500 fs and 2.9-3.4 ns were reported, possibly due to experimental limitations. Their work has therefore left a gap in the picosecond time scale.

An extensive investigation has ended up with a suggested energy-level diagram of ZnPc [6]. Figure 2.11 elucidates the energy-level diagram with the absorption wavelength of the electronic states.

In PDT the triplet state (T_1) lifetime is an essential state. A long triplet state lifetime is an advantage, as the number of interactions between the excited triplet state and the ground state of the molecular oxygen increases with the lifetime of the excited triplet state, and therefore increases the singlet state oxygen quantum yield. Several studies have shown that the triplet state lifetime depends on the solvent. For instance, the triplet state lifetime is 330 μs for ZnPc in dimethyl formamide (DMF), whereas it is 220 μs for ZnPc in air–saturated ethanol.

Chapter 3

Experimental setup and characterisation

3.1 Experimental setup for transient absorption measurement

3.1.1 Overview of setup

Investigation of energy transfer in LHC and in ZnPc was carried out by using two experimental setups. The second experimental setup was however mainly used for the study of the energy transfer in ZnPc.

The first femtosecond pump–probe experimental setup used is described below and illustrated schematically in Figure 3.1. A commercial Ti:Sapphire femtosecond oscillator (Coherent Mira 900–F), operating at a repetition rate of 76 MHz and pumped by the 5 W output of a CW diode–pumped Nd:YVO4 laser (Coherent Verdi V5), produced pulses of approximately 130 fs in duration, as measured by a home–built autocorrelator. These pulses were stretched and then amplified by a regenerative Ti:Sapphire amplifier (Coherent Legend–F), pumped by a diode–pumped Q–switched Nd:YLF laser (Coherent Evolution) at a 1 kHz repetition rate, and finally compressed to produce 130 fs pulses of up to 1 mJ per pulse. This pulse duration was also measured by a home–built autocorrelator. These pulses have a spectral bandwidth of approximately 8 nm FWHM and a central wavelength of 795 nm.

As shown in Figure 3.1, the amplified beam is split by a beam splitter (BS0) into two (90% transmitted and 10% reflected). These are the pump and probe beams, respectively. The probe beam is sent first through a half wavelength plate (WP) and a polariser (P) of horizontal polarisation. The rotation of

wavelength plate combined with the polariser allows one to adjust the pulse energy of the probe in order to have conditions for better generation of the white light continuum. In addition the probe beam is sent to a variable optical delay line, which comprises a retro–reflector mirror on a precision translation stage controlled by a computer. The optical delay is necessary in order to get a real–time rapid–scan acquisition by changing the pump and probe beam temporal overlap in the sample. A small part of energy of the probe beam is reflected by a beam splitter (BS1) to photodiodes PD1 and PD2 placed after another beam splitter (BS2). The beam splitter BS2 then reflects 50 % and transmits 50 % of this energy to PD1 and PD2 respectively. The probe beam is then focused on a sapphire plate (SP) of 2.15 mm thickness to generate a white–light continuum. A short-pass filter (F) is placed after this in the probe path in order to suppress the strong residual peak at 795 nm from the Ti:Sapphire laser. The probe beam is split into two beams, namely a reference and a signal beam. The signal is focused on the sample in such a way that it overlaps spatially with the pump beam in the liquid sample, while the reference beam is also sent through the sample as indicated in Figure 2.4. In addition, the pump beam diameter (approximately 300 µm) was kept larger than the probe at the spatial overlap in the sample. The PD1 was also used to monitor the shifting of the probe beam by investigating the power variation on the photodiode. Consequently, the PD1 allows checking of the spatial overlap between the pump and probe while taking the measurement. In addition the PD2 was used for the synchronisation of the electronics components of the pump-probe system.

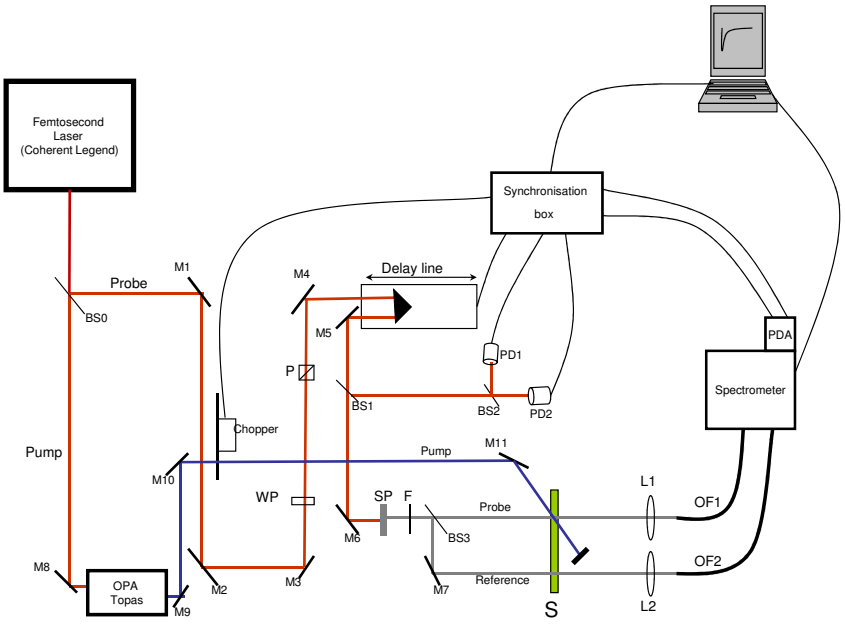

Figure 3.1: Pump–probe experimental setup used to measure transient absorption in liquid samples. BS0, BS1, BS2 and BS4: Beam splitters. M1, M2, M3, M4, M5, M6, M7, M8, M9, M10 and M11: Coated mirrors. WP: Wave plate. P: Polariser. SP: Sapphire plate. F: Cut–off filter. S: Sample. PD1 and PD2: Photodiodes. L1 and L2: Focusing lenses. OF1 and OF2: Optic fibres. PDA: Photodiode arrays. OPA: Optical parametric amplifier.

The pump pulse is sent through an optical parametric amplifier (OPA) (TOPAS C – OPA from Coherent) in order to obtain a wide tuning range of the pump beam (530–700 nm). After the OPA, a chopper is inserted in the pump beam path in order to record spectra that are classified as pumped and not–pumped, thereby reducing background effects. The probe reference and signal beams are focused on optical fibres that guide the beams into the entrance slit of an imaging spectrometer. Figure 3.2 shows the image of the pump and probe beam paths (in red the probe beam, in blue the pump beam and in white the probe after white–light generation).

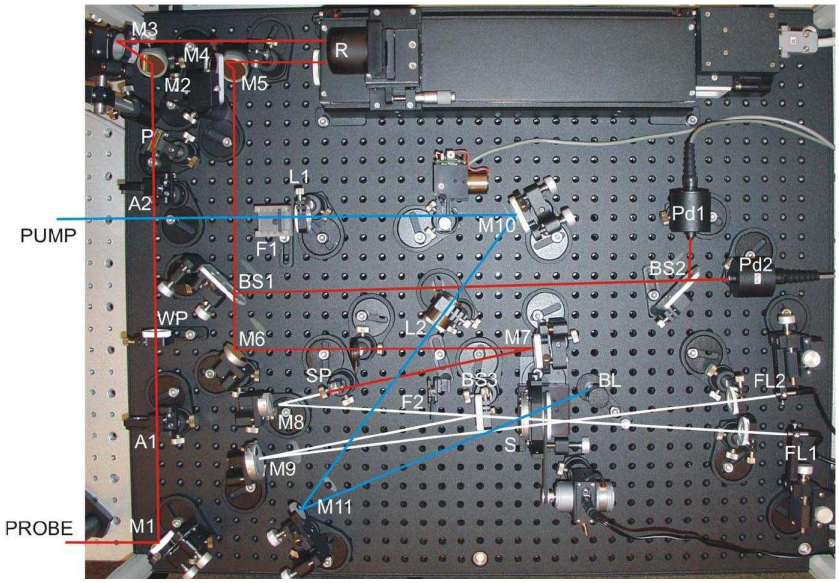

Figure 3.2: Image of pump–probe experimental setup.

The second setup was that of a regenerative Ti:Sapphire amplifier system (CPA–2101; Clark MXR) that typically produces 1 mJ pulses at 775 nm with a pulse duration of 150 fs and a repetition rate of 1 kHz. The CPA beam is then split into two beams (80 % probe and 20 % pump). The probe beam follows the same pathway as described above. However, a neutral density filter was used in order to attenuate the energy incident on the sapphire crystal that was used for white–light generation. The 20 % pump beam is sent through a two–stage phase–matched noncolinear optical parametric amplifier (NOPA). The NOPA principle has been described in the literature [23]. The chirped output beam from the NOPA is compressed using two Brewster prisms. Pulses ranging from 450 nm to 760 nm with a duration of approximately 50 fs and energy of several microjoules can then be obtained. Figure 3.3 shows the layout of the second pump–probe setup using the CPA Clark MXR laser.

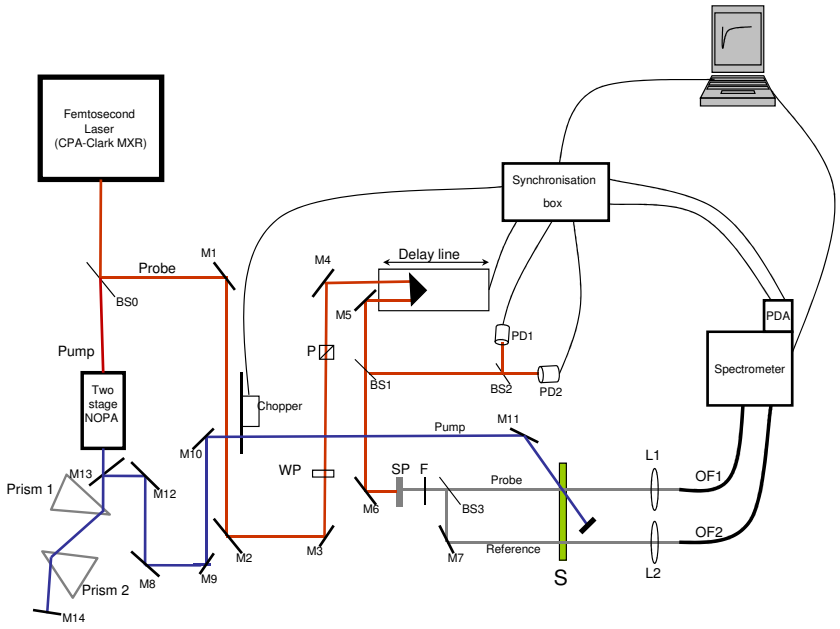

Figure 3.3: Pump–probe experimental setup used to measure transient absorption in liquid samples. BS0, BS1, BS2 and BS4: Beam splitters. M1, M2, M3, M4, M5, M6, M7, M8, M9, M10, M11, M12, M13 and M14: Coated mirrors. WP: Wave plate. P: Polariser. SP: Sapphire plate. F: Cut–off filter. S: Sample. PD1 and PD2: Photodiodes. L1 and L2: Focusing lenses. OF1 and OF2: Optic fibres. PDA: Photodiode arrays. NOPA: Noncolinear optical parametric amplifier.

The spectrometer (MS 2004 I from "solar TII") uses a Czerny–Turner optical configuration. The light, after passing through the entrance slit, is directed by a collimating spherical mirror of 165 mm focal length onto a diffraction grating. The spectrometer has two gratings. The 600 lines/mm diffraction gratings blazed at 500 nm for 335–1000 nm operation (multi–channel detection) and 300 lines/mm blazed at 1000 nm for 700–1900 nm operation (single–channel detection). Those gratings are installed on a quadruple turret in such a way that by turning the turret one can change the grating. The grating used in this study is a 600 lines/mm diffraction grating, blazed at 500 nm for 330–1000 nm operation. The grating disperses the parallel incident beams (signal and reference beams), and these are again collimated using a second collimating mirror of 200 mm onto two vertically separated Si linear photodiode arrays. This spectrometer disperses both beams to a maximum of 206 nm across the active area of the Si–photodiode arrays. Each PDA has 1024 pixels and a spectral response range from 200 nm to 1000 nm. In addition, these PDAs have a high UV sensitivity (approximately $2 * 10^4$ photon/ pixel $*$ count) with

good stability, a low dark current and a high saturation charge, which allow longer integration time for the signal. This system has a data collection rate of 833 spectra/second, which corresponds to the integration time of 1.2 ms. This longer integration time increases the signal to noise ratio.

In addition, steady-state absorption was measured using an Ocean Optics spectrometer combined with a lamp. An Ocean Optics USB–ISS–UV–VIS lamp was used as source of illumination of the sample. The USB–ISS–UV–VIS spectrometer has a sample holder whereby the sample, in a cuvette of 10 mm path length, can be inserted.

For a better data acquisition it was important to ensure that the pump and probe beams overlap spatially and temporally, and that the spatial overlap remains the same for the duration of the experiment. The spatial overlap was done manually by adjustment of the mirror M11 (see Figure 3.2) until the optimum value of absorbance change is obtained. The change of the spatial overlap was monitored by observing the power variation of the laser on the PD1. One can see from Figure 3.2 that the optical path of the probe beam inside the optical setup is much larger than the path of the excitation beam. This means that, at a relative zero delay, the pump was entering the sample before the probe. An additional optical path for the excitation beam was added outside the optical setup. This was done in order to ensure that the lengths of pump and the probe beams path are the same at a relative zero time delay. This allowed the temporal overlap of the pump and probe beams.

The quality of the spectra obtained by the spectrometer depends on coupling of the input beams (probe and reference beams) into the fibers (OF1 and OF2). Therefore to ensure best light input into the spectrometer, the fibers were positioned at the focal lengths of focusing lenses (L1 and L2) and perpendicular to the input beams. In order to have as strong as possible raw signals throughout the total spectral region, the fibers were adjusted transversally and longitudinally. In addition amplitudes of raw spectra for probe and reference beams were required to be as close as possible to each other for the duration of the experiment.

In this work, the experiments with malachite green were done not only for the characterisation of the pump-probe system but this was essential in the setup and commissioning of the system. In addition to improve the stability of the white light continuum, the position of the sapphire plate was optimized.

3.1.2 Measurement of laser pulse duration

The laser pulse duration measurement is important, as this can indicate potential problems with the laser and can ensure that pump–probe spectroscopy

experiments are done with the optimal laser pulse duration. Non–optimal pulse duration results in poorer temporal resolution of the pump–probe experiment, as well as lower energy in the OPA output, resulting in lower pump power and larger variation due to the power being closer to the threshold for the OPA conversion process. Similarly, the white–light continuum, used as probe beam, is also dependent on the intensity and hence the pulse duration. The temporal pulse duration measurements are done with a home–built background–free intensity autocorrelator. The autocorrelator has a beam splitter, two optical arms and a doubling crystal for second harmonic generation. This is an indirect technique whereby the pulse is used to measure itself. The layout of the autocorrelator is shown in Figure 3.4.

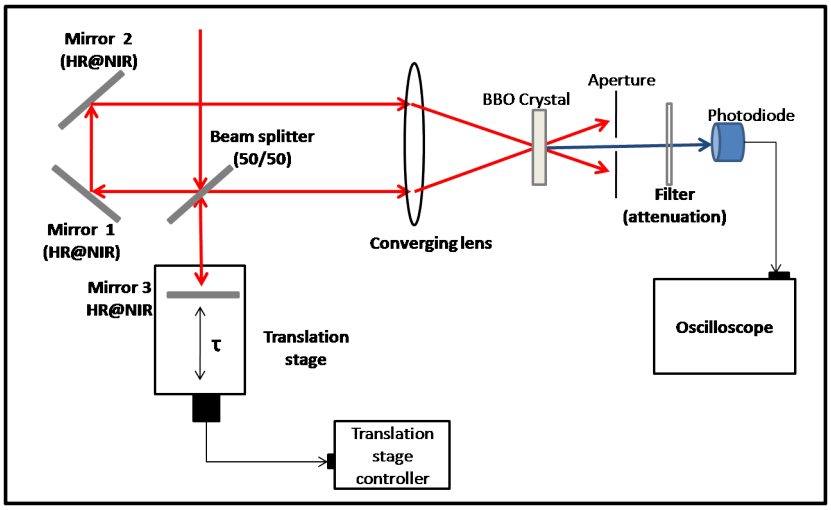

Figure 3.4: Experimental setup of background–free intensity autocorrelator

In the autocorrelator, an incoming laser beam is split into two optical arms by a beam splitter (50/50) that go through different paths. One beam passes through a fixed path length that consists of two high-reflecting mirrors at near-infrared wavelength. The other beam goes through a path, that includes variable delay line, that consists of a flat mirror mounted on a motorised translation stage. Both beams are then focused into a nonlinear crystal (BBO) by a converging lens. These two replicas are spatially and temporally overlapped in the nonlinear crystal in order to produce the second harmonic generation (SHG). By moving the delay line, one is able to scan the temporal overlap of the two pulses. The second harmonic signal created is detected using a photodiode connected to the oscilloscope. Figure 3.5 shows the SHG signal called the autocorrelator trace. The pulse duration of the laser beam is then derived from the autocorrelator trace.

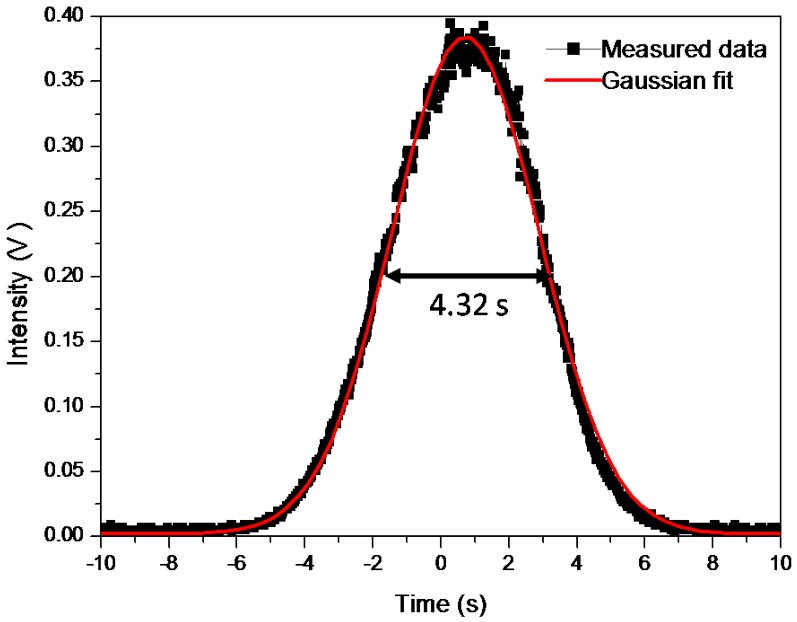

Figure 3.5: Autocorrelation trace data of background-free intensity autocorrelator with Gaussian fit used to determine the pulse duration. The time axis represents the scanning time and the scanning speed was 0.006 mm/s.

In order to obtain the pulse duration of the pulse $\triangle t$, the autocorrelation time $\triangle t_A$ is calculated. The autocorrelation trace full width half maximum (FWHM) (AC_{fwhm}) is extracted from recorded data and the scanning speed of the delay line is recorded. The autocorrelation time is given by:

$$\triangle t_A = \frac{2 * AC_{fwhm} * scanspeed}{c} \tag{3.1}$$

where the factor 2 is accounted to the pulse traveling up and down the arm of the moving delay line and c is the speed of light. For a Gaussian pulse shape, the pulse duration $\triangle t$ is given by [80]:

$$\triangle t = \frac{1}{\sqrt{2}} \triangle t_A \tag{3.2}$$

For the sake of obtaining the optimum laser pulse duration, a series of autocorrelation traces was recorded for different parameters (variation of pulse compressor) of the laser. Figure 3.5 shows autocorrelation trace data with a Gaussian fit applied. The autocorrelation trace FWHM was 4.32 s and the scanning speed was 0.006 mm/s. In this particular case, the pulse duration

found was 122 fs. This value varied from day to day by about ±20 fs. In the work done here the pulse duration was assumed to be around 130 fs. In the Clark MXR experiments, the corresponding pulse duration was approximately 170 fs.

3.1.3 Optimisation of the spectrometer

A good spectral resolution of the spectrometer is essential in order to distinguish distinctly the corresponding wavelengths of processes involved in the experiment. The spectral resolution of the spectrometer is influenced by the entrance slit width of the spectrometer, the focusing of image onto PDAs as well as the number of pixels in the PDAs. In the specification sheet of the spectrometer, the spectral resolution of the spectrometer combined with the PDAs was 0.24 nm. This spectral resolution was obtained with an entrance slit of 10 µm, the focusing lens at 200 mm and the number of pixels at 1024. In order to have a real wavelength resolution, a Helium Neon laser line was recorded with a 10 µm spectrometer entrance slit. Applying a Gaussian fit on the data obtained, it was found that an open slit of 10 µm produces a wavelength resolution of 0.67 nm.

The accuracy of the wavelength of the spectrometer is a parameter of high importance. In order to have wavelength accuracy on experimental data recorded on the pump–probe spectrometer, a calibration curve was plotted. A spectrum of an Hg–Ar lamp at room temperature was recorded using the pump–probe spectrometer. Figure 3.6 shows the plot of Hg–Ar known lines against Hg–Ar measured lines and the linear fit of data obtained. The linear fit of the data gives the calibration equation of:

$$Y = 1 * x + 10(\pm 3) \tag{3.3}$$

By comparing the recorded line peaks of Hg-Ar lamp and the real line peaks a wavelength shift of approximately 10 nm was observed. This shift can be seen in the calibration equation. With the pump–probe software it is possible to correct this wavelength shift.

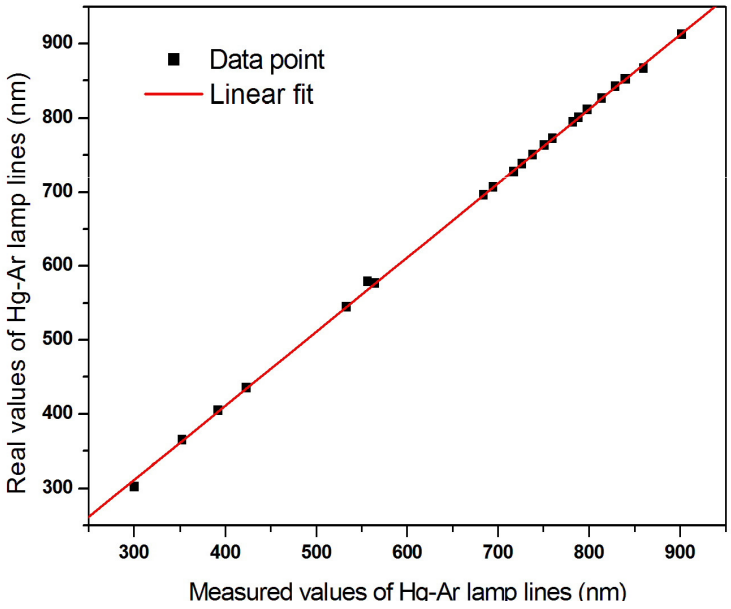

Figure 3.6: Graph of known Hg–Ar lamp lines versus measured lines using a pump–probe spectrometer with the linear fit of data obtained

3.1.4 White–light continuum

Initially a regenerative Ti:Sapphire amplifier laser (Coherent Mira 900) at 1 kHz with the centre wavelength at 795 nm and a pulse duration of 130 fs was employed for pump–probe experiments. Further experiments were performed using a Clark MXR CPA laser with the centre wavelength at 772 nm and a 1 kHz repetition rate delivering 150 fs pulses. Both lasers were used for the generation of the white–light continuum, using a sapphire plate in order to use this as a probe pulse in the pump–probe experiment. Figure 3.7 a) shows spectra of the white–light continuum generated with the Coherent Mira 900–F, recorded using an Ocean Optics USB 2000 spectrometer. Two spectra are shown, with and without a short–pass filter in order to illustrate the strong residual signal from the 795 nm laser output and hence the need for the short–pass filter. This white light was then split in two: the probe and reference beams, using a 50:50 beam splitter . For all the pump–probe experiments done here, the short-pass filter was used. As a result, the white–light continuum range used was restricted to within 400 nm to 700 nm with the strongest intensity near 500 nm. In addition, spectrometer saturation at the fundamental of the laser (795 nm) could be observed, as indicated in the Figure 3.7 a).

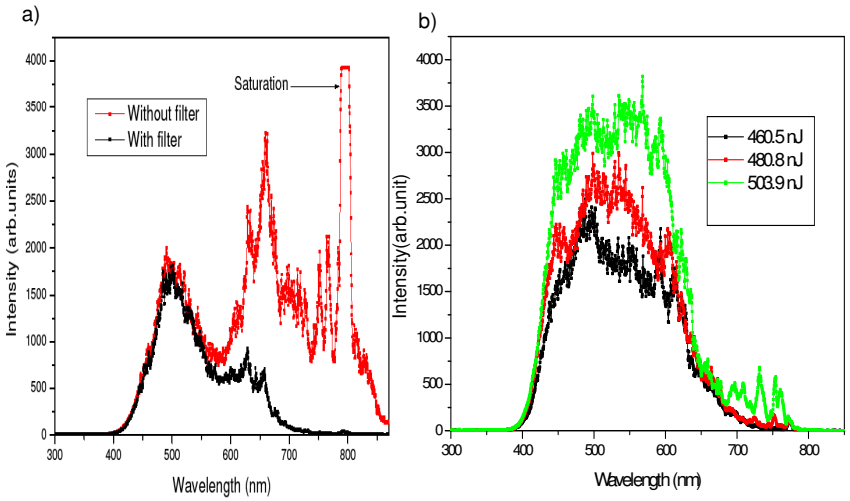

Figure 3.7: Spectra of the white–light continuum used in pump–probe system: a) white–light generated using Coherent Mira900–F laser recorded with and without short–pass filter. b) white–light generated by the Clark MXR CPA laser recorded at different energies.

The white–light continuum was also recorded for the Clark MXR CPA laser. Figure 3.7 b) shows spectra of the white–light continuum recorded with different energies using a short-pass filter. It was found that the white–light continuum ranged from 400 nm to 750 nm. In addition, it has a plateau region from 450 nm to 625 nm, which has a strong intensity. In pump–probe, the stability of the white–light continuum plays an important role in the analysis and interpretation of data. It is therefore crucial to study its variation.

For regenerative Ti:Sapphire amplifier laser (Clark MXR CPA) at 1 kHz, the white light stability was investigated by recording the white light continuum at different delay times for the entire delay line (2 ns) using the pump-probe spectrometer. Figure 3.8shows 24 white light spectra obtained at various delay times across the 2 ns range, separated by constant delays of 78 ps. The laser power before the sapphire crystal was 8 mW. It was found that the white light continuum has a maximum variation of 10%.

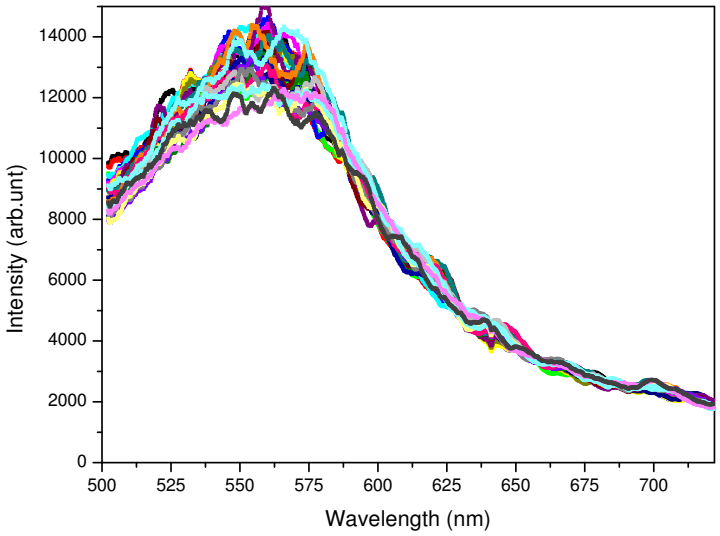

Figure 3.8: White light continuum at different delay time for the entire delay line (2 ns). A constants delay step of 78 ps was used and the power before the sapphire plate was set at 8 mW.

Furthermore the stability of the white–light continuum using the Clark MXR CPA laser was investigated by recording the power used to generate the continuum and calculating the associated standard deviation of the total white light energy. Figure 3.9 shows the result obtained. For every power before the sapphire plate, 50 measurements of white–light energy were recorded. The mean and the associated standard deviations were then calculated. The best white–light continuum generation conditions are obtained for the laser power before the sapphire crystal ranging from 25 mW to 42 mW as shown. Below 25 mW the white light continuum is not observed clearly and the maximum at 42 mW is defined by the limits of the setup. This power range is obtained by using a rotating wave plate combined with a polariser (see Figure 3.2). In this power range, the white–light continuum energy has a maximum standard deviation of 7%, as shown in Figure 3.9. These variations were acceptable for our pump–probe experiments.

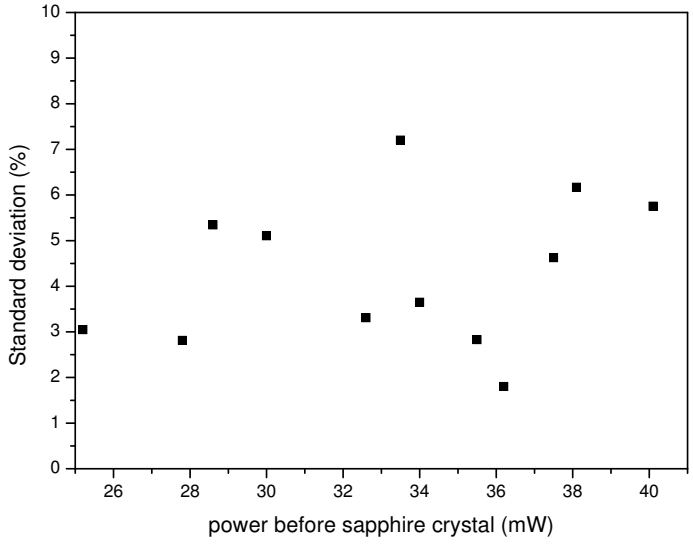

Figure 3.9: Graph of white–light continuum stability indicating the power used before the sapphire crystal to generate the continuum and the associated standard deviation of the white–light continuum energy. For every power before the sapphire plate, 50 measurements of white–light energy were recorded. The mean and the standard deviation were then calculated.

3.1.5 Pump–probe system at Stellenbosch University

Preliminary work was done on ZnPc in a DMF solvent at the Laser Research Institute (LRI) of Stellenbosch University. The femtosecond pump–probe setup used for the experiment is described elsewhere [81]. The pump–probe system is similar to our system described in Section 3.1.1. However, there are some differences compared to our setup. The white–light continuum used as a probe was a single filament white–light and no reference beam was used in the detection system. The white–light continuum spectrum extends from 350 nm to 1050 nm with the fundamental of the laser at 775 cut-off. The use of the NOPA with a prism compressor that provides a pump pulse duration of around 20 fs gives this pump–probe system with a temporal resolution below 100 fs. In addition, the pump pulse was focused into the sample with an energy of 350 nJ.

3.2 Method for transient absorption spectroscopy

3.2.1 Sample preparation

3.2.1.1 Light harvesting complex

LHC II samples were prepared from spinach leaves (with good turgor and dark green colour), as described in the literature [82, 83], with a few modifications to suit the experimental conditions. The leaves were grown at a local greenhouse and the entire experiment was performed under normal laboratory light and on ice. The spinach leaves were washed with cold water and chilled in distilled water, and then homogenised in a blender with ice cold buffer A (50 mM Hepes, 0.4 M sorbitol, pH 7.8 with NaOH). The suspension was filtered through four layers of muslin and then centrifuged at 5000 g for 5 minutes at 4°C. The pellet was resuspended in cold buffer B (20 mM Hepes, 5 mM EDTA, 50 mM sorbitol, pH 7.8 with NaOH). A medium sized brush was used for crude homogenisation of the pellet to ensure that all material was finely homogenised without visible big particles. The suspension was again centrifuged at 10000 g for 10 minutes at 4°C. The pellet was resuspended in cold buffer C (20 mM Hepes, pH 7.8 with NaOH) and again homogenised as above. Triton x–100 was added to the suspension to obtain the final detergent concentration of 0.7–0.9%, and the suspension was then stirred continuously on ice and in the dark for at least 45 minutes, followed by centrifugation at 30000 g for 40 minutes at 4°C. The supernatant predominantly contained LHC II and hence was kept at this stage and the pellet was discarded.

All the centrifugation procedures were carried out using a Beckman Coulter, Avanti J–30I centrifuge. The preparations can be stored in the dark at –87°C for up to a month without the loss of their lamellar structure. Thawing and re–freezing can lead to the destruction of these properties, therefore a sample can be used only once. The prepared sample was diluted in buffer C to obtain an absorbance of ~1 in a 1 cm optical pathlength cuvette at 430 nm for all the characterisation methods as well as the pump–probe experiments. The chlorophyll content of the sample was calculated using a method based on Arnon's equations. A 50 μL sample was added to 10 cm^3 of 80% pure acetone. The mixture was filtered and the absorbance at 665 nm and 649 nm was recorded. To obtain the chlorophyll a and b ratio in the sample, Arnon's equations were used. These are given by:

$$Chlorophyll\, a = [(A665 * 11.63) - (A649 * 2.39)] * 0.2 mg/cm^3 \qquad (3.4)$$

$$Total\,chlorophyll = [(A665 * 6.4) + (A649 * 17.72)] * 0.2 mg/cm^3 \tag{3.5}$$

and

$$chlorophyll\,b = Total\,chlorophyll - chlorophyll\,a \tag{3.6}$$

where A665 and A649 are the absorbance of the sample at 665 nm and 649 nm.

By using these equations, it was found that the chlorophyll a, chlorophyll b and total chlorophyll content were 1.68 mg/cm^3, 0.69 mg/cm^3 and 2.38 mg/cm^3, respectively. As a result, the ratio of chlorophyll a to chlorophyll b gives the value of 2.4:1 [64, 82].

An SDS–PAGE (Sodium Dodecyl Sulfate PAGE) gel technique was performed to identify proteins in the sample mixture. Figure 3.10 illustrates the results obtained from performing the SDS–PAGE using the extracted LHC II sample at room temperature. Lane 1 contained the molecular weight standards SM1811 PageRuler protein ladder which was used as protein molecular markers, while lanes 2 to 7 contained LHC II samples buffered with a 5x sample buffer in different concentrations to obtain optimal resolution. Lanes 2 to 4 contained a sample that was more concentrated and gave a better resolution, while lanes 5 to 7 contained a sample that was strongly diluted (with little protein) and hence very difficult to see using Commassie blue staining solution.

Results obtained from this technique showed that the prepared sample contained mostly the LHC II family - this can be seen from the broken down complexes of PS II, as shown in Figure 3.10. At a molecular weight of 56 kDa a band is observed in the reference (lane 1), as well as lanes 3,4,5 and 7. This corresponds to pure LHC II [84]. CP47 (45 k–50 kDa) and CP43 (35 kDa), which are complexes from the peripheral core complex of PS II together with D1 and D2 proteins closely associated to the RC, were present. All these pigment protein complexes could be detected using Commassie blue staining solution. The gel also indicated the presence of small subunits (20–25 kDa) from LHC I and CPI. This implies that the sample was not purely LHC II; it contained some components from LHC I as well as some from the PS II reaction centre.

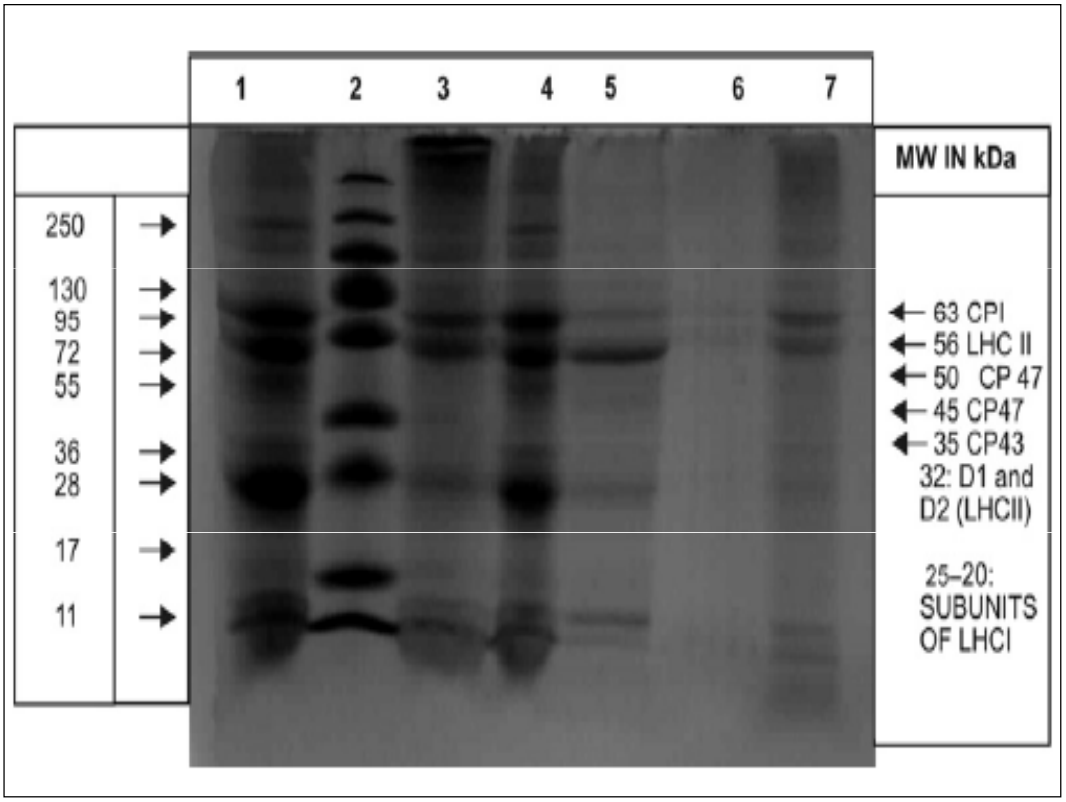

Figure 3.10: SDS–PAGE of extracted LHC II scanned using a Vacutec G:Box from syngene

3.2.1.2 Zinc phthalocyanine

ZnPc of 95% purity and DMSO were purchased from Sigma–Aldrich and used as supplied without any further purification. The ZnPc sample solution was prepared by weighing ZnPc powder using a scale. 0.3±0.02 mg of ZnPc powder was introduced into a foiled centrifuge tube and 10 ml of DMSO solvent was added. The solution obtained was stirred and mixed by using an electric motor shaking machine (Vortex mixer) in order to obtain a basic homogeneous and uniform solution. The solution obtained had a high concentration of about 5.19 x 10^{-5} mol.dm^{-3}. Different concentrations of ZnPc were obtained by dilution of this original solution. Figure 3.11 shows the absorption spectra of ZnPc acquired at different concentrations using an Ocean Optics spectrophotometer. All preparations of the sample were done in relatively dark conditions.

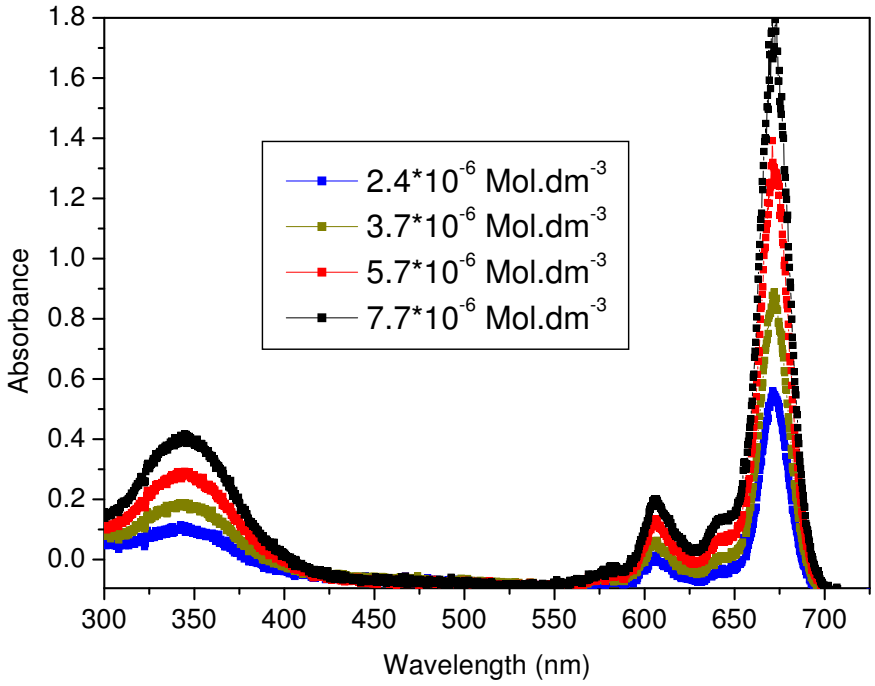

Figure 3.11: Absorption spectra of zinc phthalocyanine at indicated concentrations recorded using a USB–ISS–UV–VIS lamp combined with a UBS2000 spectrometer. The path length of the sample was 1 cm.

3.2.2 Measurement method

The transient absorption experiments were performed using a pump–probe technique based on a regenerative amplifier, the mode–locked Ti–Sapphire laser system. The details of the laser setup and spectrometer have been discussed previously in Section 3.1.1. The pump–probe system uses the white–light as probe beam. The probe beam is split into two beams, signal and reference, and focused into the sample. After the sample, these two beams are then guided into the spectrometer, which disperses the beams spectra on two linear image sensors, PDA, situated behind the spectrometer. In this case, it is possible to probe the evolution of the absorption for a wide range of wavelengths, e.g looking at this evolution for different wavelengths at different delays.

All pump–probe measurements were performed at room temperature and in dark conditions. The power of the pump beam used to study the transient absorption of LHC II and ZnPc samples were kept in the region of 2 to 6 μJ before the sample with a pulse duration of around 130 fs. In addition, the

spatial overlap between the pump and the probe was checked physically by looking at the overlap spot on the sample as well as monitoring the maximum absorbance change at τ_0. Thereafter, a fine adjustment was done by observing the absorbance change spectrum on the recording software (ExciPro software) and tuning the position of the pump beam relative to the probe beam until the maximum absorbance change is reached. These fine tuning alignments were done on a dye (Oxazine) before the sample was used. The sample was held in a rotating cuvette cell of 1 mm thickness and later a flowing cell was used. An average of 200 pulses per data point measured at each delay time for a typical delay step of 100 was used. A delay step is related to delay time. In fact, one step is a displacement of 0.234 μm of delay line, which correspond to a delay time of 0.78 fs. In addition, delay steps of 20, 50 and 100 were used in cases of investigating ultrafast processes that occur in a few hundred femtoseconds, whereas delay steps of 500 and 5000 were used for longer processes that occur with picosecond to nanosecond time constants.

3.2.3 Analysis of data

A program called ExciPro was used for data acquisition. The aim of the data acquisition was to obtain the absorbance changes induced by the pump pulse on the sample under investigation. The program provides tools and algorithms for the selection of the operational parameters and automatic recording of the absorbance change spectra at the specified optical delay line position.

In our study, the chopper was used in the pump beam path in order to record spectra that are classified as pumped and not–pumped. In the chopper mode, the algorithm will compute the $ratio\,a$ of the signal and reference acquired with the chopper open (pumped sample) and the $ratio\,b$ of the signal and reference acquired with the chopper closed (not pumped sample). As a consequence, a result ratio ($\Delta = \frac{ratio\,a}{ratio\,b}$) is calculated. To obtain absorbance changes data, a logarithm function of Δ is taken. The data recorded can be saved in the ExciPro program's format in order to reopen these data, if needed. In addition, it is possible to export data series and entire data recorded in the form of ASCII files. These files may be imported into data processing programs such as Origin, MatLab and Mathematica. Origin was used for extracting information about the absorbance changes spectra and kinetics. The time constants were determined by the use of single and double exponential decay fitting to the data. However, a program written in Matlab was designed to produce chirp-corrected 3D contour plot.

Chapter 4

Results and discussion

4.1 Characterisation

In order to study ultrafast processes in LHC II and ZnPc, it is highly important to characterise the pump–probe system used to examine these ultrafast processes. To carry out a quantitative and qualitative study on the ultrafast processes, different parameters of the pump–probe system need to be investigated, such as the temporal and spatial resolution. In addition, studies on the repeatability of the experiment, the chirp created by white–light generation, as well as the accuracy of the wavelength calibration of the spectrometer were performed.

4.1.1 Malachite green as test sample

Malachite green in ethanol was used as a sample for this proof of principle experiment to demonstrate the working of the system. A typical result of the pump–probe transient absorption signal at one particular wavelength is shown in Figure 4.1. In this experiment, the pump pulse energy was 1.5 ± 0.08 μJ with a focused beam size of roughly 300 μm, and the probe beam size was kept smaller than the pump beam. The 610 nm absorbance change as a function of delay time is presented here. Because the OPA was also set to 610 nm (pump wavelength), this is effectively a one–colour pump–probe measurement, although the probe is in fact a white–light continuum and therefore more information is available from a single experiment.

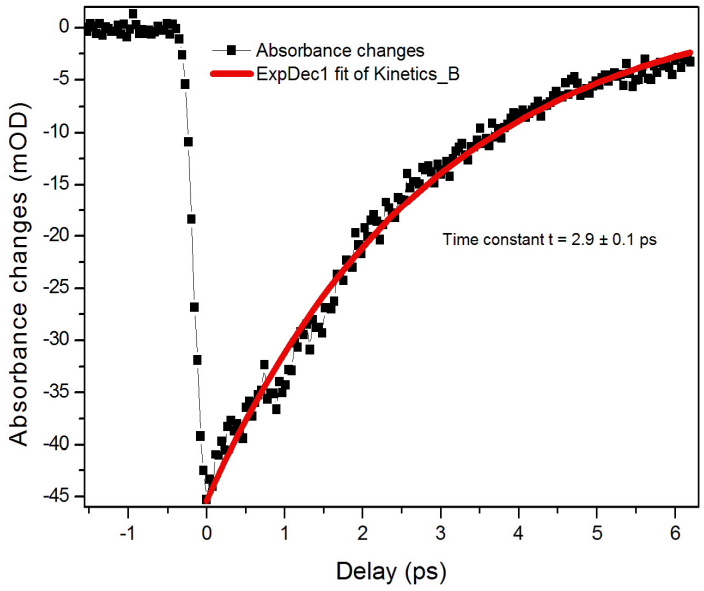

Figure 4.1: Absorbance change at 610 nm as a function of the delay between pump and probe pulses in malachite green. In this case, the pump was set to 610 nm and the probe was a white–light continuum.

The temporal delay time at which the strongest absorbance change (of 45 mOD) is observed is relative to the physical position of the retro–reflector in the optical delay line. A fast decay process after this point, which can be attributed to the excited-state decay, as expected [21] was observed. A single exponential fit of the decay data, which fits reasonably well in this case, indicates a time constant of 2.9 ± 0.1 ps. Figure 4.2 displays a contour graph of the measured transient absorption of the malachite green for the entire wavelength range of 500 to 720 nm. It can be seen in this figure that the strongest absorbance changes occurs around 610 nm as expected [21, 82, 85]. In addition, a negative broadband feature from 640 nm to 720 nm was observed. This band is related to the stimulated emission which was explained in section 2.2.5. The maximum absorbance changes for our experimental measurements were between 0.055 and 0.060 OD, and the noise level was 0.002 OD for malachite green. This noise level was consistent in all experiments with this laser (Coherent Mira 900–F).

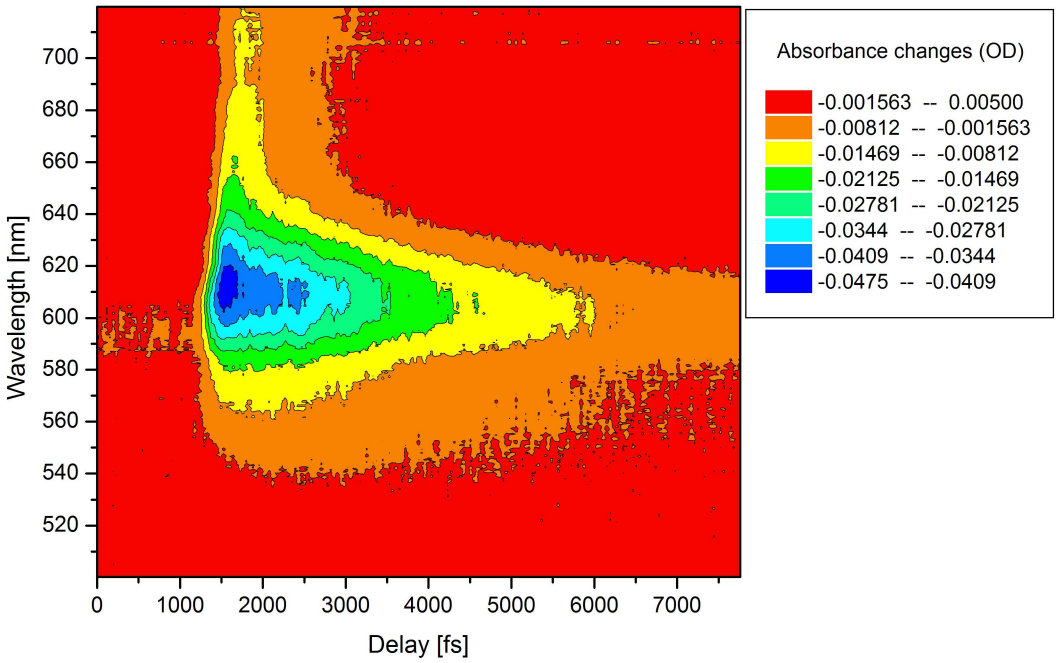

Figure 4.2: Transient absorption contour graph indicating measured absorbance difference spectra for a range of delay times between pump and probe pulses. The strongest absorbance change occurred at 610 nm and at a relative delay of 1 900 fs in this experiment.

4.1.2 Temporal resolution

The temporal resolution of the pump–probe system is determined by the convoluted temporal profile of the pump and probe pulses [15]. It also depends on the step size of the delay line. The time delay must be taken into account when determining the temporal resolution of the pump–probe setup. The time delay obtained is based on the relation between the speed of light and the spatial displacement of the delay line. In our pump–probe setup, for a typical step giving a spatial displacement of 0.234 µm, the probe is delayed by 0.78 fs compared to the pump. The minimum step size used was 20, which corresponds to a temporal delay of 15.6 fs.

In order to measure the temporal resolution of the pump–probe setup experimentally, a kinetic transient absorption measurement was done on malachite green for the purpose of determining the rise time. The rise time refers to the time required for the value of the absorbance change signal to change from

a specified minimum value, which is 10% of the minimum of the absorbance change, to a specified maximum value, which is 90% of the highest value of the absorbance change, as shown in Figure 4.3. The rise time obtained is approximately 200 fs. The rise time is the temporal resolution limit of the setup. This means that the true temporal evolution of ultrafast processes taking place on timescales shorter than 200 fs cannot be distinguished.

The temporal resolution depends on the pulse duration of the pump pulse, which is 130 fs. The temporal resolution also depends on the degree of chirp of the white–light continuum. In conclusion, the temporal resolution of the pump–probe setup is approximately 200 fs.

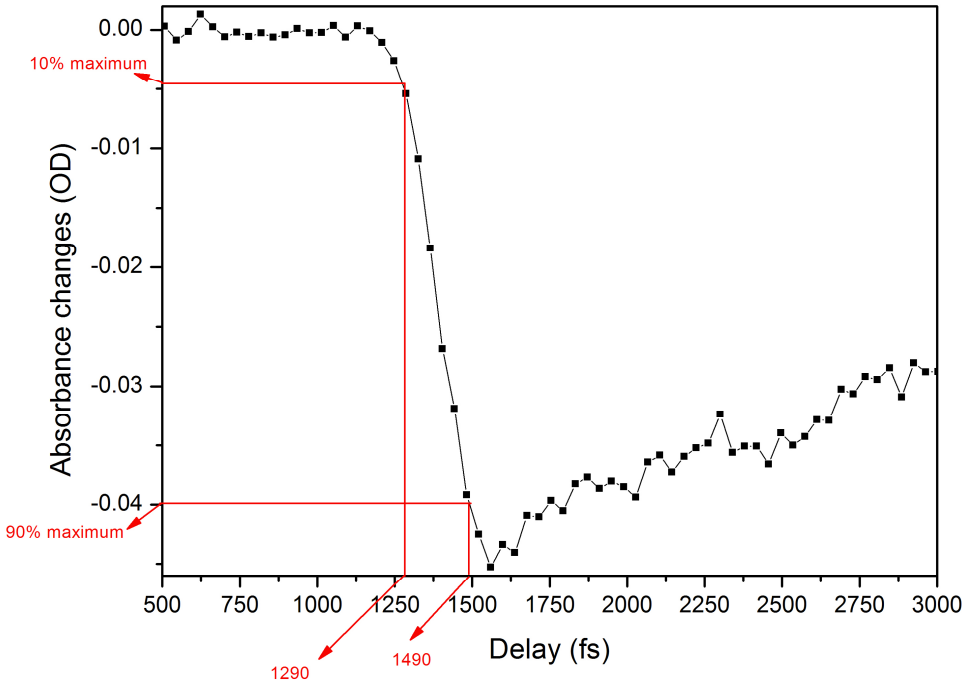

Figure 4.3: Transient absorption kinetics of malachite green obtained by using a step size of 20 (1 step of size 20= 15.6 fs) pumped at 610 nm and probed at 620 nm. It was used to determine the temporal resolution of the setup, which is 200 fs .

4.1.3 Reproducibility

In transient absorption spectroscopy, reproducibility is an important issue. The reproducibility of measurement allows us to demonstrate that the results obtained are consistent. Transient absorption measurement was done on mala-

chite green and the same sample was used for the different experiments. The power output of the amplifier was set at 950 ±1.506 mW. It was necessary to record the power of the pump at the exit of the OPA and before the sample as well as the probe power after the beam splitter used to generate the white–light continuum. Table 4.1 summarises the powers used for the experiment.

Table 4.1: Summary of power used for the experiment

	Power	Standard deviation
Amplifier output @ 795 nm	950 mW	1.506 mW
Pump power at TOPAS output @ 620 nm	55.11 mW	0.322 mW
Pump power before sample @ 620 nm	2.50 mW	0.463 mW
Probe power use to generate WLC (after beam splitter)	91.4 mW	0.504 mW

For this experiment, the pump pulse wavelength was set at 620 nm, the averaging at 100 and the steps at 500. The transient absorption kinetics of malachite green were recorded. Figure 4.4 presents the results obtained for four different scans done on the same sample. This was done in order to demonstrate the reproducibility of the experiment by looking at the variation of respective time constants. Table 4.2 presents the time constants obtained for these different scans.

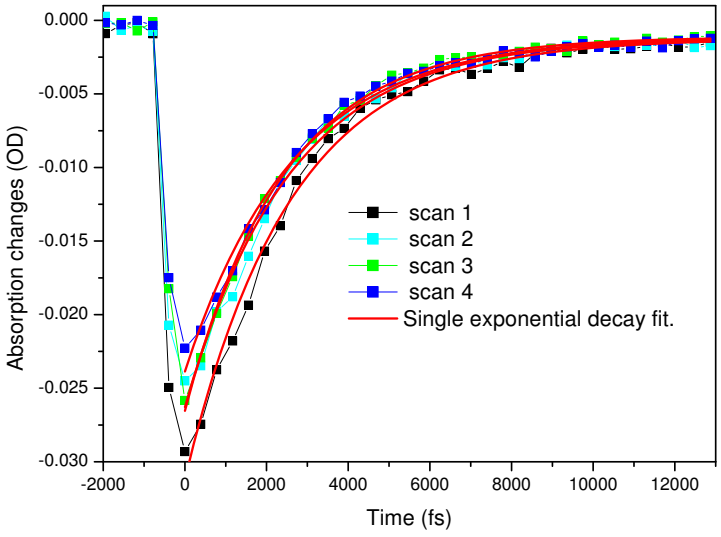

Figure 4.4: Graph of kinetics of malachite green indicating four different scans done on the same sample in order to investigate the reproducibility of the experiment

Table 4.2: Summary of time constants obtained for different scans.

	Scan 1	Scan 2	Scan 3	Scan 4	Average
Time constant t (ps)	2.574	2.562	2.414	2.658	2.552
Error margin	±0.092	±0.095	±0.043	±0.096	±0.082

The analysis of these results shows that the time constants obtained in the four respective experiments are in agreement within the accuracy of the experiment. This demonstrates the reproducibility of the experiment with regard to the time constant results. However, the time constants obtained here are slightly different from the time constants 2.1 ps and 2.3 ps reported in the literature [21, 85, 86]. This difference is due to the solvent used and the concentration of the sample [21, 85, 86] as well as the sample handling. The recovery time constant depends on the viscosity of the solvent. It has been demonstrated that malachite green in methanol exhibits a time constant of 2.1 ps [86] while it becomes 2.3 ps in buthanol [85]. In addition a high concentration may cause aggregation which results in the lengthening of the recovery time constant.

4.1.4 Influence of pump power and sample concentration

Different powers of the pump were used to determine the minimum power able to excite the sample. These experiments were done on the malachite green, on LHC II as well on ZnPc. In this section the characterisation done on the malachite green is presented. Figure 4.5 shows the transient absorption spectra of malachite green pumped at 610 nm with different pump powers. A threshold near 2.1 mW below which the excitation is too low to detect was found. On the other hand, too high power can produce problems such as bleaching of the sample.

By increasing the power of the pump, the value of the power appropriate to the excitation of the malachite green was obtained. However, the value of the power needed to excite the sample also depends on the concentration of the sample. For that reason, the sample was prepared in such way that only 20% of the pump was absorbed. It was found that a high concentration (> 20% absorption) of the sample can cause reabsorption, thereby influencing the value of the time constant and misleading the interpretation of the data.

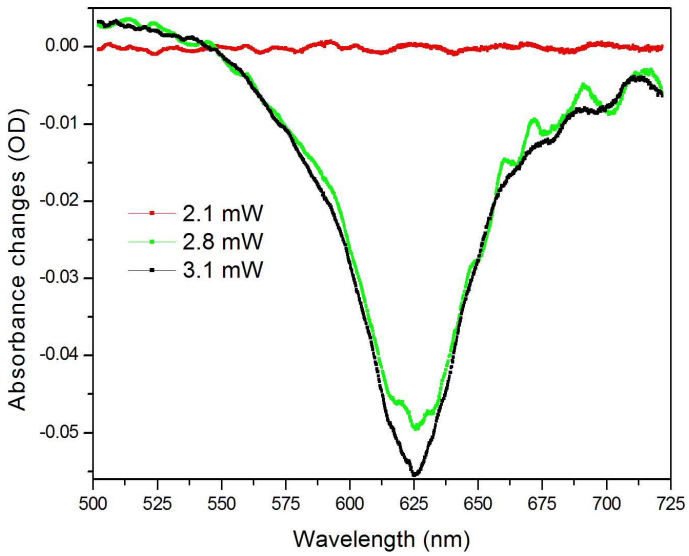

Figure 4.5: Transient absorption spectra of malachite green pumped at different pump powers

The same work was done on LHC II and ZnPc. For these two samples, the minimum power used to excite LHC II sample was 2 mW, whereas a minimum power of 3 mW was used to excite ZnPc. Figure 4.6 shows the transient absorption spectra of LHC II which indicates the minimum power used to excite the sample.

In order to obtain the concentrations required in the pump-probe experiments, the prepared extracted LHC II sample and the prepared ZnPc were diluted in buffer and solvent respectively. Steady state absorption at different concentrations was recorded using an Ocean Optics spectrophotometer. The samples were prepared such that they exhibited an absorbance of ~ 1 in a 1 cm optical pathlength at 436 nm and 678 nm for LHC II and 672 nm for ZnPc. This was deemed suitable for use in the pump-probe experiments. This condition resulted in approximately 20% absorption of the pump in pump-probe experiment which is a necessary condition to avoid reabsorption which can occur with stronger concentrations. Furthermore it was noticed that samples diluted to yield absorbance ≤ 0.3 over a 1 cm path length could not give a signal in the pump-probe experiment.

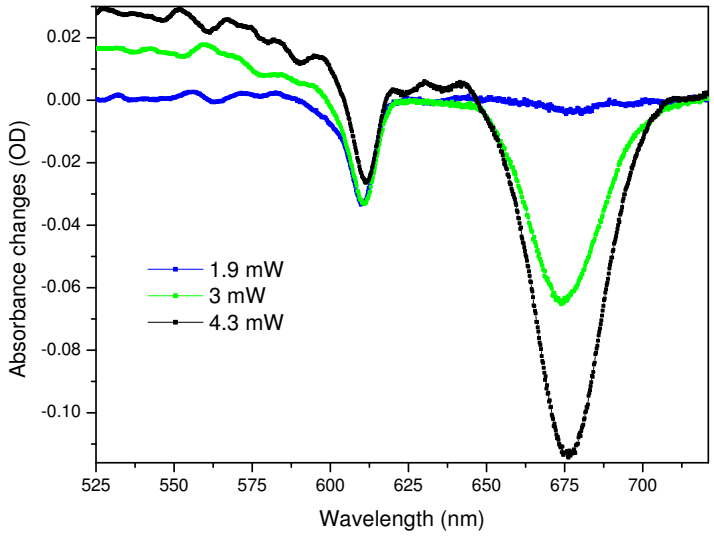

Figure 4.6: Transient absorption spectra of LHC II sample pumped at different pump powers. A sample with a steady state absorption around 1 was used.

4.1.5 Choice of delay step size

It is crucial to choose an appropriate delay step size according to the need of the experiment. In our experiment, the delay between the pump and probe pulse trains is controlled by a stepper motor translation stage set on an optical delay line. The time and step size ratio of our optical delay line was 0.78125 fs/step and the total time window of the optical delay line was 2 ns.

In our optical delay line, in order to set the value of the step size, a numerical input was used to specify the rate of the motor stepping. This numerical input ranged from 20 to 30 000 steps. This implies that the minimal step size used was 15.6 fs, while the maximum was 23.44 ps. This step range was appropriate for our study. The step size used in our study was 20, 50, 100, 500 and 5 000. In order to observe the femtosecond range time constants the 20, 50, and 100 delay steps was used, whereas the 500 and 5 000 steps were used for the investigation of the picosecond range time constants.

4.1.6 Chirp measurement and correction

When analysing transient absorption data that were measured using the white–light continuum as a probe, there appears to be a time delay between ultrafast processes occurring in the blue and the red regions. This time delay is introduced

by the white–light continuum. The white–light continuum is obtained by focusing a femtosecond pulse onto an optical medium (a sapphire plate in our case). The interaction of the femtosecond pulse with this medium leads to the broadening of its spectrum, as well as the lengthening of the pulse duration due to the delay of spectral components relative to one another, called chirp. The spectral components with low frequency (red components) propagate faster than those with high frequency (blue components). Therefore, light of different wavelengths arrives at different times at the sample. As a result, the timescales of the transient absorption kinetics data of different probe wavelengths are shifted in time relative to one another. In order to correct for these shifts and place all dynamics on the same timescale, it is important to correct the chirp introduced by the white–light generation.

Before tackling the problem of chirp correction, an explanation of how the chirp gives a time delay between shorter and longer wavelength components is necessary. In our experiment, the probe beam was temporally delayed with respect to the pump beam, as shown in Figure 4.7. In principle, this delay time between probe and pump can be compared to the autocorrelator whereby the one pulse is scanned through another. Using the moving stage, the delay time between pump and probe is changed in such a way that the probe beam is scanned over the pump beam.

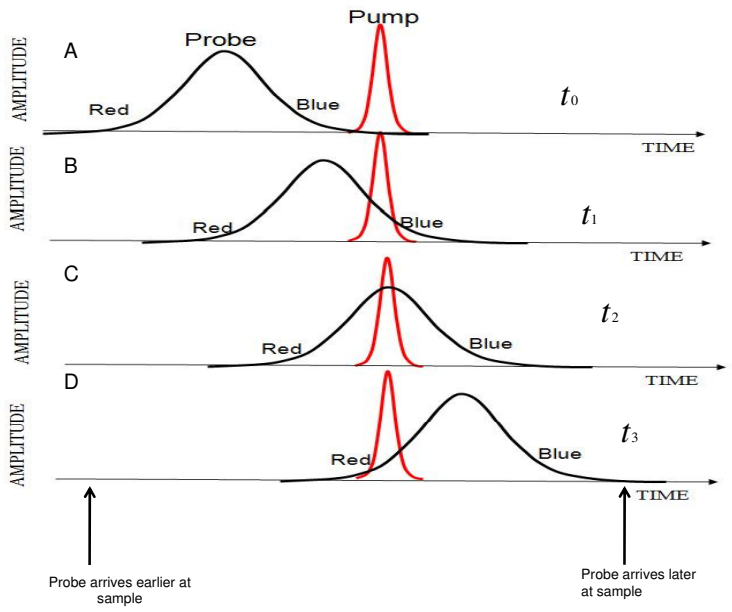

Figure 4.7: Graph indicating the timing of the pump and probe at different pump–probe delay times

The experiment started with the probe beam going through the sample, whereafter the pump beam entered the sample at time t_0 (Figure 4.7 A). By measuring the variation of absorption of the probe, no signal was observed as a result of the sample not being pumped at the time the probe beam went through the sample. As the delay time was changed to t_1, the pump started overlapping with the blue part of the probe pulse, as indicated in Figure 4.7 B. As a result, only the ultrafast dynamic processes in the blue could be detected. Further delay times (Figure 4.7 C and 4.7 D) saw dynamic processes in the green, yellow and red start appearing in that order.

Correction of this chirp is necessary for the investigation of ultrafast processes. In order to accomplish compensation, the kinetic of a known sample that exhibits localised temporal response in the spectral range of interest must be recorded. In our experiment, dyes were used as specimens that have localised temporal responses in the spectral range from 400 to 700 nm (Oxazine 170 and Sulforhodamine B dyes). Pump–probe measurements were done on these dyes and the absorbance changes spectra and kinetics were recorded. These experiments were carried out with the pump beam power set to 1.5 mW. The absorbance changes as a function of delay between pump and probe pulses was plotted.

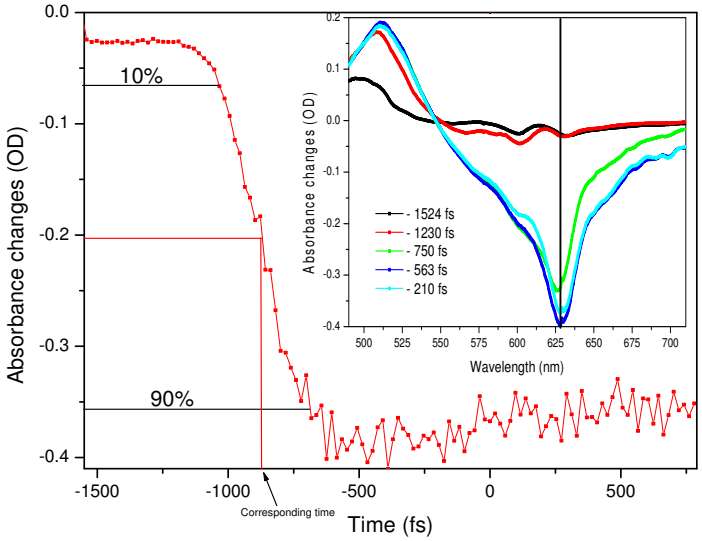

Figure 4.8: Absorbance change at 628 nm as a function of delay between pump and probe pulses (outer graph) and transient absorption in the indicated wavelength interval and time delay (inner graph) of Oxazine 170 dye with pump wavelength set at 560 nm from our pump–probe setup

For every chosen wavelength of the Oxazine 170 recorded spectra (Figure 4.8 inner graph), a corresponding kinetics profile (Figure 4.8 outer graph) was used to find the delay time. The delay time is calculated from the kinetics profile by determining the delay values where the signal reaches 90% and 10% of the maximum value of the absorbance change. The average of the 90% delay value and the 10% delay value is calculated and is considered as the delay value for that wavelength. In this work it was assumed that the rise time was limited by the temporal resolution of our setup and that presumably no sequential ultrafast processes contributed to this. Figure 4.8 illustrates how to determine the delay time corresponding to a specific wavelength. A set of relative delay time values are then obtained in the 400–700 nm spectral range. It is therefore possible to plot the relative time delay against the wavelength, as illustrated in Figure 4.9, for two different dyes.

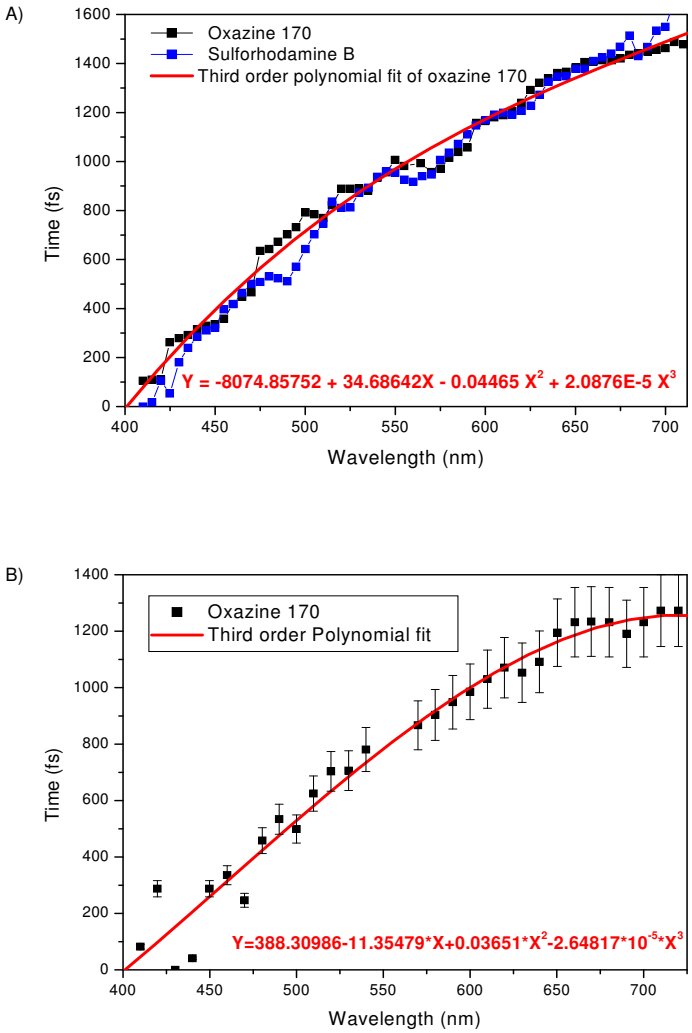

Figure 4.9: A relative time delay against wavelength of: A) Oxazine 170 and Sulforhodamine dyes with polynomial fit and the time correction equation for chirp obtained using the coherent/TOPAS setup; B) Oxazine 170 dye with polynomial fit and the time correction equation for chirp obtained using the Clark/NOPA setup to generate white–light

It was observed that under the same conditions the two dyes exhibit the same behaviour, as shown in Figure 4.9 A. As the wavelength increases (from blue towards red), the relative time delay increases. In addition, Figure 4.9 A demonstrates that in our experiment, the white–light spanning the spectral range from 410 nm to 710 nm had a temporal span of approximately 1.5 ps for the coherent setup. Figure 4.9 A shows the third order polynomial fit as

well as the polynomial equation generated by the fit (in red). This equation gives the value of delay time at a specific wavelength. This equation is used to compensate for the chirp introduced by the white–light. The kinetics graph for a specific wavelength is corrected for chirp by calculating the delay time at the relevant wavelength using the equation in Figure 4.9 A and subtracting this delay time from all time data of the kinetics graph. The same work on chirp measurement and correction was done for the white–light generated using the CPA Clark laser. Figure 4.9 B indicates the results obtained. In this case a total temporal span of 1.25 ps was obtained.

In conclusion, the generation of the white–light continuum engenders a temporal broadening of the pulse. In addition, this white light is positively chirped because of the fact that the long wavelength components of the pulse precede the short wavelength components. It is possible to compensate for the chirp introduced by the white–light generation. The method of recording the kinetics of processes with a dye that exhibit a well localised temporal response, such as Oxazine 170 dye, and determining the correction equation can be used to correct or compensate this delay difference (chirp). In addition, the temporal span values obtained using the coherent legend and CPA Clark lasers are quite similar.

4.2 Light harvesting complex II (LHC)

4.2.1 Steady-state absorption measurements on LHC II

The absorption spectrum of our samples containing LHC II extracted from spinach leaves was recorded using an Ocean Optics lamp and spectrometer (Ocean Optics, USB 2000) at room temperature and is shown in Figure 4.10. This spectrum shows similar shapes and peak positions to those indicated in the literature [87]. The absorption spectrum shows one main peak in the red region, around 672 nm, which is mainly due to chlorophyll a [60] and a shoulder at 650 nm as well as a small peak at 625 nm, which are related mostly to chlorophyll b. In addition, the absorption spectrum exhibits a broad feature from 400 nm to 520 nm, with the main peak positioned at 440 nm and shoulders on both sides of this. The peak at 440 nm represents chlorophyll a, while the peak at 467 nm represents chlorophyll b, both in the blue absorption region of LHC II [27].

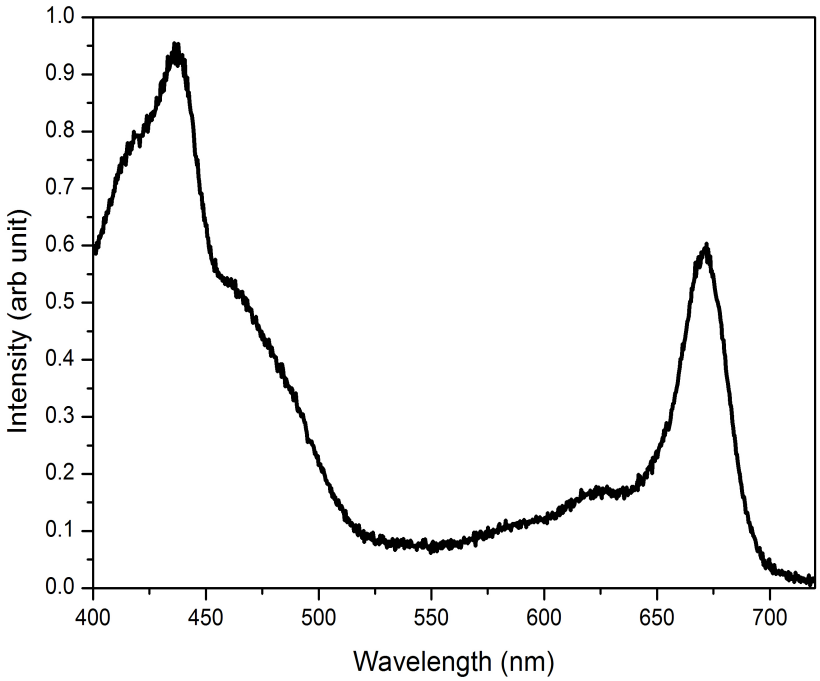

Figure 4.10: Absorption spectrum of LHC II extracted from spinach leaves recorded at room temperature

4.2.2 Transient absorption measurement on LHC II

Figure 4.11 shows the transient absorption spectra obtained in the range 350 nm to 800 nm, although the white–light continuum only had significant intensity from 420–700 nm. In this case, in order to excite both chlorophyll a and b components (Chla/b), the LHC II sample was pumped by a wavelength of 610 nm. See last paragraph on page 61 for motivation. Although 610 nm does not correspond to the peak absorption wavelength, our system provides high pulse energies and good pulse-to-pulse stability at this wavelength. Figure 4.11 exhibits five broadband absorbance changes of interest. The negative absorbance change with peaks at 436 nm and 678 nm corresponds to ground state bleaching of Chlorophyll a. The pump excites many molecules into the higher excited state, which results in a reduction of the number of molecules in the ground state. Therefore, when the probe pulse arrives, there are fewer molecules in the ground state, causing negative absorbance changes. The broadband positive absorbance change (approximately 500–640 nm), with a peak at approximately 542 nm, is due to excited state absorption. This signal is caused by the excited-

state population, which is then excited further to a higher energy level by the probe pulse. This causes an increase of the absorption of the probe beam. In addition, shoulder bands observed at 472 nm (Figure 4.11 outer graph) and 650 nm (Figure 4.11 inner graph) can be ascribed to GSB of chlorophyll b.

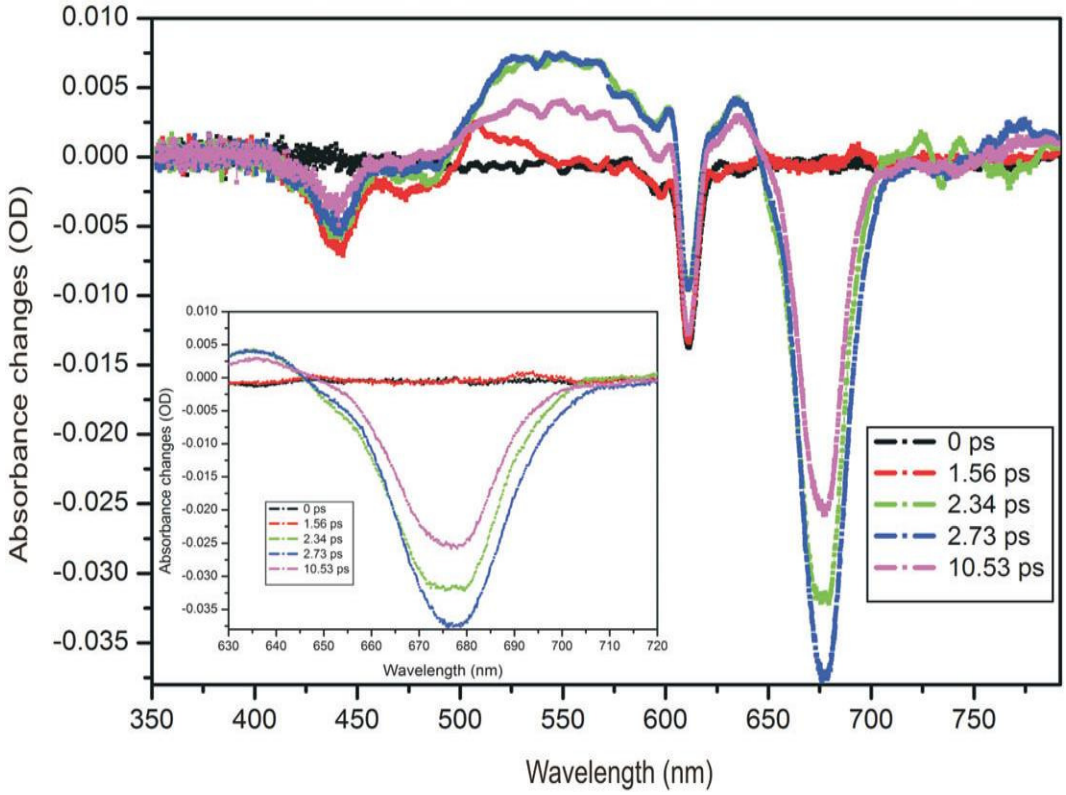

Figure 4.11: Transient absorption of LHC II in the wavelength interval 350–790 nm and time delays as indicated with the pump wavelength set at 610 nm (outer graph) and an enlarged reproduction of the 630–720 nm region of the same spectra in which the shoulder at 650 nm is clearly observable (inner graph)

The large contribution of the broadband ESA (positive absorbance change from 500–640 nm) results in a less pronounced chlorophyll b shoulder at 650 nm than expected. The peak observed at 610 nm is due to laser scatter from the sample due to particles in the sample, indicating imperfect sample preparation. During sample preparation, a crude homogenisation of the sample pellet was done, however small particles were still present in the sample and these caused the scattering of the pump beam. Upon 610 nm excitation, chlorophyll a and b are excited and the energy transfers are expected to occur among the chlorophyll molecules. Several studies have been done on the energy transfer among the chlorophylls and these have shown that the transfer takes place mainly from

chlorophyll b to chlorophyll a [33, 61]. In addition, as mentioned in Chapter 2 there is also energy equilibration that takes place from chlorophyll a to chlorophyll a and from chlorophyll b to chlorophyll b. The energy transfer from chlorophyll b to chlorophyll a within the monomer exhibits three components: a very fast component that occurs around 100–150 fs and two further components, which have lifetimes of 600–800 fs and 5–7 ps [61]. In order to obtain complete information on the five bands observed in Figure 4.11, a contour graph can be plotted (Figure 4.12). Figure 4.12 shows the transient absorption of LHC II as a function of wavelength and relative delay time between pump and probe. It is possible to observe the pump at 610 nm in this case, which remains constant over all experimental time delays and is due to laser scatter. The detection system of the spectrometer records signals continuously such that small contributions from the pump light from scattering, for example, can enter the spectrometer. Even though this is not part of the probe pulse at its corresponding delay time, it can be observed as a constant signal independent of probe delay time. In addition, the variation of the GSB at 678 nm and 436 nm, and the ESA with a peak around 542 nm can be observed clearly.

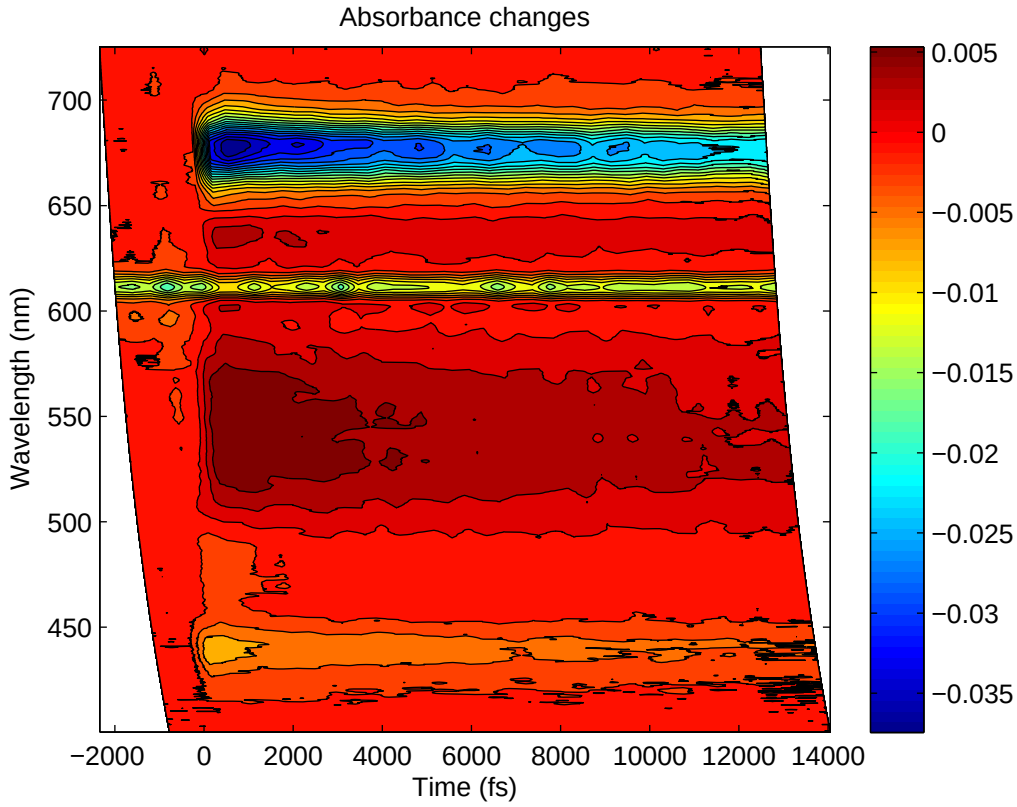

Figure 4.12: Transient absorption contour graph indicating measured absorbance changes in OD for a range of delay times between pump and probe pulses. The pump was set at 610 nm and the probe was a white–light continuum. The chirp correction equation was applied to the data.

To extract further information of the energy transfer of the LHC II from the experiment, time constants are extracted. Figure 4.13 shows the evolution of the absorbance change of 678 nm (the strongest absorption in Figure 4.11), 542 nm, 472 nm and 436 nm as a function of delay time. In the 678 nm, 472 nm and 436 nm bands, a fast drop in the absorbance change to quickly reach a minimum, which was followed by a slower recovery was observed. Whereas in the 542 nm transient a fast increase followed by a slower downturn was seen. To obtain the time constants, a second order exponential fit procedure was applied to the data set obtained of each peak (436 nm, 472 nm, 548nm and 678 nm). This was done because it was expected for the sample to exhibit at least two separate energy transfer mechanisms with different time constants, and because a single exponential did not fit the data well. The experimental values of the energy transfer time constants are tabulated in Table 4.3. The results of the second order exponential fit gave us two time constants of 1.3±

0.5 ps and 25± 4 ps for the 678 nm peak. The 1.3 ps time constant can be ascribed to singlet–singlet annihilation within the LHC II monomer and the 25 ps component to the annihilation in the trimer. Comparable time constants of 1.9 ps and 20 ps for monomer and trimer annihilation respectively at 679 nm have been reported in the literature [17]. In fact, the annihilation process that takes place can increase the energy transfer [17]. This result demonstrates that our LHC II was composed of monomers and trimers.

Table 4.3: Summary of observed time constants of different probe wavelengths: 436 nm, 472 nm, 542 nm and 678 nm, for a pump wavelength of 610 nm

Probe wavelengths	436 nm	472 nm	542 nm	678 nm
t_1(ps)	0.86±0.2	0.75±0.1	4.76±1	1.3±0.5
t_2(ps)	45±4	29±2	43±6	25±4

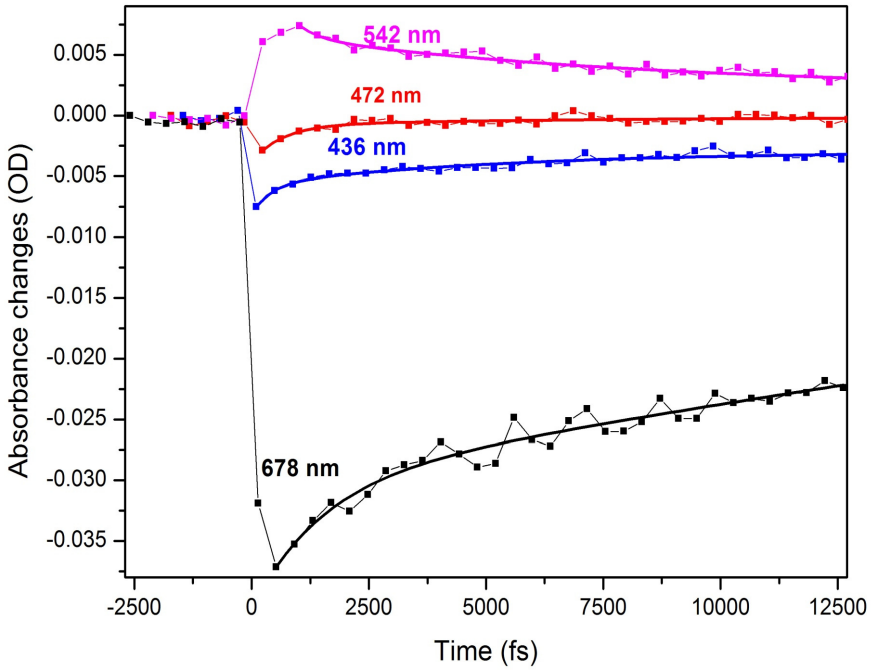

Figure 4.13: Absorbance change as a function of relative delay time between pump and probe pulses for LHC II at different wavelengths (436 nm, 472 nm, 542 nm and 678nm) pumped at 610 nm after the chirp correction equation was applied

In the blue absorption region it was possible to detect the time constants of

energy transfer between chlorophylls. The 436 nm peak relates to chlorophyll a and gives us two time constants of 860 ± 200 fs and 45 ± 4 ps, whereas the 472 nm peak relates to chlorophyll b and gives us two time constants of 750 ± 100 fs and 29 ± 2 ps. The 29 and 45 ps are not accurate extracted values, as the measurement was only done over a total range of 15 ps in this set of data. However, the time constant of 750 fs is related to the energy transfers from chlorophyll b to chlorophyll a. This energy transfer is reflected in the disappearance of the chlorophyll b bleaching (472 nm peak) after approximately 800 fs, as indicated in Figure 4.11. The time constant of the major component of energy transfer from chlorophyll b to chlorophyll a was reported in the literature to be approximately 600 fs [17, 33, 61, 62, 63]. Time constants obtained for 542 nm are 4.76 ± 1 ps and 43 ± 6 ps, again the latter value is less accurate due to the limited range of the experimental measurement. These time constants were extracted from a broadband feature ranging from 500 nm to 640 nm (with peak at 542 nm) associated with ESA. Upon 610 nm excitation by the pump pulse, the LHC II molecules are excited to a high vibrational energy level of the electronic excited state. The molecules will then undergo vibrational relaxation through internal conversion (IC) from high vibrational levels to the lowest vibrational level of the electronic excited state [62, 79, 89]. A broadband excited-state absorption spectrum is obtained due to the overlap of absorption spectra of different vibrational energy levels at the probe wavelengths. The dynamics of this spectrum is therefore related to the relaxation of the vibrational energy of the excited state of the chlorophyll a and chlorophyll b molecules.

The time constants obtained for LHC II at 610 nm pump wavelength for the absorbance change at 678 nm correspond well with those expected, while the others are less accurate, probably due to a long–lived state being populated and not resolved temporally here due to its long lifetime. The observation of a long–lived state could be due to the presence of LHC I, D1 and D2 residue in our sample. These complexes are expected to have long lifetimes in the order of hundreds of picoseconds up to the nanosecond regime [90, 91, 92].

The transient absorption experiment was also carried out at different pump wavelengths in order to compare results obtained for the energy-transfer times from different degrees of pump excitation. Figure 4.14 indicates the absorbance changes of the same sample containing LHC II pumped at different wavelengths: 610 nm, 630 nm, 650 nm and 680 nm at zero time delay (or strongest absorption change). As expected, the strongest absorbance change was observed (approximately 0.052 OD) when the pump was set at 680 nm. The pump of 650, 630 and 610 nm produced the strongest absorption changes of 0.027, 0.020 and 0.013 OD respectively. By changing the pump wavelengths, different pigments (Chla, Chlb or Chla/b) were excited, which resulted in different energy-transfer pro-

cesses taking place, namely different combinations of chlorophyll b to chlorophyll a and chlorophyll a to chlorophyll a energy transfer. Different time constants were therefore expected. In addition, the scattering of the pump wavelength, as shown on Figure 4.14 was present. However, the scattering at 650 nm and 680 nm were not resolved due to the overlap of the signal and the scattered light.

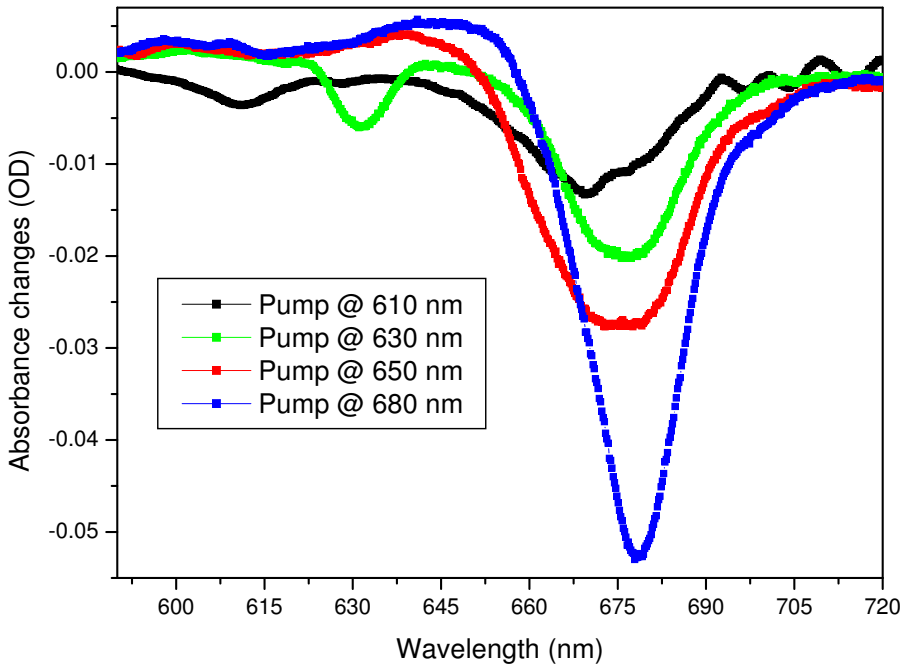

Figure 4.14: Transient absorption of LHC II of sample from spinach leaves for different pump wavelengths. The spectra were recorded at relative time t=0 when the pump and probe overlapped.

Time constants extracted from each of these experiments for the 678 nm peak are given in Table 4.4 below. By setting the pump at 650 nm, which is the strongest chlorophyll b absorption wavelength, it was possible to observe two time constants of 0.81 ± 0.3 ps and 9.95 ± 1 ps, which are related to the energy transfer from chlorophyll b to chlorophyll a. These values are within the same order of magnitude as the values of 600 fs and 5–7 ps reported in the literature [17, 33, 61, 63]. Previous studies of the energy transfer in LHC II by transient absorption have revealed that upon 650 nm excitation the energy transfer from Chl b to Chl a takes place with two major time constants of 0.15–0.3 ps and 600 fs together with a minor 4–9 ps component [63]. In addition the investigation

of energy transfer from Chl b to Chl a in CP29 sample upon 653 nm excitation has shown the presence of the time constants of 0.8–1 ps and 5–6 ps [61]. The fastest transfer time (0.15–0.3 ps) was absent in our data. However the fast and the slow components are observed in our analysis.

The excitation of the sample at 680 nm gives us time constants of approximately 0.35± 0.1 ps and 6.90 ± 0.3 ps. These values are correlated to the Chl a – Chl a energy equilibration and are in agreement with the values reported in the literature [63, 88]. Upon 670 nm excitation time constants of 300 fs and 6 ps were reported, whereas a time constant of 400 fs was found upon 672 nm excitation [63]. These time constants were attributed to the energy equilibration of chlorophyll a. Taking into consideration the uncertainties, the results obtained in this work under 650 nm, and 680 nm excitations are within the same magnitude as the values obtained in literature.

By using a pump wavelength of 630 nm, 2.8 ± 1.1 ps and 47 ± 17 ps time constants were obtained whereas using a pump wavelength of 610 nm 1.3 ± 0.5 ps and 25 ± 4 ps were observed. To our knowledge, the investigation of energy transfer in LHC II upon 630 nm excitation has not been studied. The longer time constants obtained upon 630 nm and 610 nm excitation are the result of the combination of the vibrational relaxation and energy transfer. Pumped at 630 nm and 610 nm, molecules will relax from the higher-lying vibrational states into which the molecules were excited down to the lower ones from which the energy transfer can take place. The energy transfer occurs within chlorophylls. At 630 nm and 610 nm the Chl a and Chl b can be excited. However the calculation of the ratio of Chl a to Chl b in our sample was found to be 2.4:1 (see section 3.2.1.1). This means that there was more Chl a than Chl b. One could then speculate that the major energy transfer occurs from Chl a to Chl a (equilibration).

Table 4.4: Summary of observed time constants for probe wavelength of 678 nm at different pump wavelengths: 610 nm 630 nm, 650 nm and 680 nm.

Pump Wavelengths	610 nm	630 nm	650 nm	680 nm
t_1(ps)	1.3±0.5	2.8±1.1	0.81±0.3	0.35±0.1
t_2(ps)	25±4	47±17	9.95±1	6.90±0.3

In the present study, the ultrafast energy-transfer components that occured below 200 fs were not resolved due to the temporal limitation of our setup. The precision of the time constant results obtained in this work may be improved further by making longer range measurements (temporally) and by fitting a function with more than two time constants as fitting parametres. These are challenges for future work on improvements in the extracted time constants.

4.3 Zinc Phthalocyanine

4.3.1 Steady-state absorption measurement on ZnPc

A steady-state absorption spectrum of ZnPc in DMSO at a concentration of 10 μM was acquired using a Xe–Kr lamp combined with a USB2000 Ocean Optics spectrometer (Figure 4.15) in order to confirm the optimum pump pulse wavelength. One can see that ZnPc in DMSO presents two major absorption bands, a B- or soret band with a peak at 345 nm and a Q-band ranging from 600 nm to 700 nm with a strong and sharp absorption peak near 672 nm. The Q-band exhibits at least three bands: a strong peak at 672 nm as mentioned before, a shoulder at 645 nm and a small peak at 605 nm. The 672 nm peak can be explained as the transition from the singlet ground state to the first singlet excited state ($S_0 \rightarrow S_1$). This band has been assigned to the ZnPc monomer [73]. The shoulder at 645 nm is related to the vibrational mode of the ZnPc [93] and the 605 nm is attributed to the dimer form of ZnPc [73]. Furthermore, the B-band with a peak at 345 nm is allocated to the transition from the singlet ground state to the second singlet excited state ($S_0 \rightarrow S_2$) [6, 11].

It has been proven in the literature that the photodynamic action of an aggregated sample is usually less efficient than its action in monomer form [93, 94]. In fact, in aggregate form, the PDT drug has a short-lived excited-state lifetime. This short lifetime is expected to be inefficient in singlet oxygen generation, therefore inefficient in the damage of cancer cells. However, previous studies have indicated that ZnPc displays a strong tendency for dimer formation and strongly aggregates further in water [30]. Moreover, several studies have been done on steady-state absorption of ZnPc to investigate the ZnPc form in DMSO. These studies have indicated that ZnPc in DMSO is mostly in the monomeric form. In our results, the spectral profile of ZnPc in DMSO, as indicated in Figure 4.15, shows a substantially narrow peak at 672 nm, and this peak has a relatively high intensity compared to the 605 nm peak. These spectrum structures are comparable to those reported in the literature [30, 93, 94]. These structural forms of the absorption spectrum of ZnPc in DMSO prove effectively that the monomer/dimer ratio of the ZnPc in our sample is large.

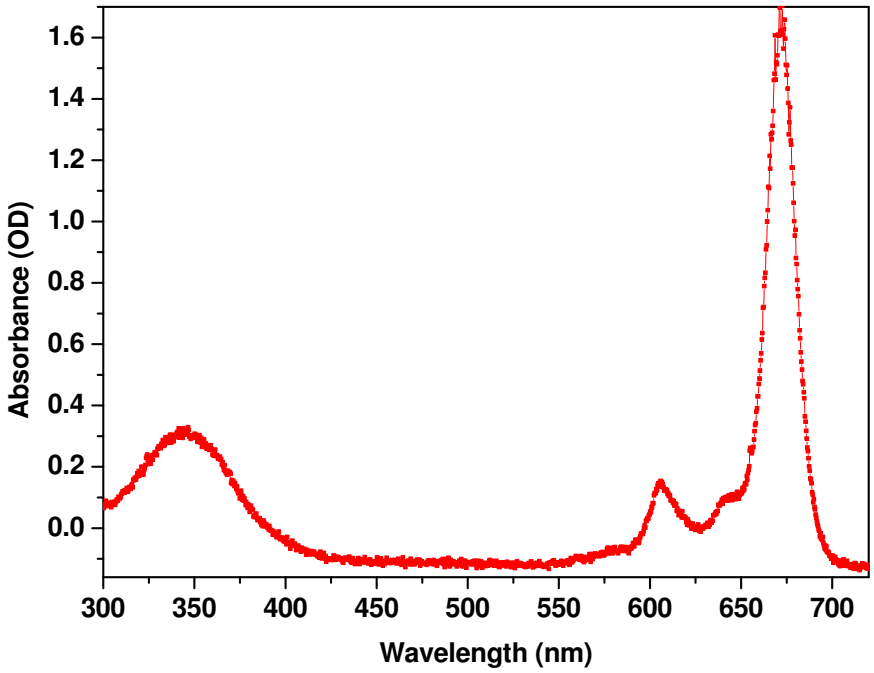

Figure 4.15: Steady-state absorption spectrum of ZnPc in DMSO at a concentration of 10 μM in a 10 mm path length cuvette recorded using a Xe–Kr lamp combined with a USB2000 Ocean Optics spectrometer

To confirm the presence of ZnPc in monomeric form in our sample, a careful investigation of the variation in the absorbance of the 672 nm peak as a function of the ZnPc concentration in DMSO was performed. Figure 4.16 shows the variation of the absorbance peak versus the sample concentration. The points (black) show the experimental data obtained and the red line indicates the linear fit of this data. One can see the absorbance changes linearly with the ZnPc concentration in DMSO. This linear behavior was observed within the sample concentration range that was used in our experiment. However, beyond a certain concentration, a nonlinear behaviour is observed, as indicated in the literature [30], which is an indication of aggregation. The linear behaviour implies that in our sample, ZnPc in DMSO, the monomer/dimer ratio of the ZnPc does not change significantly with concentration in the concentration range used in the experiment. This result is in agreement with the Beer–Lambert law. In addition, the wavelength position of the strong peak and the FWHM of the Q-band for different sample concentrations were checked. It appears that the wavelength remains at 672 nm and the FWHM is 18 nm. This proves that there

is no red shift and there is no broadening of the Q-band, which are features associated with aggregation.

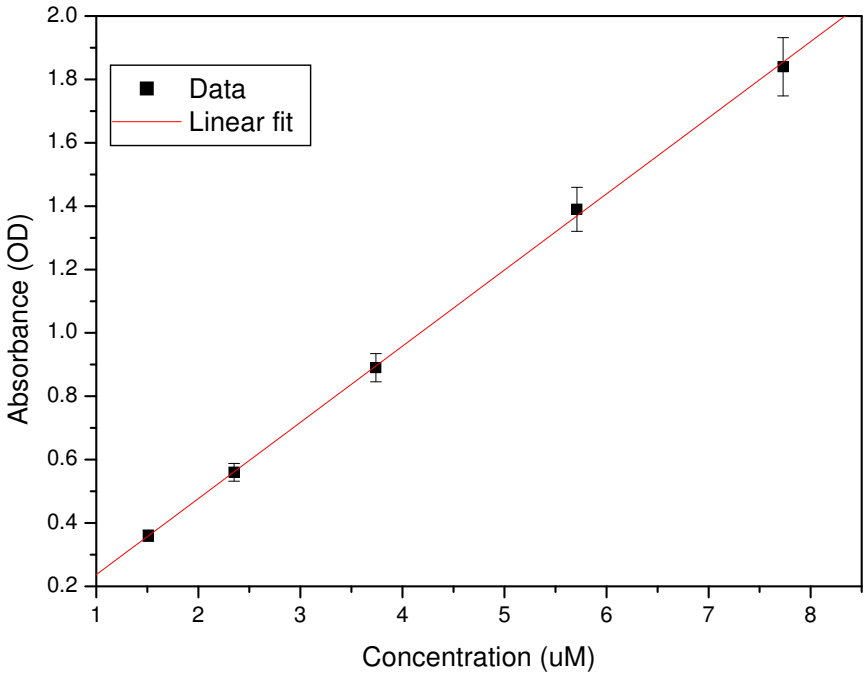

Figure 4.16: Variation of the absorbance at a 672 nm peak as a function of ZnPc concentration in DMSO.

All the steady-state absorption spectra of ZnPc in DMSO measurements were recorded using a USB2000 Ocean Optics spectrometer, and the sample holder in this spectrometer had a path length of 10 mm. However, in the pump–probe setup the path length of the sample is 10 times less than in the Ocean Optics spectrometer (1 mm). As the work was done in a relatively low concentration, according to the Beer–Lambert law, the absorbance depends on the path length d of the cell, as indicated by the following equation:

$$A = -\varepsilon dc$$

where A is the absorbance, ε is the absorption coefficient, d is the absorption path length and c is the concentration of the sample.

It is evident that the absorbance in the pump–probe spectrometer will be 10 times less than in the Ocean Optics spectrometer.

4.3.2 Transient absorption measurement on ZnPc

In this experiment, the Coherent TOPAS laser system was used, the pump was set at 672 nm with a pulse energy of 3–4.5 μJ and the other settings of the experiment remained the same, as described in Section 3.2.2. In this experiment, the sample concentration was 10 μM. Figure 4.17 illustrates the transient absorption contour plot measurement of ZnPc. This figure shows three main bands. The first band has a peak at 672 nm, which is caused by the ground-state bleach dynamics. It exhibits a negative absorbance change and the dynamics of this band show how the ground state is repopulated after excitation ($S_1 \rightarrow S_0$). This broad spectral band also includes the SE. The second band has a peak at 630 nm, which is due to the excited state absorption ($S_1 \rightarrow S_{n1}$). The third band has a broad spectral range from 460 nm to 600 nm with a major peak at 480 nm. This broad band is a potential combination of two processes: the triplet–triplet ESA ($T_1 \rightarrow T_n$) and the singlet–singlet ESA ($S_1 \rightarrow S_{n2}$).

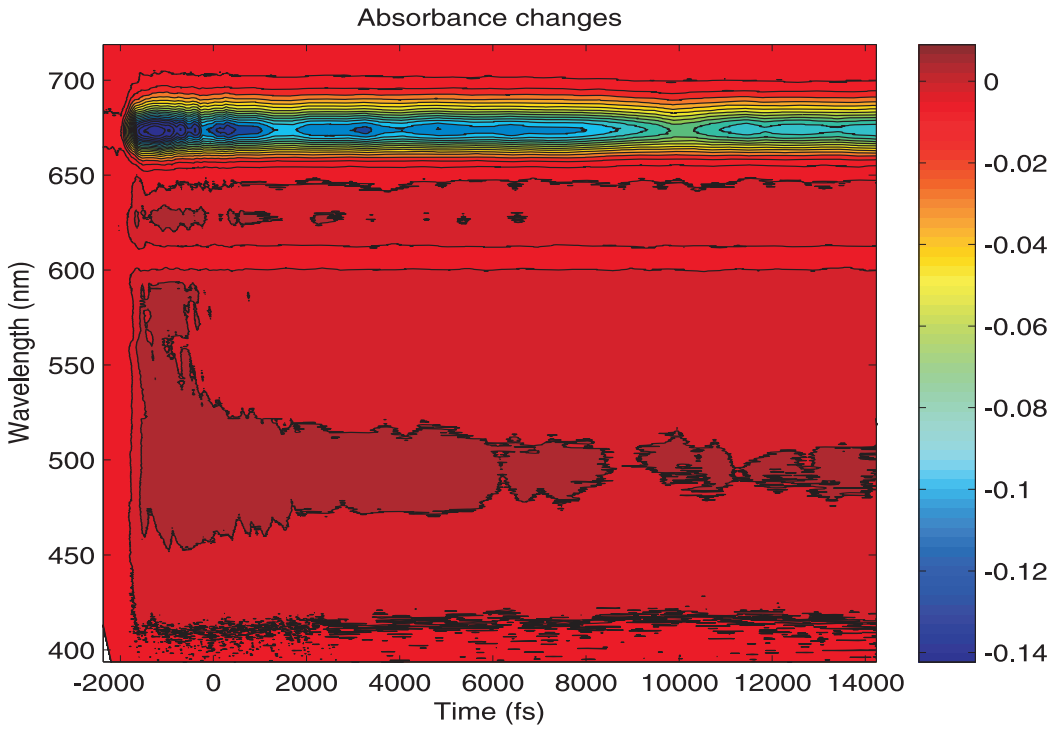

Figure 4.17: Transient absorption contour plot of ZnPc in DMSO (at a concentration of 10 μM) pumped at 672 nm, indicating measured absorbance changes for a range of delay times between pump and probe pulses

Table 4.5: Decay times of ZnPc in DMSO and DMF pumped at 630 nm, 660 nm and 672 nm for different concentrations and probes at different wavelengths

Solvent	ZnPc concentration (μM)	Pump wavelength (nm)	Probe wavelength (nm)	Time constant (ps) τ_1 τ_2
DMSO	10.4	672	686	4.7 ± 1.6, 45.1 ± 7.5
			672	1.82 ± 0.1, 38.9 ± 2.6
			668	1.5 ± 0.1, 29.3 ± 3.9
			630	1.4 ± 0.3, 17 ± 2.6
			485	1.4 ± 0.5, 14 ± 1.8
DMSO	10.4	630	672	1.8 ± 0.1, 34.2 ± 2.3
			630	2.7 ± 0.3
			485	2.5 ± 0.3, 38.4 ±0.6
DMSO	5.2	630	672	1.3 ± 0.3, 39.6 ± 8.3
DMF	6.3	660	690	38.5 ± 7.4
			670	45.7 ± 5.7
			660	42.9 ± 3.8
			624	44.8 ± 5.7
			480	38.3 ± 2.1

After excitation one can observe a negative absorbance change signal of around 672 nm, as indicated in Figure 4.18. The absorbance change goes from 0 OD to a maximum of –0.14 OD, immediately at zero delay, that corresponds to the spatial and temporal overlap between the pump and the probe beam. The negative absorbance change indicates that the signal at the 672 nm band is dominated by the GSB and SE. It was observed that this was moving toward the red, as shown in Figure 4.18. At zero delay, the GSB peak was at 672.5 nm, whereas after 4.68 ps and 24.92 ps, the peak was at 673.9 nm and 674.5 nm, respectively. This red shift is attributed to the decrease of energy of the excited state (S_1) due to solvent redistribution [6]. One has to notice that the ground-state molecules are not affected by solvent rearrangement, therefore their absorption (and bleach signal) stays at the same wavelength. In addition, the solvent rearrangement only affects the excited molecules, and therefore will have an effect on the SE that originates from the excited molecules. Upon excitation, the excited state of ZnPc possesses a new electron distribution. This charge distribution causes the rearrangement of solvent around the molecule, which will shift the energy of the excited state S_1 down. As solvent rearrangement

proceeds, the wavelength of the SE shifts towards the red, causing a red shift of the absorbance change peak. The energy decrease of the excited state is therefore due to the solvent's (DMSO) molecule redistribution.

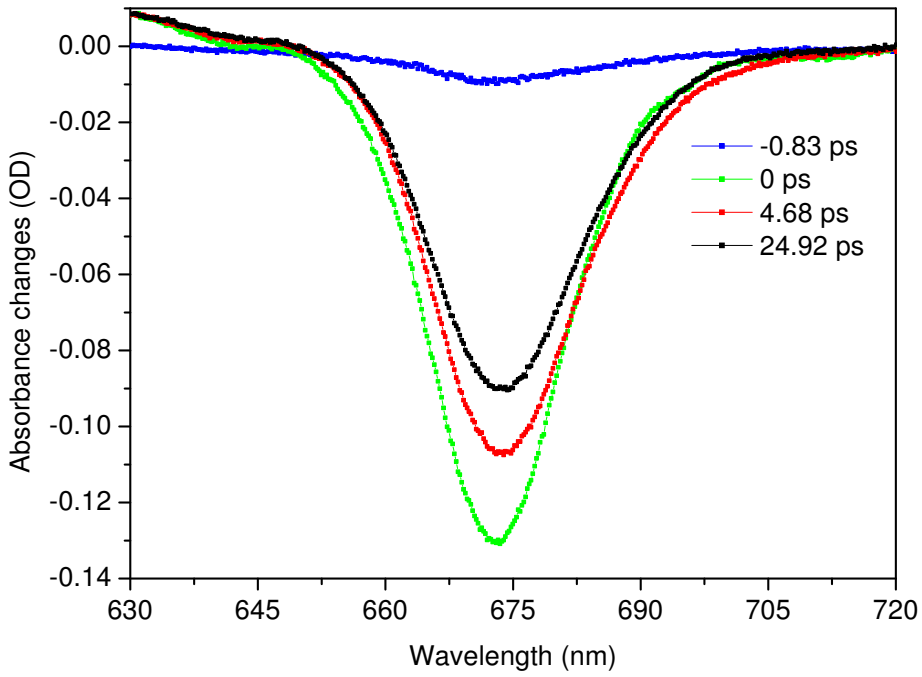

Figure 4.18: Transient absorption spectra of ZnPc in DMSO (at a concentration of 10 μM) pumped at 672 nm indicating the wavelength peak of the Q-band moving toward the red. At 0 ps (green curve), 4.68 ps (red curve) and 24.92 ps (black curve) the peak was at 672.5 nm, 673.9 nm and 674.5 nm, respectively.

The dynamics were investigated further by making bi–exponential fits to the data at different wavelengths in the band. The results obtained show a fit to a bi–exponential decay at the 672 nm band peak, comprising a fast process with a time constant of 1.82 $\pm$ 0.1 ps and a slower process with a time constant of approximately 38.9 $\pm$ 2.6 ps. See table 4.5 on the preceding page for a summary of all measured time constants discussed in this section. This decay was attributed to solvation dynamics. The solvation process is a non-exponential process and can be characterised only by approximation by a set of exponential decay times. These decay times tend to span several orders of magnitudes [95, 96, 97, 98]. The solvation of Coumarin 153 in the same solvent used here, DMSO [98] has been fitted with time constants of 214 fs, 2.29 ps and 10.7 ps, and

the solvation of ZnPc in DMSO in a previous study [6] by 250 fs and 2.5 ps. In both studies, the fs components were assigned to the inertial solvation dynamics and the ps timescales to dielectric solvation dynamics. In our experiment, the fs timescale component could not be measured. The ps time constants that were measured agree approximately with the dielectric solvation dynamics times of previous studies. The 38.9 ± 2.6 ps time constant is of the same order observed by Rao and Rao [7], although our association of the time constant with solvation dynamics differs from their interpretation. The decay curve does not return to 0 OD even after a time delay of 1.2 ns as shown in Figure 4.19. This indicates that the timescale of the processes that depopulate S_1 state is much longer, approximately 3 ns, as known from the literature [6].

In order to have a more detailed view of the dynamic of the Q-band, the dynamics of the blue and red side of the band were analysed. The decays of data at 668 nm and 686 nm were fitted by a bi–exponentials as shown in Figure 4.19. The time constants were 1.5 ± 0.5 ps, 29.3 ± 3.9 ps and 2.1 ± 1.6 ps, 41.1 ± 7.5 ps for 668 nm and 686 nm, respectively. The two time constants at 668 nm were relatively short compared to those at 686 nm. This implied that there is a fast decay in the blue side of the Q-peak whereas the red side has a slow decay. These results indicate once again that the peak of Q-band shift toward the red.

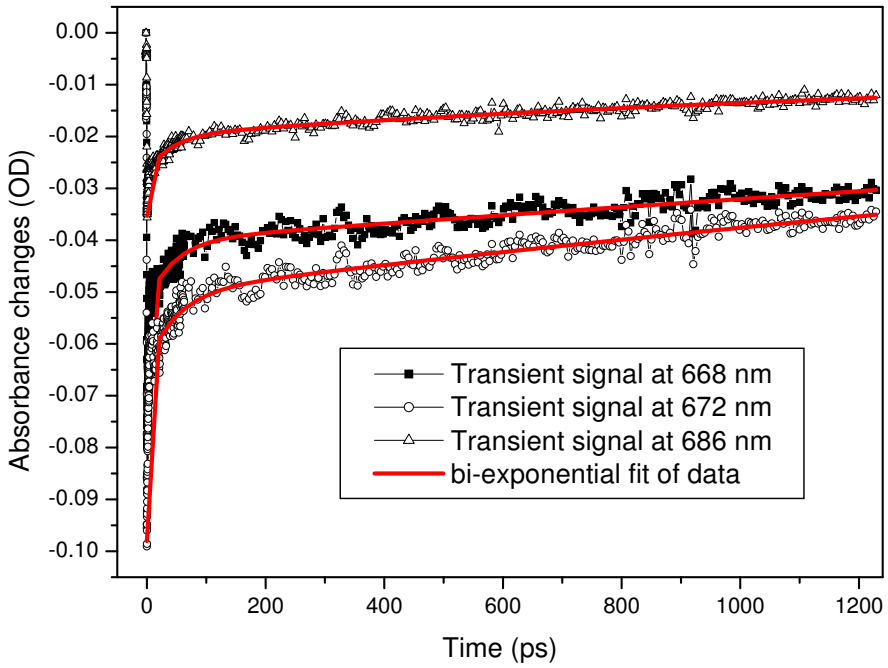

Figure 4.19: Transient signal of absorbance changes of ZnPc in DMSO at a concentration of 10 μM pumped at 672 nm and probed at 668 nm, 672 nm and 686 nm

In addition, further ultrafast dynamics were resolved, as indicated in Figure 4.17. In the region of 430 nm to 600 nm with the peak band around 485 nm, a bi–exponential was resolved. The time constants of the bi–exponential fit, as shown in Figure 4.20, are 1.4 ± 0.5 ps and 14 ± 1.8 ps. This region in principle contains the combination of two processes: the triplet–triplet ($T_1 \rightarrow T_n$) ESA at 480 nm and the singlet–singlet ($S_1 \rightarrow S_{n2}$) ESA at 485 nm. However, the transfer of population to the T_1 triplet state after excitation takes place on a 3 ns timescale and our experimental measurements covered only the first ∼ 70 ps after excitation. This means that during our measurements, the T_1 triplet state still has a negligible population and the band at 480 nm was caused by the $S_1 \rightarrow S_{n2}$ singlet–singlet ESA only. The last ultrafast dynamic observed was in the region of 610 nm to 650 nm with the peak around 630 nm. The decay was found to be a bi–exponential and was fitted with time constants of 1.4 ± 0.3 ps and 17 ± 2.6 ps (Figure 4.21). This band is related to the singlet–singlet ESA ($S_1 \rightarrow S_{n1}$).

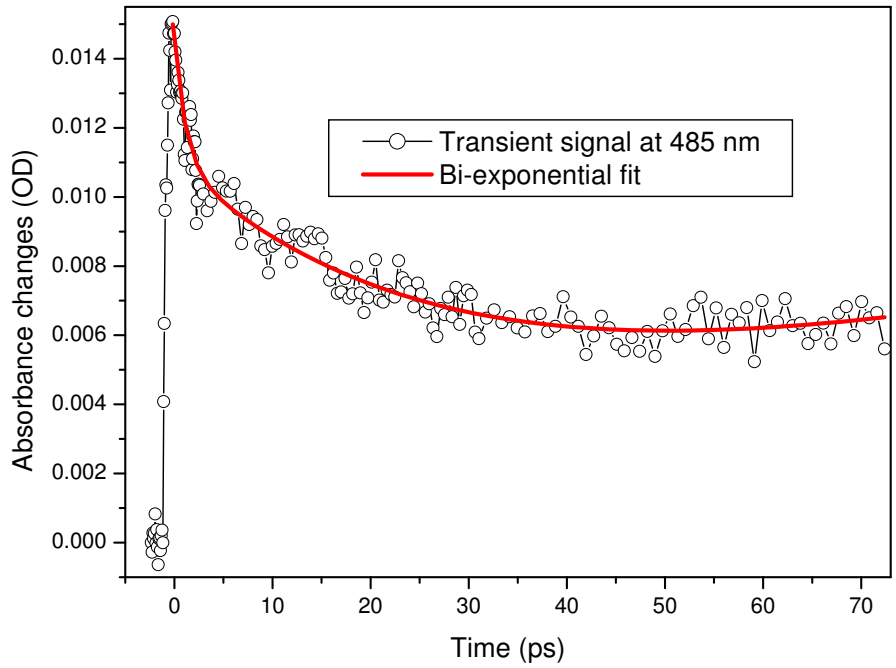

Figure 4.20: Transient traces and exponential fits at 485 nm of ZnPc in DMSO at a concentration of 10 μM pumped at 672 nm. The time constants found were 1.4 ± 0.5 ps and 14 ± 1.8 ps.

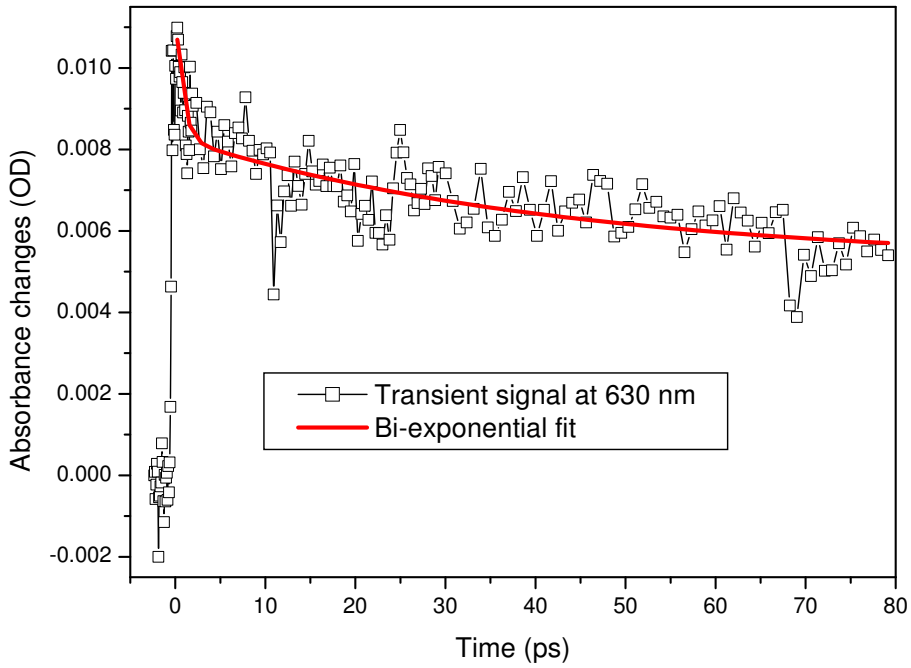

Figure 4.21: Transient traces and exponential fits at 630 nm of ZnPc in DMSO at a concentration of 10 μM pumped at 672 nm. The time constants found were 1.4 $\pm$ 0.3 ps and 17 $\pm$ 2.6 ps.

In the literature there is only one paper by Savolainen et al [6] reporting a pump–probe experiment similar to this study, using ZnPc in DMSO. In the experiment of Savolainen et al, the pump wavelength was 672 nm and the concentration 12.6 μM. In the paper of Savolainen, a bi–exponential decay at 672 nm is reported with time constants of 250 fs and 2.5 ps, but without any evidence for a longer lifetime in the range of 10–100 ps, although time constants in this range have been observed by others. Howe and Zhang [72] observed 10 and 160 ps using sulphonated ZnPc and Rao and Rao [7] observed a time constant of 35 ps using the technique of degenerate four–wave mixing. The 250 fs and 2.5 ps of Savolainen et al [6] were attributed to the solvation dynamics of the DMSO solvent. It is important to point out that the results given by Rao and Rao were obtained using the degenerate four-wave mixing technique, which is different from the femtosecond pump-probe technique used in this work. In addition the results presented by Howe and Zhang were also obtained with a modified sample ($ZnPcS_4$). Furthermore, in the work presented by Savolainen et al, obtained using femtosecond pump-probe spectroscopy, data in the picosec-

ond time scale is lacking, probably due to limitations in their setup. In their work only 250 fs, 450 fs and 2.5 ps time constants were presented.

In this work, new results obtained complement the work done by others by providing data in the picosecond time scale. In our experiments, time constants of 1.82 ps and 38.9 ps at 672 nm were observed. However, a 250 fs component could not be resolved. The 450 fs component was not observed, although it should be possible to resolve such a process. The 1.82 ps observed at 672 nm is comparable to the 2.5 ps time constant of Savolainen et al [6] and can be attributed to the solvent effect. In addition, the 38.9 ps component that was not observed by Savolainen et al [6] was resolved. Rao and Rao [7] assigned the 35 ps time constant that they observed to population relaxation from the excited state to the ground state ($S_1 \rightarrow S_0$). This cannot be a correct assignment. The lifetime of the excited singlet state is approximately 3 ns. If there was a population relaxation with a time constant of 35 ps, this would have depopulated the excited S_1 singlet state and the lifetime of the excited single state could then not be 3 ns. The depopulation of the excited state (S_1) occurs via the combination of fluorescence (F), IC and ISC. This means that the decay of ground-state bleach (S_0) should be the combination of three exponential decays with lifetimes associated with the three processes. It has been proven that the combination of these three processes for depopulation of the excited state holds only for the dynamics on the nanosecond timescale [6]. It is in the light of this argument that the association of a 38.9 ps component to population relaxation was rejected and interpreted as a slower term in a multi–exponential approximation of the solvent dynamics.

For the time constants obtained for the 630 and 485 nm bands, literature values were not available for direct comparison. Savolainen et al. [6] reported a single exponential time constant for the decay of the 630 nm band of 250 fs. Similarly, Savolainen et al observed a 450 fs decay of the 485 nm band, but no ps time constants. It may be possible that the timescales chosen in their measurements were designed to record fs and ns dynamics, but that they were not suited for dynamics in the 10–100 ps timescales. In our work, a bi–exponential fit with 1.4 ps and 17 ps time constants for the 630 nm band and 1.4 ± 0.5 ps and 14 ± 1.8 ps for the 485 nm band were obtained, as mentioned above. The observation that these time constants of the singlet ESA are smaller than those of the GSB 672 band possibly indicates the presence of vibrational relaxation processes with time constants of the same order that lengthens the decay time of the lower vibrational levels in the S_1 state possibly associated with the 672 nm transition. The ESA, at 630 nm and 485 nm, may originate from higher vibrational levels in the S_1 state due to favorable Franck Condon factors, meaning that vibrational relaxation will shorten the decay time observed in these

bands. The report of time constants as short as 3 ps associated with vibrational relaxation by Rao and Rao [7] supports this speculative explanation.

The difference between the numerical values of the time constants from our results and those obtained by Savolainen et al [6] may be attributed to the fact that in our setup the "magic angle" was not used. The magic angle allows one to avoid the effect that the rotational motion of molecules in the excited state has on the measurements. The rotational dephasing of the molecules adds an additional decay to the dynamics. This decay induced by the rotational dephasing has a typical time scale of the order of 100 ps [99] or may be longer since it involves rotation of the large sample molecules in the solvent. In our setup the white light is unpolarised and for unpolarised white light, the rotational dephasing should cause a loss of only approximately 17% [99]. In summary, the fact that the magic angle was not used may introduce additional time constants (>100 ps) and a signal loss ($\sim$ 17%) in the results. The measured time constants and signal losses measured at the CSIR setup are partially due to the rotational dephasing, but the losses seen are larger than expected from the theory of rotational dephasing. Solvation dynamics may also contribute to the signal loss as will be discussed on page 83.

Additional transient absorption measurements on a ZnPc sample were conducted by pumping at a different wavelength. The ZnPc in DMSO at different concentrations were pumped at 630 nm and probed with white–light and the energy of the pump was set at 4–6 μJ. At this pump wavelength it was observed that the GSB wavelength peak of the Q-band was extended further toward the red, as shown in Figure 4.22. At zero delay, the GSB peak was at 671.9 nm, whereas after 4.68 ps and 24.92 ps, the peak was shifted to 674.9 nm and 676 nm, respectively. It could be noticed that after 24.92 ps there was a red shift of 4 nm for the Q-band peak, whereas a 2 nm red shift was observed for the sample pumped at 627 nm. This red shift indicates the decrease of energy of the excited state (S_1) due to solvent redistribution, as mentioned above, when the sample was pumped at 672 nm. In addition, a negative signal at 630 nm was observed, as shown in Figure 4.22, in contrast to the positive signal observed when the sample was pumped at 672 nm (see Figure 4.18). This negative signal is due to the scattering of the pump wavelength (630 nm) and this is dominant over the ESA expected at this wavelength. This signal was confirmed as scatter due to the fact that it is present at all delay times. In Figure 4.23 the dynamics at 672 nm are analysed for the three concentrations used here with the maximum absorbance changes depending on the concentration. In general, after excitation there is a very fast rise to a peak followed by a typical bi–exponential decay. Once again, the decay did not return to zero as observed previously. The transient signals decay exhibited bi–exponential components with lifetimes

summarised in table 4.5. One can observe that the lifetimes measured at different concentrations for the 672 nm peak are of the same magnitude. The longer time constant at 485 nm shows that the ESA to S_{n2} probably results from lower lying vibrational levels in S_1 so that the lifetime is lengthened by vibrational relaxation from the higher lying vibrational states into which the molecules were pumped by 630 nm down to the lower ones from which the ESA occur.

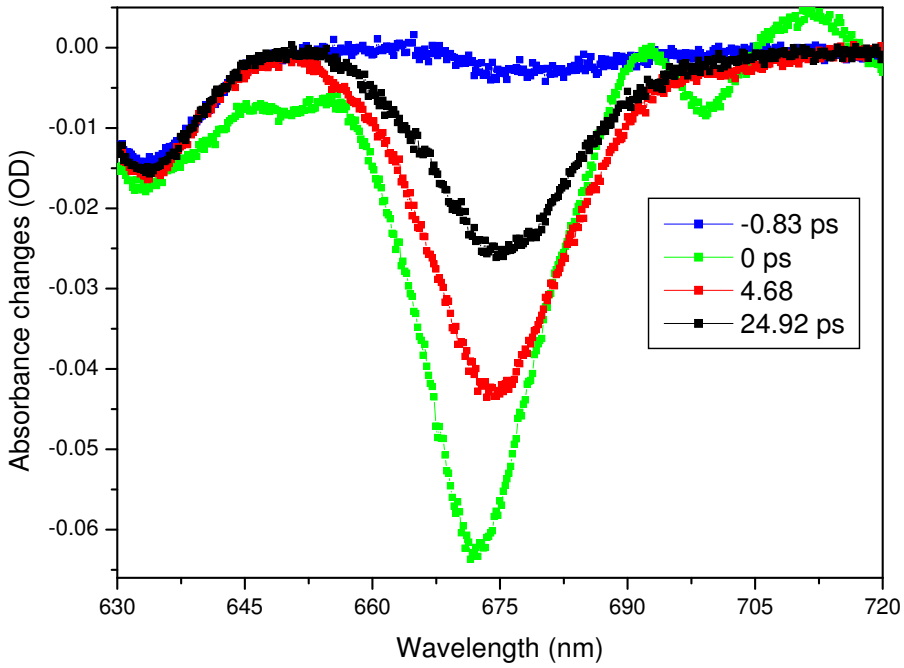

Figure 4.22: Transient absorption spectra of ZnPc in DMSO (at a concentration of 10 μM) pumped at 630 nm, indicating the wavelength peak of the Q-band moving toward the red. At 0 ps (green curve), 4.68 ps (red curve) and 24.92 ps (black curve) the peak was at 671.9 nm, 674.9 nm and 676 nm, respectively.

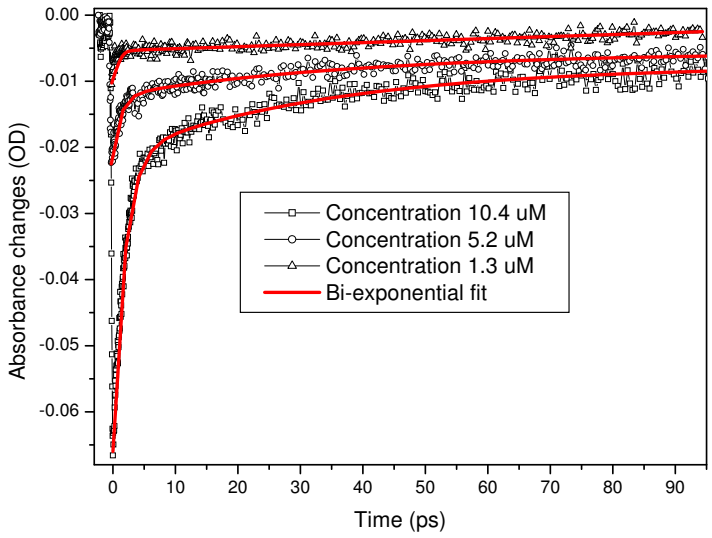

Figure 4.23: Transient signals of ZnPc in DMSO at 672 nm pumped at 630 nm for different concentration: $1.3*10^{-6}$ mol.dm^{-3}, $5.2*10^{-6}$ mol.dm^{-3} and $10*10^{-6}$ mol.dm^{-3}

The investigation of ZnPc in DMSO by pumping at 630 nm has to our knowledge never been reported before. The change of sample concentration did not have any significant impact on the time constants. These time constants remained in the range of 1.3–1.8 ps for the fastest time and 34–39 ps for the slow time constant. When pumping at 630 nm, time constants for the GSB band at 672 nm of 1.3–1.8 ps and 34–39 ps (for $5–10*10^{-6}$ mol.dm^{-3}) were observed and can be considered similar to the results when pumping at 672 nm when taking the uncertainties into account. However a 2.7± 0.3 ps time constant was observed for the 630 nm band and a bi–exponential fit with 2.5 ± 0.3 ps and 38.4 ± 0.6 ps time constants for the 485 nm band. The 2.7 ps and 2.5 ps are of the same magnitude and significantly longer than the 1.4 ps time constant obtained with 672 nm pumping. The interpretation of these time constants is complex due to the possible overlap of a GSB/$S_1 \rightarrow S_0$ SE and $S_1 \rightarrow S_{n1}$, $S_1 \rightarrow S_{n2}$ ESA at 630 nm and 485 nm, respectively, when the pump wavelength is 630 nm, pumping into higher vibrational levels. These 2.7 ps and 2.5 ps time constants could be attributed to vibrational relaxation. Upon excitation at 630 nm, the molecules relax from the vibrational levels into which they were pumped down to lower vibrational levels of the excited singlet state. This vibrational relaxation has been reported to be around 3 ps [6, 7]. The difference in time constants of the ESA obtained, 2.7 ps and 2.5 ps, could be due to the contribution of the

scattering pump wavelength and the signal at 630 nm. The 38.4 ± 0.6 ps of the 485 nm band is significantly longer than the 14 ps time constant obtained with 672 nm pumping. However, the 38.4 ps time constant is of the same order as the time constant obtained for the GSB band at 672 nm. It is associated with the solvation dynamics.

In all the results on ZnPc in DMSO, one can observe a reduction of the signal within the first 100 ps. This reduction of the signal might be attributed to the rotational motion of ZnPc molecules. The basic principle of this rotational motion of molecules (rotational dephasing) is that the pump pulse excites their molecules that only have the transition dipole moments aligned with its electric field. At the excited state, because the molecules possess different angular momenta, they will rotate away from their initial alignment. Therefore, when the probe pulse arrives 100 ps later than the pump pulse, the molecule has had enough time to rotate and the probe will only interact with molecules that still have the dipole moment aligned with its electric field. This rotational dephasing usually occurs in timescale of 100 ps [15]. In order to overcome the reduction in signal due to the rotation of the molecules, one has to change the angle between the polarisation direction of the pump and the probe light. It has been demonstrated that if one uses the magic angle (54.7^0) one can avoid the rotational dephasing of the molecules [99]. However in our setup, the measurement was done without the magic angle which could be the reason for the partial reduction of the signal. Despite the signal reduction by the rotational dephasing, the solvation dynamics and vibrational relaxation of the ZnPc were still present.

Preliminary transient absorption work was done on ZnPc in DMF at a concentration of 6.3 μM. Figure 4.24 shows the transient signal contour plot of ZnPc in DMF obtained in the range from 440 nm to 700 nm when it was pumped at 660 nm. The transmission changes contour plot exhibits three broadband features. The first band has a peak at 670 nm which is caused by the GSB dynamics. This broad spectral band also includes the SE. The second band has a peak at 624 nm, which is due to the ESA ($S_1 \rightarrow S_{n1}$). The third band has a broad spectral range from 440 nm to 600 nm with a major peak at 480 nm. This broad band is a potential combination of two processes: the triplet–triplet ESA ($T_1 \rightarrow T_n$) and the singlet–singlet ESA ($S_1 \rightarrow S_{n2}$), as mentioned previously. ZnPc in DMF exhibits a GSB band with a peak at 670 nm, as indicated in Figure 4.25, whereas this peak is at 672 nm for ZnPc in DMSO. This shift was also noticed in the second band, where the band has a peak at 624 nm for ZnPc in DMF rather than 630 nm, as observed for ZnPc in the DMSO solvent. The position of the Q-band is in agreement with what has been reported in the literature [8, 68, 100]. The position of the Q-band peak depends on the solvent

used and on its polarity. It has been reported that the position of the Q-band is further red-shifted as the polarity of the solvent increases [8]. In this experiment the solvent (DMF) used is less polar than DMSO. Therefore, the Q-band peak is expected to be around the value found. In order to improve our understanding of the solvent effect, the investigation of the peak shift of the GSB/SE peak at 670 nm was done. It was observed that the peak has a relatively small shift toward the red, as shown in Figure 4.25, inner graph. At zero delay, the GSB peak was at 670.5 nm, whereas after approximately 200 ps, the peak was at 671.5 nm, which is a shift of approximately 1 nm. This shift was approximately 2 nm and 4 nm after 24 ps for ZnPc in DMSO pumped at 672 nm and 630 nm, respectively. If the shift of the peak is interpreted as the shift in the peak wavelength of the SE from excited molecules as explained before, this means that the solvent rearrangement of the less polar DMF should cause a smaller decrease in the S_1 level energies than with DMSO. This can be expected, as the rearrangement of more polar solvent molecules should change the environment of the ZnPc molecule more than in the case of less polar or non–polar solvent molecules. Therefore, the smaller red shift of the Q-band in the case of DMF is expected.

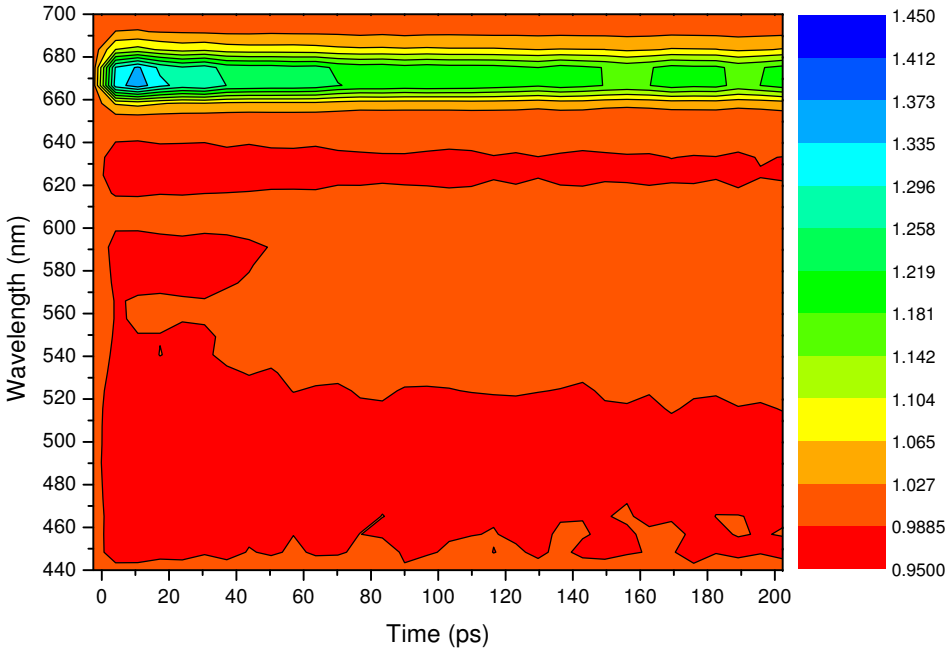

Figure 4.24: Transient signal contour plot of ZnPc in DMF (at a concentration of 6.3 μM) pumped at 660 nm, indicating measured transmittance changes for a range of delay times

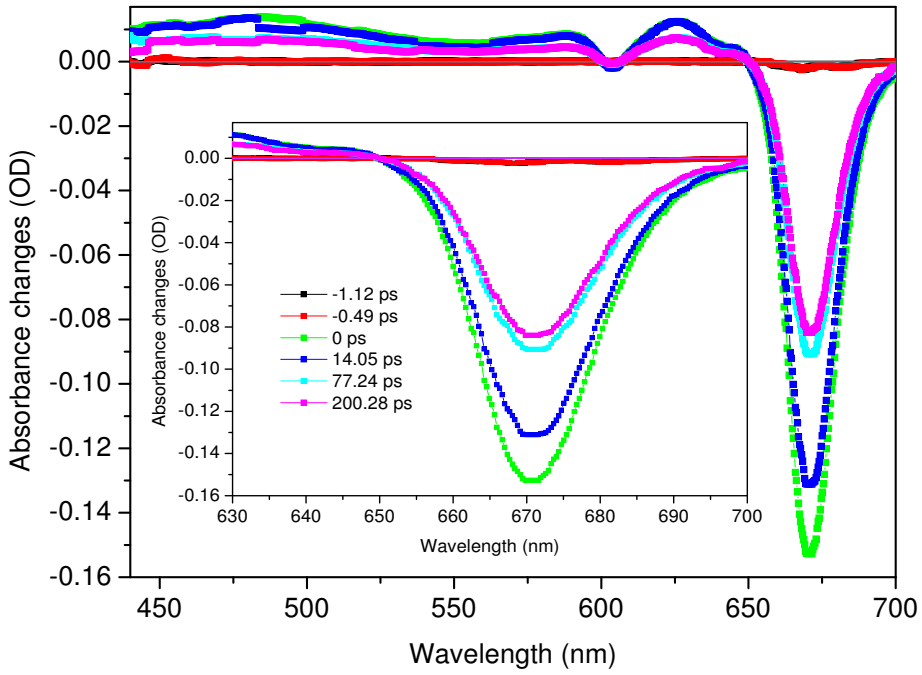

Figure 4.25: Transient signal of ZnPc in DMF sample at a concentration of 6.3 μM pumped at 660 nm (outer graph) and the transient signal in 630–720 nm region which clearly indicates the wavelength peak of the Q-band moving toward the red-shift (inner graph)

Figures 4.26 shows the transient absorption profiles of ZnPc in the DMF solvent at a concentration of 6.3 μM. The sample was excited at 660 nm and the dynamics of the Q-band was probed at 660 nm, 670 nm and 690 nm. As observed in Figure 4.26, the transient signal features a quick rise and is followed by exponentials decays. The data were fit by a bi–exponential decay. However, the result obtained for the double exponential fitting gave us the same time constant. At wavelengths of 660 nm, 670 nm and 690 nm, the time constants were 42.9 $\pm$ 3.8 ps, 45.7 $\pm$ 5.7 ps and 38.5 $\pm$ 7.4 ps respectively. Similar results were obtained for the double exponential fit at 624 nm and 480 nm, as summarised in table 4.5. One can see that the time constants obtained here at different wavelengths are of the same magnitude when the uncertainty is taken into consideration. Time constants observed at 670 nm in DMF agree with the time constants observed at 672 nm with a 672 nm pump that was reported in the investigation of the ZnPc in DMSO above. However, the time constants observed at 624 nm and 480 nm in DMF are significantly longer than

the corresponding time constants in DMSO. As stated above, this time constant can be interpreted as a slower term in a multi–exponential approximation of the solvent dynamics. However, in this experiment, the fast time component was not obtained as observed above.

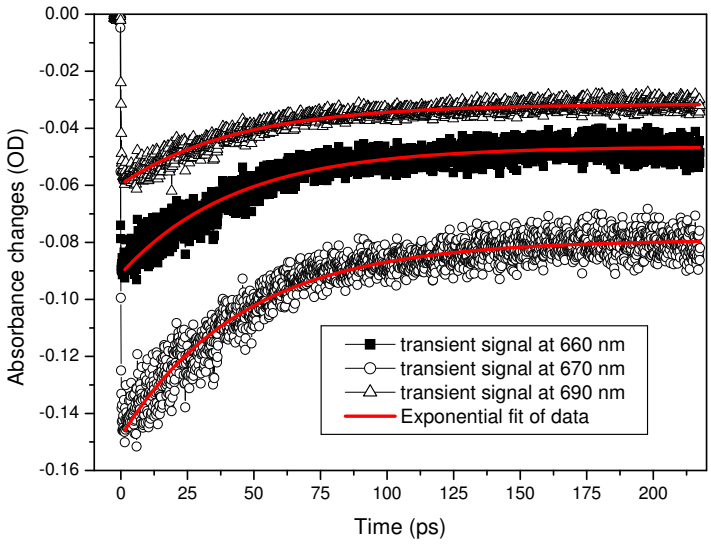

Figure 4.26: Transient absorbance change of ZnPc in DMF sample at a concentration of 6.3 μM pumped at 660 nm with energy of 350 nJ and at 668 nm, 670 nm and 686 nm

There are a number of aspects that could explain this different result. Firstly in this experiment, DMF was used, which is less polar than DMSO. It has been proven that the nature of the lowest excited state varies with the change of the solvent polarity [101]. Upon excitation, the charge redistribution of the DMF solvent around the ZnPc molecule appears to exhibit only a slow relaxation due to the polarity of DMF. In addition, the solvation dynamic effect is related to the dipole of the solvent [101]. The dipole moment of DMF is 3.79 compared to 3.96 for DMSO [68]. This difference in dipole moment could be at the root of the difference in our result.

Secondly, the experiment with DMF as solvent was performed using the experimental setup at Stellenbosch University and not our own experimental setup. The difference in the signal to noise ratio between our experimental setup and the Stellenbosch setup is indicated in Figure 4.27. For comparison, one can see that the signal to noise ratio was lower in the Stellenbosch setup. This might be the reason why the fast time constant that was observed in our

experiment could not be seen. In addition, the pump energy was 350 nJ with the beam size of 100 μm for a concentration 6.3 μM. This concentration might have influenced the detection of the fast time constant component.

Thirdly, the measurements done in Stellenbosch were done at the magic angle, unlike the other measurements. The magic angle was use to eliminate the decay of the signal due to rotational dephasing, as discussed on page 75. The measurements taken in Stellenbosch at the magic angle serves to some extent as a test for the effect of the magic angle. Even at the magic angle there is a significant loss in signal of 35% over 100 ps (as shown in Figure 4.26). This proves without a doubt that the losses seen in our previous results are not completely due to rotational dephasing.

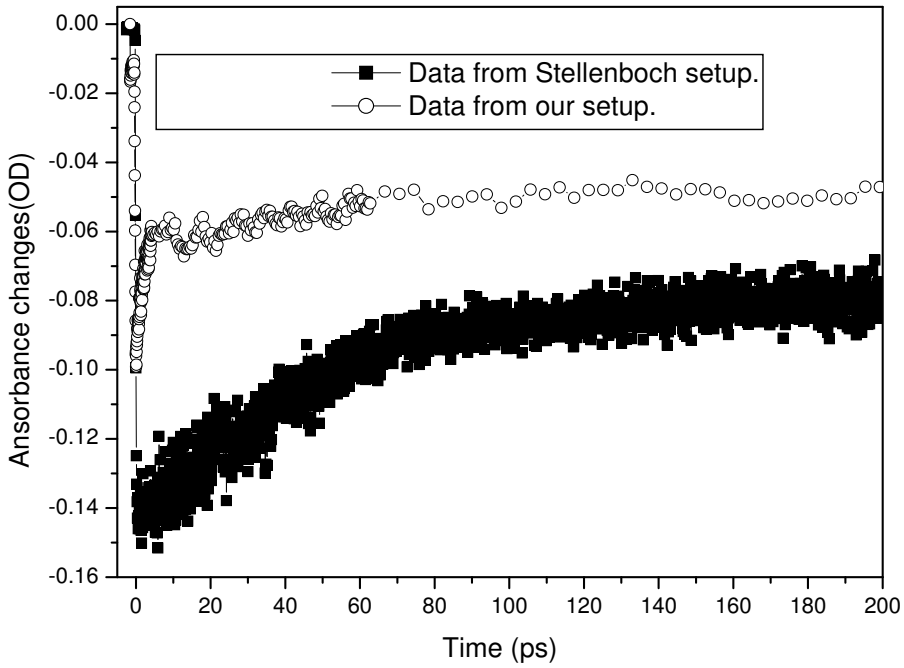

Figure 4.27: Transient absorbance change of ZnPc in DMF at 6.3 μM pumped at 660 nm (in black square) from the Stellenbosch setup and transient absorbance change of ZnPc in DMSO at 5 μM pumped at 672 nm (circle) from our setup

The investigation of the solvent effect on ZnPc reveals that there is a longer red shift of the Q-band peak of ZnPc in DMSO than in DMF. This observation is consistent with the explanation of the red shift by solvent rearrangement around the excited molecule. The rearrangement of a more polar solvent should

cause a larger change in the electronic environment and therefore energy levels of the sample molecule than that of a less polar solvent. In addition, the change of the excitation wavelength does not influence the solvation time, but affects the red shifts of the Q-band.

In literature the dynamics are usually fitted with multi-exponential functions, but only the time constants (exponentials) are extracted, and the coefficients of the different exponential terms which indicates how much the signal drops in that specific time, are often neglected. For the sample studied using the CSIR setup with concentration of $10*10^{-6}$ mol.dm^{-3} in DMSO and pumped at 672 nm, the signal changes from -0.10 OD to -0.05 OD within 100 ps, as shown in Figure 4.19. This indicates a signal loss of >50%. In addition, when samples at different concentrations in DMSO are pumped at 630 nm using the CSIR setup, the signal exhibits losses of 60-75% as observed in Figure 4.23. In order to extract more precise information on signal loss without complications from peak shifts, the area under the 672 nm peak was evaluated as a function of time. Figure 4.28 indicates the variation of the area under the 672 nm peak shown in Figure 4.18 ($10*10^{-6}$ mol.dm^{-3} concentration in DMSO, pumped at 672 nm) as a function of time showing that within 100 ps a signal loss of 53% is observed.

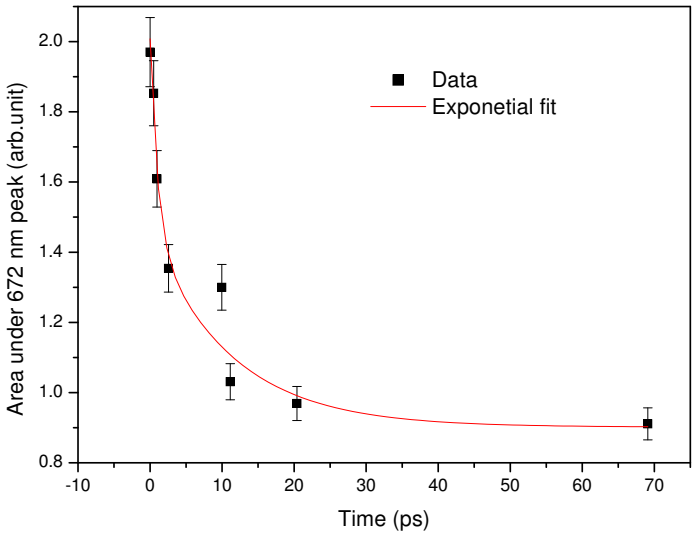

Figure 4.28: Variation of area under 672 peak as function of time for ZnPc in DMSO with a concentration of $10.4*10^{-6}$ mol.dm^{-3} pumped at 672 nm.

In this work a relatively large signal loss, around 50-75%, was observed in all the ZnPc dynamics. Such a large signal loss is not expected. The 3 ns lifetime

of S_1 suggests a small population decrease of about 2-3% within the first 100 ps, and the signal losses in the femtosecond time scale detected by Savolainen et al are also a few %. If this loss is due to depopulation of the S_1 state it is very relevant for PDT, as it will reduce the quantum efficiency. The loss observed is not purely ascribed to the fact that the magic angle was not used in these experiments. The results of the measurements in Stellenbosch where obtained with the magic angle, however a signal loss of at least 35% was also observed in those results.

The signal loss can possibly be caused by the solvent dynamics. The solvent rearrangement around the excited molecule can change the properties of the molecule such as its absorption and emission coefficient [104], the so called Einstein B coefficient. This reduction in absorption or emission coefficient will reduce the ESA signals and the SE signal. However the GSB will not be reduced. The use of a wide range of solvents, including non-polar solvent should also be useful to determine whether the solvent dynamics causes the signal loss.

Chapter 5

Conclusions and future work

5.1 Conclusions

In this dissertation the characterisation work and the results achieved using the technique of femtosecond pump–probe spectroscopy for ultrafast time–resolved spectroscopy were presented. Our experimental setup was characterised and benchmarked using malachite green dye and the measured lifetime of 2.9 ps corresponds well to those quoted in the literature for this dye. The method of correcting for chirp induced in the white–light continuum generation process was presented, as this is required for accurate time resolution of the measurements.

Measurements of the ultrafast energy transfer in LHCs extracted from spinach leaves were also presented. Upon 610 nm excitation measurement of the time constants of the energy transfer among the chlorophylls, as well as annihilation processes, was possible. The pump–probe technique allowed the extraction of the time constants of the energy transfer from Chlb to Chla as well as the energy equlibration from Chla to Chla in LHC II. The time constants obtained are in agreement with the values given in the literature. A detailed study of the energy-transfer lifetimes as a function of pump laser intensity and wavelength was presented. In addition the confirmation of the ultrafast dynamics of the extracted LHCs as well as the interpretation of energy-transfer information from the pump–probe measurements were discussed. A time constant of 6.90 ps which is related to energy transfer from Chla to Chla was extracted whereas two time constants were attributed to Chlb–Chlb energy transfer. These results with the natural LHCs serve to confirm previous work, and demonstrate the potential for measurements of a similar nature on artificial systems.

The transient absorption of ZnPc using the pump–probe setup was studied. This study indicated that there are three time constants. The transient decay dynamic of the ZnPc in DMSO revealed that the dynamics observed on

a timescale of a few picoseconds are associated with solvent relaxation and vibrational relaxation. The longer time constant (in the order of 40 ps) is related to the the dielectric solvent dynamic relaxation of S_1. This time constant is in agreement with the value obtained using ZnPc in DMF. These new results obtained complement the work done by Savolainen et al [6] which lacks data in the picosecond time scale. It was also proved that the change of sample concentration, within the range used in this study, does not influence the solvent effect. The time constants remained in the range of 1.3–1.8 ps for the fast time constant and 38–45 ps for the slower time constant. In addition the excitation of the sample at 630 nm produced lengthening of the time constants due to vibrational relaxation.

The investigation of the solvent effect on ZnPc revealed that there is a longer red shift of the Q-band peak of ZnPc in DMSO than in DMF. This observation is expected due to the difference in polarity of these two solvents. The results here agree with trends known from literature in terms of the solvent polarity [8, 100]. However, the change of the pump wavelength caused a further red shift of the Q-band.

In this work, it was found that within 100 ps there is a large signal loss of 50-75% in our experimental results. Even results of some measurements where the magic angle was used still gives a significant signal loss of at least 35%. Therefore the large signal loss observed in our results was not only due to rotational dephasing. Such a signal loss of 35% is still high compared to what is reported in literature. Solvent dynamics could explain this signal loss, but more work is required in order to confirm this.

5.2 Future work

The results obtained on natural LHC II serve as a proof of principle that the energy transfer in these types of complexes can be measured using the pump-probe setup at the CSIR. Future work could entail the use of this system to characterise the energy transfer of artificial light harvesting complexes, to ensure their efficiency and how they are similar or different from natural systems.

Most measurements in this work were done without using the magic angle. More specifically, all measurements done with the pump-probe system at the CSIR was without the magic angle. As is well known and has been observed here, the rotational dephasing did have an influence on the signal loss. Therefore it will be important in future investigations to use the magic angle in order to suppress the contribution of the rotational motion to the signal, and thereby investigate further the unexpected large loss of signal over 100 ps. In addition, further investigation needs to be done into a wide range of solvents, including

a non-polar solvent in order to improve the discrimination between the effect of the rotational dephasing of the sample and the solvent effect.

Bibliography

[1] Cinque G., Croce R., Holzwarth A. and Bassi R. (2000). "Energy transfer among CP29 chlorophylls: Calculated Forster rates and experimental transient absorption at room temperature". Biophysical Journal, 79, 1706–1717.

[2] Brabec C.J., Zerza G., Cerullo G., De Silvestri S., Luzzati S., Hummelen J.C., and Sariciftci S. (2001). "Tracing photoinduced electron transfer process in conjugated polymer/fullerene bulk heterojunctions in real time". Chemical Physics Letters, 340, 231–236.

[3] Zewail A.H. (2000). "Femtochemistry: Atomic–scale dynamics of the chemical bond". Journal of Physical Chemistry A, 104, 5660–5694.

[4] Zewail A.H. (1988). "Laser femtochemistry". Science, New Series, 242, 1645–1653.

[5] Reid G.D. and Wynne K. (2000). "Ultrafast laser technology and spectroscopy". In Meyers R.A. (Ed), Encyclopedia of Analytical chemistry, 13644–13670.

[6] Savolainen J., Van der Linden D., Dijkhuizen N. and Herek J.L. (2008). "Characterizing the functional dynamics of zinc phthalocyanine from femtoseconds to nanoseconds". Journal of Photochemistry and Photobiology A: Chemistry, 196, 99–105.

[7] Rao S.V. and Rao D.N. (2002). "Excited state dynamics in phthalocyanines studies using degenerate four wave mixing with incoherent light". Journal of Porphyrins and Phthalocyanines, 6, 233–237.

[8] Ogunsipe A., Maree D. and Nyokong T. (2003). "Solvent effects on the photochemical and fluorescence properties of zinc phthalocyanine derivatives". Journal of Molecular Structure, 650, 131–140.

[9] Cerullo G., Manzoni C., Luer L. and Polli D. (2007). "Time–resolved methods in biophysics 4. Broadband pump–probe spectroscopy system with

sub–20 fs temporal resolution for the study of energy transfer processes in photosynthesis". Photochemical & Photobiological Sciences, 6, 135–144.

[10] Cogdell R.J., Issacs N.W., Howard T.D., McLuskey K., Fraser N.J. and Prince S.M. (1999). How photosynthetic bacteria harvest solar energy. Journal of Bacteriology, 181, 3869–3879.

[11] Savolainen J. (2008). "Coherent control of biomolecules". PhD dissertation, Universiteit Twente, Enschede.

[12] Vengris M (2005). "Biological photoreactions explored by multi–pulse ultrafast spectroscopy" PhD dissertation, Vrije Universiteit, Amsterdam.

[13] Demtroder W (2003). "Laser spectroscopy: basic concepts and instrumentation". Third edition. Berlin: Springer–Verlag.

[14] Jeong J. and Gusev A (2007). "Ultrafast, Ultrawide–band spectroscopy". Biophotonics, Laurin publishing.

[15] Dantus M. and Gross P (1998). "Ultrafast spectroscopy". Encyclopedia of applied physics, 22.

[16] Wendling M., Van Mourik F., Van Stokkum I.H.M., Salverda J.M., Michel H. and Van Grondelle R. (2003). "Low–intensity pump–probe measurements on the B800 Band of Rhodospirillum molischianum". Biophysical Journal, 84, 440–449.

[17] Visser H.M., Kleima F.J., Van Stokkum I.H.M., Van Grondelle R., Van Amerongen H. (1996). "Probing the many energy–transfer processes in the photosynthetic light–harvesting complex II at 77 K using energy–selective sub–picosecond transient absorption spectroscopy". Chemical Physics, 210, 297–312.

[18] Visser H.M., Somsen O.J.G., Van Mourik F., Lin S., Van Stokkum I.H.M. and Van Grondelle R. (1995). "Direct observation of sub–picosecond equilibration of excitation energy in the light–harvesting antenna of Rhodospirilum rubrum". Biophysical Journal, 89, 1083–1099.

[19] Visscher K.J., Bergström H., Sundström V., Hunter C.N. and Van Grondelle R. (1989). "Temperature dependence of energy transfer from the long wavelength antenna BChl–896 to reaction center in Rhodospirillum rubrum, Rhodobacter sphaeroides (w.t. and M21 mutant) from 77 to 177 k, studied by picosecond absorption spectroscopy". Photosynthesis Research, 22, 211–217.

[20] Luo.T. (2008).“Femtosecond time–resolved studies on the reaction pathways for the generation of reactive oxygen species in photodynamic therapy by indocyanine green”. Master thesis, University of Waterloo, Ontario.

[21] Schweitzer G., Xu L., Craig B. and DeSchryver F.C. (1997). “A double OPA femtosecond laser system for transient absorption spectroscopy”. Optics Communications, 142, 283–288.

[22] Jonas D.M, Lang M.J, Nagasawa Y., Joo T. and Fleming G.R. (1996). “Pump–probe polarization anisotropy study of femtosecond energy transfer within the photosynthetic reaction center of rhodobacter sphaeroides R26”. Journal of Physical Chemistry B, 100, 12660–12673.

[23] Megerle U., Pugliesi I., Schriever C., Sailer C.F. and Riedle E. (2009). “Sub–50 fs broadband absorption spectroscopy with tunable excitation: Putting the analysis of ultrafast molecular dynamics on solid ground”. Applied Physics B, 96, 215-231.

[24] Buehler Ch., Dong C.Y., So P.T.C., French T. and Gratton E. (2000). “Time–resolved polarization imaging by pump–probe (stimulated emission) fluorescence microscopy”. Biophysical Journal, 79, 536–549.

[25] Dong–Hui Q., Shi–Lin L., Lei Z., Jian Y., Li W., Guo–Zhen Y., and Yu–Xiang W. (2003). “Experimental study on chirped structure of the white–light continuum generation by femtosecond laser spectroscopy”. Chinese Physics Society, 12, 986–991.

[26] Muller A.M., Witzel B., Uiterwaal C.J.G.J., Wanner J., and Kompa K.L. (2002). “White–Light–induced Fragmentation of Toluene”. Physical Review Letters, 88(2), 023001(1)-023001(4).

[27] Gradinaru C.C., Van Stokkum I.H.M., Pascal A.A., Van Grondelle R. and Van Amerongen H. (2000). “Identifying the pathways of energy transfer between carotenoids and chlorophylls in LHC II and CP 29. A multicolor, femtosecond pump–probe study”. Journal of Physical Chemistry B, 104, 9330–9342.

[28] Polivka.T., Van Stokkum I.H.M., D. Zigmantas D., Van Grondelle R., Sundetrom V. and Hiller R.G. (2006). “Energy transfer in the major intrinsic light–harvesting complex from Amphidinium carterae”. Biochemistry, 45, pp 8516–8526.

[29] Hartland G.V.(2004). “Measurement of material properties of metal nanoparticles by time–resolved spectroscopy”. Physical Chemistry Chemical Physics, 6, pp 5263–5274.

[30] Nunes S.M.T., Sguilla F.S. and Tedesco A.C. (2004). "Photophysical studies of zinc phthalocyanine and chloroaluminum phthalocyanine incorporated into liposomes in presence of additives". Brazilian Journal of Medical and Biological Research, 37, pp 273–284.

[31] Doust A.B., Van Stokkum I.H.M., Larsen D.S., Wilk K.E., Curmi P.M.G., Van Grondelle R. and Scholes G.D. (2005). "Mediation of ultrafast light–harvesting by a central dimer in phycoerythrin 545 studied by transient absorption and global analysis". Journal of Physical Chemistry B, 109, 14219–14226.

[32] Zinth W. and Wachtveitl J. (2005). "The first picoseconds in bacterial photosynthesis – Ultrafast electron transfer for the efficient conversion of light energy". Journal of Chemical Physics and Physical Chemistry, 6, 871–880.

[33] Van Grondelle R. and Novoderezhkin V.I (2006). "Energy transfer in photosynthesis: experimental insights and quantitative models". Physical Chemistry Chemical Physics, 8, 793–807.

[34] Mančal T., Valkunas L., Read E.L., Engel G.S., Calhoun T.R. and Fleming G.R. (2008). "Electronic coherence transfer in photosynthetic complexes and its signatures in optical spectroscopy". Spectroscopy, 22, 199–211.

[35] Liu Z., Yan H., Wang K., Kuang T., Zhang J., Gul L., An X. and Chang W. (2004). "Crystal structure of spinach major light–harvesting complex at 2.72 A resolution". Nature, 428, 287–292.

[36] McDermott G., Prince S.M., Freer A.A., Hwathornthwaite–Lawless, Papiz M.Z. and Cogdell R.J. (1995). "Crystal structure of an integral membrane light–harvesting complex from photosynthetic bacteria". Nature, 374, 517–521.

[37] Müh F., Renger T. and Zouni A. (2008). "Crystal structure of cyanobacterial photosystem II at 3.0 A resolution: A closer look at the antenna system and the small membrane–intrinsic subunits". Plant Physiology and Biochemistry, 46, 238–264.

[38] Conçalves R.P., Busselez J., Lévy D., Seguin J. and Scheuring S. (2005). "Membrane insertion of Rhodopseudomonas acidophila light harvesting complex 2 investigated by high resolution AFM". Journal of Structural Biology, 149, 79–86.

[39] Bahatyrova S., Frese R.N., Siebert C.A., Olsen J.D., Van der Werf K.O., Van Grondelle R., Niederman R.A., Bullough P.A., Otto C. and Hunter C.N. (2004). "The native architecture of a photosynthetic membrane". Nature, 430, 1058–1062.

[40] Scheuring S., Boudier T. and Sturgis J.N. (2007). "From high–resolution AFM topographs to atomic models of supramolecular assemblies". Journal of Structural Biology, 159, 268–276.

[41] Goc J., Hara M., Tateishi T. and Miyake J. (1996). "Reconstructed light–harvesting system for photosynthetic reaction centres". Journal of Photochemistry and Photobiology A: Chemistry, 93, 137–144.

[42] Kramer H., Jones M.R., Fowler G.J.S., Francke C., Aartsma T.J., Hunter C.N. and Amez J. (1995). "Energy migration in rhodobacter spaeroides mutants altered by mutagenesis of the peripheral LH2 complex or by removal of the core LHI complex". Biochimica et Biophysica Acta – Bioenergetics, 1231, 89 –97.

[43] Zuber H. and Cogdell R.G. (1995). "Structure and organisation of purple bacterial antenna complexes". In Blankenship, Madigan and Bauer (Ed). Anoxygenic photosynthetic bacteria. Dordrecht: Kluwer, 315–348.

[44] Zuber H. and Brunisholz R.A. (1991). "Structure and function of antenna polypeptides and chlorophyll protein complexes: Principles and versatility". In Scheer (Ed) The chlorophylls. City: Publisher 627–703.

[45] Hu X., Damjanovic A., Ritz T. and Schulten K. (1998). "Architecture and mechanism of the light–harvesting apparatus of purple bacteria". Proceedings of the National Academy of Sciences USA, 95, 5935–5941.

[46] Harvey P.D., Stern C., Gros C.P. and Guilard R. (2008). "Comments on the through–space singlet energy transfers and energy migration (exciton) in the light harvesting systems". Journal of Inorganic Biochemistry, 102, 395–405.

[47] Bradforth S.E, Jimenez R., Van Mourik F., Van Grondelle R. and Fleming G.R. (1995). "Excitation transfer in the core light–harvesting complex (LH–1) of rhodobacter sphaeroides: An ultrafast fluorescence depolarization and annihilation study". Journal of Physical Chemistry, 99, 16179–16191.

[48] Hess S., Chachisvilis M., Timpmann K., Jones M.R., Fowler G.J.S., Hunter C.N. and Sundström V. (1995). "Temporally and spectrally re-

solved sub picosecond energy transfer within the peripheral antenna complex (LH2) and from LH2 to the core antenna complex in photosynthetic purple bacteria". Proceedings of the National Academy of Sciences USA, 92, 12333–12337.

[49] Gradinaru C.C., Kennis J.T.M., Papagiannakis E., Van Stokkum I.H.M, Cogdell R.J., Fleming G.R., Niederman R.A., and Van Grondelle R. (2001). "An unusual pathway of excitation energy deactivation in carotenoids: singlet–to–triplet conversion of an ultrafast timescale in a photosynthetic antenna". Proceedings of the National Academy of Sciences USA, 98, 2364–2369.

[50] Groot M.L., Breton J., Van Wilderen L.J.G.W., Dekker J.P. and Van Grondelle R. (2004). "Femtosecond visible/visible and visible/mid–IR pump–probe study of the photosystem II core antenna complex CP47". Journal of Physical Chemistry B, 108, 8001–8006.

[51] Jansson S. (1994). "The light–harvesting chlorophyll a/b–binding proteins". Biochimica et Biophysica Acta – Bioenergetics, 1184, 1–19.

[52] Van Oort B., Van Hoek A., Ruban A.V. and Van Amerongen H. (2007). "Aggregation of Light–Harvesting Complex II Leads to formation of efficient excitation energy traps in monomeric and trimeric complexes". Federation of European Biochemical Societies Letters, 581, 3528–3532.

[53] Nield J. and Barber J. (2006). "Refinement of the structural model for the photosystem II supercomplex of higher plants". Biochimica et Biophysica Acta – Bioenergetics, 1757, 353–361.

[54] De Weerd F.L., Van Stokkum I.H.M., Van Amerongen H., Dekker J.P. and Van Grondelle R. (2002). "Pathways for energy transfer in the core light–harvesting complexes CP43 and CP 47 of photosystem II". Biophysical Journal, 82, 1586–1597.

[55] Kühlbrandt W., Wang D.N. and Fujiyoshi Y. (1994). "Atomic model of plant light–harvesting complex by electron crystallography". Nature, 367, 614–621

[56] Croce R., Cinque G., Holzwarth A.R. and Bassi R. (2000). "The soret absorption properties of carotenoids and chlorophylls in antenna complexes of higher plants". Photosynthesis Research, 64, 221–231.

[57] Novoderezhkin V.I., Palacios M.A., Van Amerongen H. and Van Grondelle R. (2005). "Excitation dynamics in the LHC II complex of higher

plants: Modeling based on the 2.72 Å crystal structure". Journal of Physical Chemistry B, 109, 10493–10504.

[58] Simidjiev I., Barzda V., Mustárdy L. and Garab G. (1997). "Isolation of lamellar aggregates of the light–harvesting chlorophyll a/b protein complex of photosystem II with long–range chiral order and structural flexibility". Analytical Biochemistry, 250, 169–175.

[59] Lambrev P.H., Várkonyi Z., Krumova S., Kovács L., Miloslavina Y., Holzwarth A.R. and Carab G. (2007). "Importance of trimer–trimer interactions for the native state of the plant light–harvesting complex II". Biochimica et Biophysica Acta – Bioenergetics, 1767, 847–853.

[60] Palacios M.A, Standfuss J., Vengris M., Van Oort B.F., Van Stokkum I.H.M., Kuhlbrandt W., Van Amerongen H. and Van Grondelle R. (2006). "Comparison of the three isoforms of the light harvesting complex II using transient absorption and time resolved fluorescence measurement". Photosynthesis Research, 88, 269–285.

[61] Croce R., Müller M.G., Bassi R. and Holzwarth A.R. (2003). "Chlorophyll b to chlorophyll a energy transfer kinetics in the CP29 antenna complex: A comparative femtosecond absorption study between native and reconstituted proteins". Biophysical Journal, 84, 2508–2516.

[62] Croce R., Müller M.G., Bassi R. and Holzwarth A.R. (2001). "Carotenoid–to–chlorophyll energy transfer in recombinant major light–harvesting complex (LHCII) of higher plants. I. Femtosecond transient absorption measurements". Biophysical Journal, 80, 901–915.

[63] Novoderezhkin V.I., Palacios M.A., Van Amerongen H. and Van Grondelle R. (2004). "Energy–transfer dynamics in the LHCII complex of higher plants: modified redfield approach". Journal of Physical Chemistry B, 108, 10363–10375.

[64] Molukanele P. (2009). "Dynamics of energy transfer in light harvesting photosynthetics systems". Master's thesis, North–west University, Potchefstroom.

[65] Nitschke C., O'Flaherty S.M., Kroll M., Doyle J.J. and Blau W.J. (2004). "Optical properties of zinc phthalocyanine nanoparticle dispersions". Chemical Physics Letters, 383, 555–560.

[66] Howe L. and Zhang J.Z. (1997). "Ultrafast studies of excited–state dynamics of phthalocyanine and zinc phthalocyanine tetrasulfonat in solution". Journal of Physical Chemistry A, 101, 3207–3213.

[67] Abramczyk H. and Szymczyk I. (2004). "Aggregation of phthalocyanine derivatives in liquid solutions and human blood". Journal of Molecular Liquids, 110, 51–56.

[68] Ogunsipe A. and Nyakong T. (2004). "Effects of substituents and solvents on the photochemical properties of zinc phthalocyanine complexes and their protonate derivatives". Journal of Molecular Structure, 689, 89–97.

[69] Dougherty T.J., Gomer C.J., Henderson B.W., Jori G., Kessel D., Korbelik M., Moan J. and Peng G. (1998). " Photodynamic therapy". Journal of the National Cancer Institute, 90, 889–905.

[70] Dolmans D.E.J.G.J., Fukumura D. and Jain R.K. (2003). "Photodynamic therapy for cancer". Nature Reviews Cancer, 3, 380–387.

[71] Ogunsipe A., Chen J.Y. and Nyokong T. (2004). "Photophysical and photochimical studies of zinc (II) phthlalocyanine derivatives–effects of substituents and solvents". New Journal Chemistry, 28, 822–827.

[72] Howe L. and Zhang J.Z. (1998). "The effect of biological substractes on the ultrafast excited–state dynamics of zinc phthlalocyanine". Photochemistre and Photobiology, 67, 90–96.

[73] Brozek–Pluska B., Jarota A., Kurczewski K. and Abramczyk H. (2009). "Photochemistry of tetrasulphonated zinc phthalocyanine in water and DMSO solution by absorption, emission, Raman spectroscopy and femtosecond transient absorption spectroscopy". Journal of Molecular Structure, 924–926, 338–346.

[74] Koval'skaya N.E., Kuznetsova N.A., Kaliya O.L., Gretsova N.S. and Sokolova I.V. (2000). "Study of spectral properties of zinc phthalocyanines used as sensitizers in photodynamic therapy". Optics and Spectroscopy, 89, 724–726.

[75] Idowu M., Ogunsipe A. and Nyokong T. (2007). "Excited state dynamic of zinc phthalocyanine carboxylates". Spectrochimica Acta Part A, 68, 995–999.

[76] Ogunsipe A., Durmus M., Atilla D., Gurek A.G., Ahsen V. and Nyokong T. (2008). "Synthesis, photophysical and photochemical studies on long chain zinc phthalocyanine derives". Synthetic Metals, 158, 839–847.

[77] Abramczyk H., Brozek–Pluska B., Kurczewski K., Szymczyk I., Krzyczmonik P., Blaszczyk T., Scholl H., and Czajkowski W. (2006). "Femtosecond transient absorption, raman, and eletrochemistry studies of tetra-

sulfonated copper phthalocyanine in water solution". Journal of Physical Chemistry A, 110, 8627–8636.

[78] Bishop S.M., Beeby A., Parker A.W., Foley M.S.C., and Phillips D. (1995). "the preparation and photophysical measurements of perdeutero zinc phthalocyanine". Journal of Photochemistry and Photobiology A: Chemistry, 90, 39–44.

[79] Berera R., Herrero C., Van Stokkum I.H.M., Vengris M., Kodis G., Palacios R.E., Van Amerogen H., Van Grondelle R., Gust D., Moore T.A., Moore A.L. and Kennis J.T.M. (2006). "A simple artificial light–harvesting dyad as a model for excess energy dissipation in oxygenic photosynthesis". PNAS, 103, 5343–5348.

[80] Kienle F., (2007). "Temporal measurements on ps–fs laser systems: Autocorrelation technique". Diploma thesis, Aalen University of Applied sciences, Germany.

[81] Griessel A. (2009). "The investigation of resveratrol with conventiaonal and ultrafast pump–probe spectroscopy technique". Master's thesis, Stellenbosch University, Stellenbosch.

[82] Ombinda-Lemboumba S., du Plessis A., Sparrow R.W., Molukanele P., Botha L.R., Rohwer E.G., Steenkamp C.M. and van Rensburg L. (2009). "Femtosecond pump probe spectroscopy for the study of energy transfer of light-harvesting complexes from extractions of spinach leaves". South African journal of Science, 105, 376-386.

[83] Krupa Z., Huner N.P.A., Williams J.P., Maissan E. and James D.R. (1987). "Development at cold hardening temperatures–the structure and composition of purified rye LHCII". Plant Physiology, 84, 19–24.

[84] Dinkins R.D., Bandaranayake H., Beaza L., Griffiths A.J.F. and Green B.R. (1997) "hcf5, a nuclear photosynthetic electron transport mutant of arabidopis thaliana with a pleiotropic effect on chloroplast gene expression". Plant Physiology, 113, 1023-1031.

[85] Fukuda M., Kajimoto O., Terazima M. and Kimura Y. (2007). "Application of the transient grating method to the investigation of the photo–thermalization process of malachite green in room temperature ionic liquids". Journal of Molecular Liquids, 134, 49–54.

[86] Shank C.V., Ippen E.P., Fork R.L., Migus A. and Kobayashi T. (1980). "Application of subpicosecond optical techniques to molecular dynamics". Philosophical Transactions of Royal Society of London A, 298, 303–308.

[87] Holt N.E., Kennis J.T.M. and Fleming G.R. (2004). "Femtosecond fluorescence upconversion studies of light harvesting by β–carotene in oxygenic photosynthetic core proteins". Journal of Physical Chemistry B, 108, 19029–19035.

[88] van Amerongen H. and van Grondelle R. (2001). "Understanding the energy transfer function of LHC II, the major light-harvesting complex of green plants". Journal of Physical Chemistry, 105, 604-617.

[89] Barzda V., Gulbinas V., Kananavicius R., Cervinskas V., van Amerongen H., van Grondelle R. and Valkunas L. (2001). "Singlet-singlet annihilation kinetics in aggregates and trimers of LHCII". Biophysical Journal, 80, 2409-2421.

[90] Dekker J.P. and Boekema E.J. (2005). "Supramolecular organization of thylakoid membrane proteins in green plants". Biochimica et Biophysica Acta, 1706, 12-39.

[91] Croce R., Mozzo M., Morosinatto T., Remeo A., Hienerwadel R. and Bassi R. (2007). "Singlet and triplet state transition of carotenoids in the antenna complexes of higher-plant photosystem I". Biochemistry, 46, 3846-3855.

[92] Engelmann E.C.M., Zucchelli G., Garlaschi F.M., Casazza A.P. and Jennings R.C. (2005). "The effct of outer antenna complexes on the photochemical trapping rate in barley thylakoid photosystem II". Biochimica et Biophysica Acta, 1706, 276-286.

[93] Sibata M.N., Tedesco A.C. and Marchetti J.M. (2004). "Photophysicals and photochemicals studies of zinc (II) phthalocyanine in long time circulation micelles for photodynamic therapy use". European Journal of Pharmaceutical Sciences, 23, 131–138.

[94] Frackowiak D., Planner A., Waszkowiak A., Bojuta A., Ion R.M. and Wiktorowicz K. (2001). "Yield of intersystem (singlet–triplet) crossing in phthalocyanines evaluated on the basis of a time in resolved photothermal method". Journal of Photochemistry and Photobiology A: Chemistry, 141, 101–108.

[95] Rosenthal S.A., Xie X., Du M. and Fleming G.R. (1991). "Femtosecond solvationdynamics in acetonitrile: Observation of the inertial contribution to the solvent response". Journal of Chemical Physics, 95, 4715–4718.

[96] Rossky P.J. and Simon J.D. (1994). "Dynamics of chemical processes in solvents". Nature, 370, 263–269.

[97] Tie–Qiao Z., Shu–Feng W., Hong Y., Jian–Liang L., and Qi–Huang G. (1999). "Solvation dynamics of methanol investigated by femtosecond time–resolved fluorescence up–conversion technique". Chinese Physical Sociaty, 8, 383- 389.

[98] Horng M.L., Gardecki J.A., Papazyan A. and Maroncelli M. (1995). "Subpicosecond measurement of polar solvation dynamics: Coumarin 153 revisited". Journal of Physical Chemistry, 99, 17311–17337.

[99] http://frog.gatech.edu/UFOBook/16–Ultrafast–Techniques–Fourkas.pdf

[100] Chauke V., Ogunsipe A., Durmus M. and Nyokong. (2007). "Novel gallium (III) phthalocyanine derivatives: Synthesis, photophysics and photochemistry". Polyhedron, 26, 2663–2671.

[101] Gumy J.C., Nicolet O. and Vauthey E. (1999). "Investigation of the solvation dynamics of an organic dye in polar solvents using the femtosecond transient grating technique". Journal of Physical Chemistry A, 103, 10737–10743.

[102] Wang H.C., Lu Y.C., Chen C.Y., Chi C.Y., Chin S.C. and Yang C.C. (2005). "Non–degenerate fs pump–probe study on InGaN with multi–wavelength second–harmonic generation". Optics Express, 13, 5245–5252.

[103] Brozek–Pluska B., Czajkowski W., Kurczewska M. and Abramczyk H. (2008). "Photochemistry of tetrasulphonated magnesium phthalocyanine in water and DMSO solution by Raman, femtosecond transient absorption and stationary absorption spectroscopies". Journal of Molecular Liquids, 141, 140–144.

[104] Reichardt C. (2003). "Solvent and solvent effects in organic chemistry". Weinheim, Wiley-VCH verlag.